Optimisation and Integration of Variable Renewable Energy Sources in Electricity Networks

Wang Zhang

Centre for Future Energy Networks, School of Electrical and Information Engineering, B.E M.E.
The University of Sydney

This dissertation is submitted for the degree of
Doctor of Philosophy

School of EIE June 2017

I would like to dedicate this thesis to my loving family …

Declaration

I hereby declare that except where specific reference is made to the work of others, the contents of this dissertation are original and have not been submitted in whole or in part for consideration for any other degree or qualification at this or any other university. This dissertation is my own work and contains nothing that is the outcome of work done in collaboration with others, except as specified in the text and acknowledgments. This dissertation contains fewer than 60,000 words including appendices, bibliography, footnotes, tables and equations and has fewer than 150 figures.

Wang Zhang
June 2017

Thesis Authorship Attribution Statement

Chapter 2 of this thesis is published as [21]. I designed the study, formulated the model and simulation, analysed the data and wrote the drafts of the manuscript.

Chapter 3 of this thesis is published as [58, 59]. I designed the study in [58] and co-designed the study in [59] with the co-authors, formulated the system model, conducted the simulation, analysed the data and wrote the drafts of the manuscripts.

Chapter 4 of this thesis is published as [73, 74]. I designed the studies, formulated the models and conducted the simulations, analysed the data sets and wrote the drafts of the manuscripts.

Chapter 5 of this thesis is published as [87]. I designed the studies, formulated the models and conducted the simulations, analysed the data sets and wrote the drafts of the manuscripts.

In addition to the statements above, in cases where I am not the corresponding author of a published item, permission to include the published material has been granted by the corresponding author.

Wang Zhang,  February 2017.

As supervisor for the candidature upon which this thesis is based, I can confirm that the authorship attribution statements above are correct.

Zhao Yang Dong,  February 2017.

Acknowledgements

I would like to express my deepest appreciation and most sincere gratitude to my supervisors Prof. Zhao Yang Dong and Dr. Guo Chen. I would also like to express my sincere thanks to Dr. Ke Meng and Dr. Yan Xu. They were exceptional mentors for me throughout my research. Moreover, I would also like to express my sincere appreciation to Prof. David John Hill for his support and wisdom, and for giving me the opportunity to work with him. Furthermore, my most sincere gratitude and appreciation go to my parents, who have provided me with love, support, and understanding throughout my life and especially throughout my PhD. The research presented in this thesis would not have been possible without the contributions and support.

I would also like to express my thanks, to my cousin, for being supportive and a very close friend while we are both far away from family; to Mr.Zhuoyang Wang, for being an amazing colleague and for always having a different point of view; and to Susan, for being there and a true friend, and for the wonderful moments and adventures.

Furthermore, I would like to thank all members of the Centre for Future Energy Networks at the school of Electrical and Engineering, the University of Sydney, for being such a dynamic team and for making being supportive and encouraging.

Finally, I would like to dedicate this thesis to my grandparents. I have been extremely fortunate in my life to have grandparents who have shown me unconditional love and support, reminding me to be a person with an ambitious brain and a kind and warm heart.

Abstract

The growing penetration of renewable energy sources (RESs) into the electricity power grid is profitable from a sustainable point of view and provides economic benefit for long-term operation. Nevertheless, balancing production and consumption is and will always be a crucial requirement for power system operation. However, the trend towards increasing renewable energy penetration has raised concerns about the stability, reliability and security of future electricity grids. The clearest observation in this regard is the intermittent nature of renewable generation sources [1], such as wind and solar generation. Moreover, the location of renewable generation tends to be heavily defined by meteorological and geographical conditions [2, 3], which makes the generation sites distant from load centres. These facts make the analysis of electricity grid operation under both dynamic [4] and the steady state more difficult, posing challenges in effectively integrating variable RESs into electricity networks.

The thesis reports on studies that were conducted to design efficient tools and algorithms for system operators, especially transmission system operators for reliable short-term system operation that accounts for intermittency and security requirements. In particular, the following points are addressed through chapters in this thesis: What are the impacts of renewable generation on the grid steady state operations? What are the existing modeling and solving methods, and why are they inadequate when modelling to account for intermittencies? How could a transmission system operator effectively coordinate conventional controllable generators with various renewable sources with increasing penetration levels? What challenges and opportunities do new elements at different levels of the electricity network, such as networked microgrids, distributed renewable generations, and demand side management (DSM) present with regard to the steady state operation in transmission networks? Finally, what is the requirement for computation efficiency and convergence of the algorithms? Overall, this thesis aims to provide an efficient tool for modeling and analyzing the steady state of electricity grids with a high penetration of RESs.

Initially, the impact of renewable generation on the steady state is studied in the operation stage [5], in terms of the optimal dispatch decision-making process and load flow on an hourly basis. The problem is formulated into a security constraint optimal power flow

(SCOPF) problem, and the goal is to minimise the cost of operating the power system by identifying the setpoints of the controllable components - for example generators, transformers, capacitor banks, etc. - within system limits for a reliable, secure and economic power supply under uncertainties. In particular, different approaches to accounting for uncertainties brought by random variables are studied in details, with discussions on the advantages and disadvantages of each approach in the application of the optimal dispatch problems. In addition, the computation complexity of SCOPF is brought to an even higher level regarding uncertainties. Therefore, the first study also looks into strategies for solving such large-scale computationally expensive problems, where decomposition techniques are applied. The second chapter subsequently presents a new and efficient approach to address the uncertain factors that arise from load demand and renewable generation in power systems; this is done using a robust SCOPF model. The proposed algorithm is then tested on a modified IEEE 14-bus system and IEEE 118-bus system, showing promising results to effectively and efficiently integrate RESs into the electricity power grid operation.

Then, based on the first study, more sophisticated modeling on the electricity network are investigated in the third and fourth chapters.

First, the behaviour of a meshed ac and high voltage direct current(HVDC) grid connecting large-scale offshore wind farms is studied in the scope of SCOPF. A hierarchical SCOPF model is proposed for a meshed ac/multi-terminal HVDC (MTDC) system with high wind penetration. Two interacting levels regulates the power flow in an MTDC grid according to reference signals from the high level. In this way, the proposed method utilises an MTDC system to provide support for the ac system by redistributing power flow across the entire grid and reducing control costs. Second, the raising of microgrids in the distribution network warrants further attention.

Extending the previous studies, the fourth chapter explores the potential of using multiple microgrids to support the main grid's security control. Corrective control is compared with the preventive control method, and employed to relieve post-contingency overflows by effectively coordinating system generators and multiple microgrids. An incentive-based mechanism is designed to encourage the microrgrids to actively cooperate with the main grid for post-contingency recovery, which distinguishes the proposed method from the previous models by using a traditional centralised control method, such as direct load control. A scenario-decomposition based approach is then developed to solve the proposed robust SCOPF problem. Numerical simulations on the IEEE14- and 118-bus systems demonstrate the effectiveness and efficiency of the proposed method.

Finally, the questions regarding to the computational efficiency and convergence analysis are addressed in chapter 5 and a DSM model in a real-time pricing environment is introduced.

This model presents an alternative way of using flexibility in the demand side to compensate for the uncertainties on the generation side. To start with, a summary of previous chapters is provided in terms of reducing the calculation complexity. In particular, a linearised power flow model is adopted for optimal dispatch scheduling problems, while it is normally formulated with a quadratic objective function and linearised constraints. This clearly alleviates the computational burden by approximating the optimal power flow into a convex optimisation problem, but it also neglects some system physical constraints, such as reactive power and voltage limits. To overcome this disadvantage, two approaches are described in detail for computation efficiency improvement. First, the chapter introduces approach that applies a dc optimal power flow model with an ac power flow N-1 contingency analysis security check using the Benders Decomposition is introduced, which is applied in the models in chapter 3 and 4. The chapter also describes the details regarding effectiveness, merit, drawbacks, and limitations. Next, a fast-distributed dual gradient algorithm is proposed to accelerate the convergence rate and overcome the possible non-convergence during the iteration process for non-differentiable convex problem. The proposed algorithm is applied to a widely adopted social welfare optimisation problem under a real-time pricing environment to demonstrate its effectiveness.

Table of contents

List of figures

List of tables

Nomenclature

Functions

$\bullet^{+}$	Optimistic optimisation variable in confident interval
$\bullet^{-}$	Pessimistic optimisation variable in confident interval
$\mathscr{D}(\bullet)$	Dual problem
$\mathscr{L}(\bullet)$	Lagrangian function of a given problem
$\mu(\bullet)$	Mean value of normally distributed random variables
$\sigma^2(\bullet)$	Variance of normally distributed random variables
$\widetilde{\bullet}$	Optimistic optimisation variable in confident interval
$f(\bullet)$	Operation cost function for optimal power flow
$p_i(\bullet),\ p_t(\bullet)$	Proximity functions for double smoothing techniques

Indices

c	index of voltage source converters
i	Bus number or from bus for a transmission line
j	Bus number or to bus for a transmission line
k	Index for contingency
l	index for branches
m	Iteration for the dc grid droop control
s	Index for scenarios

Parameters

$\alpha_{m,i}$ corrective control action cost coefficient for participated microgrid i

$\alpha_{g,i}$ Redispatch cost coefficient for generator i

β_w Scale parameter for Weibull distribution

$\Delta\mathbf{u_k}$ Allowed deviation of control vector from pre-contingency to contingency k

ε Terminate criterion

η Robust degree

γ Step size for sub-gradient method

Λ Estimated upper bound for Lagrangian multiplier λ

$\mathbf{B}$ Admittance matrix of the grid

$\mathbf{J_{DC}}$ Jacobian matrix for dc grid

$\mathbf{p^{ac}_{vsc,k}}$ Vector of active power generation of all VSC on the ac side in contingency k

$\mathbf{q^{ac}_{vsc,k}}$ Vector of reactive power generation of all VSC on the ac side in contingency k

$\mathbf{Y}$ Admittance matrix

$\overline{i^{dc}_{ij}}$ Upper limit for current rating on the dc line from bus i to bus j

ρ^k Probability of contingency k to occur

ρ^s Probability of scenario s to occur

$\sigma_i,\ \sigma_t$ Convex parameters

τ TLDSCOPF Algorithm iteration termination criteria on $\mathbf{p}^{ac}_{vsc}$

$\theta_{slack}, \theta_{ref}$ Voltage angle at the reference bus or slack bus

$\underline{K_i}, \overline{K_i}$ Lower and upper limit for droop constant of VSC on dc bus i

$\varphi^{min}_{ij}, \varphi^{max}_{ij}$ Minimum and maximum voltage angle shift by voltage shift transformer between bus i and j

$a_i, b_i and c_i$ Quadratic, linear and constant coefficients for quadratic cost function for generation unit i

b_{ij} Series susceptance between bus i and bus j

g_{ij} Series conductance between bus i and bus j

H Power transfer distribution factors

k_w Shape parameter for Weibull distribution

n_b Number of Buses in the grid

n_b^{dc} Number of dc buses

n_b^{dc} Total number of dc buses in dc grid

n_g Total number of generators in the grid

n_k Number of contingencies

n_m Number of microgrids

n_s Number of scenarios

n_φ Number of the phase shifting transformers in the system

n_{rad} Number of random variables in a system

n_{tr} Number of the Tap changing transformers in the system

$p_{g,i}^{dn}, p_{g,i}^{up}$ Ramp down and ramp up limits on generation unit i

$p_{g,i}^{min}, p_{g,i}^{cap}$ Minimum and maximum active power generation of generation unit i

$p_{ij}^{min}, p_{ij}^{cap}$ Minimum and maximum active power flow from bus i to j

$p_{m,i}^{dn}, p_{m,i}^{up}$ Minimum and maximum adjustment on microgrid i

P_{rated} Rated power for wind turbine

$p_{vsc,c}^{ac,max}, p_{vsc,c}^{ac,min}$ Maximum and minimum active power generation rating of VSC c on the ac side

$p_{vsc,i}^{dc,ref}$ Reference value for active power generation of grid VSC on dc bus i in dc grid

$p_{w,j}^{\rho^{max}}$ Most probable(forecast) active power generation on wind farm connected to the node j

$q_{g,i}^{min}, q_{g,i}^{cap}$ Minimum and maximum reactive power generation of generation unit i

$q_{ij}^{min}, q_{ij}^{cap}$ Minimum and maximum reactive power flow from bus i to j

$q_{vsc,c}^{ac,max}, q_{vsc,c}^{ac,min}$ Maximum and minimum reactive power generation rating of VSC c on the ac side

r_{ij} Resistance of the dc lines from node i to node j

T_k Allowed post-contingency recovery time for contingency k

$tr_{ij}^{min}, tr_{ij}^{max}$ Minimum and maximum voltage tap rate by voltage tapping transformer between bus i and j

V_i^{min}, V_i^{max} Minimum and maximum voltage magnitude on bus i

V_k Vector of all voltages of Ac buses in contingency k

$v_{c_{in}}$ Cut in wind speed for wind power

$v_{c_{out}}$ Cut out wind speed for wind power

$V_{def,i}$ Predefined nominal voltage at bus i

v_{rated} Rated wind velocity for wind turbine

Sets

$\mathbf{Z}$ System Z

$\mathcal{N}$ Set of users subscribed to an aggregator in the real time pricing model

S_K^C Sets of corrective controlled contingencies

$S_K^N il$ Sets of Contingencies without solutions

S_K^P Sets of preventive controlled contingencies

Variables

$\Delta\widetilde{\mathbf{p}}$ Vector of changes of active power injections on buses

$\Delta\widetilde{\mathbf{p}}_L$ Vector of changes of active power flow on branches

$\hat{u}$	Control vector for not considering any contingency
$\hat{x}$	State vector for not considering any contingency
λ^t	Lagrangian multiplier, often used to indicate the electricity rate of a given time slot t
λ_k	Dual variables for problem k
$\lambda_{c,k}$	Dual variable for $\mathbf{p}_{vsc}^k$
$\lambda_{g,k}$	Dual variable for $\mathbf{p}_g^k$
θ	Vector of voltage angles
φ	Vector of Voltage angle shift
$\mathbf{I^{dc}}$	Vector of current in dc grid
$\mathbf{p_d}$	Vector of active power to loads on all buses
$\mathbf{p_g}$	Vector of active power from conventional generation units on all buses
$\mathbf{p_L}$	Vector of active power flow on all branches
$\mathbf{p_r}$	Vector of active power from renewable generation units on all buses
$\mathbf{p}$	Vector of active power
$\mathbf{p}_d^{\rho^{max}}$	Vector of the most probable load demand
$\mathbf{p}_r^{\rho^{max}}$	Vector of the most probable renewable energy generation
$\mathbf{p}_H^{max}$	Vector of equivalent upper limit on active power flow for all branches in robust formulation
$\mathbf{p}_H^{min}$	Vector of equivalent lower limit on active power flow for all branches in robust formulation
$\mathbf{q}$	Vector of reactive power
$\mathbf{r}$	Vector of random variables
$\mathbf{tr}$	Vector of tap setting
$\mathbf{u_0}$	Control vector for pre-contingency

$\mathbf{u_k}$	Control vector for contingency k
$\mathbf{u}$	Control variable vector
$\mathbf{V^{dc}}$	Vector of voltage in dc grid
$\mathbf{V}$	Vector of voltage magnitudes
$\mathbf{x_0}$	State vector for pre-contingency
$\mathbf{x_k}$	State vector for contingency k
$\mathbf{x}$	State variable vector
$\mathbf{z}$	Optimisation variable vector
ω	Optimal value for sub-problems' objective function
θ_i	Voltage angle at bus textiti
θ_{ij}	Voltage angle difference between node bus i and j
$\tilde{p}_{a,l}^{max}$	Aggregated upper bound for branch l all loads and line flow
$\tilde{p}_{a,l}^{min}$	Aggregated lower bound for branch l all loads and line flow
$\varkappa$	Lagrangian multiplier
φ_{ij}	Voltage angle shift between node bus i and j
$\widetilde{p}_{ij}$	Random active power flow from bus i to bus j
$\widetilde{p}_{r,i}$	Random active power from renewable generation on bus i
ξ	User's consumption preference parameter
$C_{cc,m}$	Corrective control cost by microgrids
$C_{cc}^{m\&g}$	Corrective control cost by microgrids and generation units
C_{ESCC}^{m}	Total contingency control cost by microgrids
C_{ESCC}^{base}	Total contingency control cost without considering microgrids' supports
$C_{pc,m}$	Preventive control cost by microgrids
$C_{pc}^{m\&g}$	Preventive control cost by microgrids and generation units

K_i Droop constant of VSC on dc bus i

L_t Aggregated consumption in the real time pricing model in the time slot t

p_i Active power injection on bus i

$p_{d,i}$ Active power demand on bus i

$p_{g,i}$ Active power generation at generator i

$p^s_{g,i}$ Active power generation of generation unit i in scenario s

$p^{max}_{h,l}$ Equivalent upper limit on active power flow for branch l in robust formulation

$p^{min}_{h,l}$ Equivalent lower limit on active power flow for branch l in robust formulation

p_{ij} Active power flow from bus i to bus j

p^{dc}_{ij} Power flow from node i to node j on the dc line

$p^{(S)}_{r,1}$ Testing scenario S generated from OA library for variable $p_{r,1}$

$p_{r,i}$ Active power from renewable generation on bus i

$p^a_{vsc,i}c$ Active power generation on the ac side

$p^{ac,k}_{vsc,i}$ Active power generation of VSC in the ac grid on ac bus i in contingency k

q_i Reactive power injection on bus i

$q_{d,i}$ reactive power demand on bus i

q_{ij} Reactive power flow from bus i to bus j

$q_{r,i}$ reactive power from renewable generation on bus i

$r_{i,k}$ Slack variables for branch l in problem k

tr_{ij} Tap setting for tap changing transformers between bus i and j

v Wind velocity

V_i Voltage magnitude on bus textiti

$V^{ac,k}_i$ Voltage on ac bus i in contingency k

V^{dc}_i Voltage on node i in the dc grid

x^t_i User i's consumption in time slot t in the real time pricing model

Chapter 1

Introduction

1.1 Background and Motivation

Currently, the on-going endeavour of deploying massive variable renewable energy sources (RESs) in the electricity grid is commonly observed. By the end of 2015, at least 173 countries had set renewable energy targets, of which 146 countries had supporting renewable energy policies.

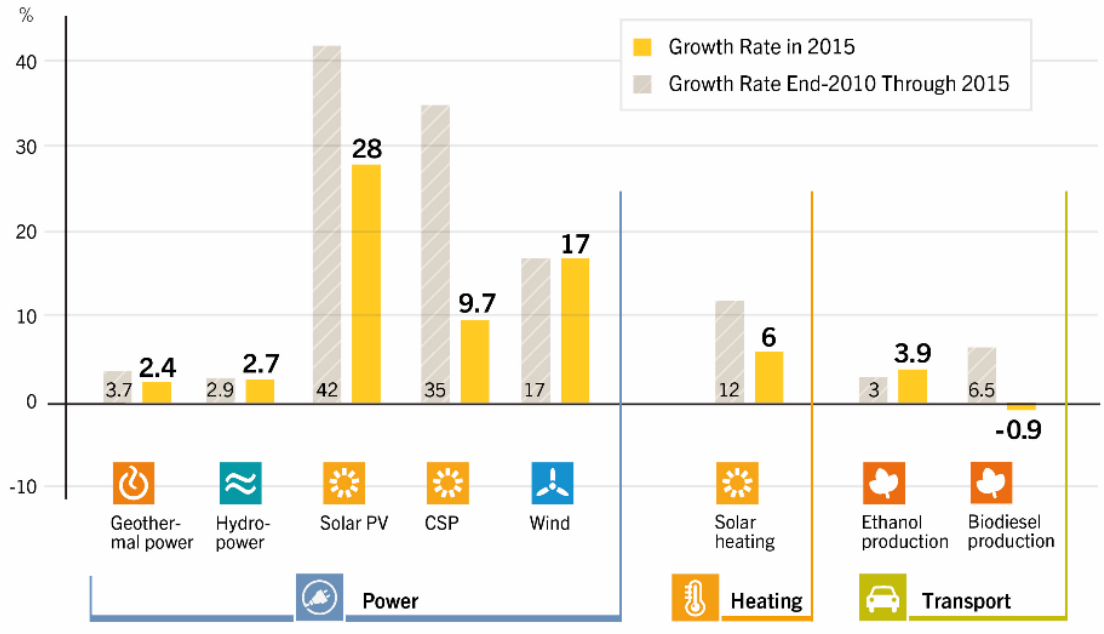

Fig. 1.1 Average annual growth rates of renewable energy capacity and bio-fuels production, end of 2010 to end of 2015 [6]

To achieve these targets, the last decade saw a steady increase in the global demand for renewable energy, with an overall 30% increase. According to the Renewables 2016 Global Status Report [6], between 2004 to 2014 the installed capacity of RESs has experienced a rapid growth globally, with 270 GW growth for wind power; up to 136 GW for photovoltaics; 285 GW for wave and tidal power; and up to 49 GW for biomass. The growing penetration of RESs into the electricity power grid is profitable from a sustainable point of view and provides economic benefit for long-term operation. Reliable and secure energy supply is of high priority for modern society [8]; unfortunately, however, this has arisen because of concern about the trend towards increasing renewable energy penetration, due to the intermittent nature of renewable generation sources, such as wind and solar generation.

In addition, security requirements for the system to withstand contingencies also plays an important role in supplying reliable and secure energy to the consumer. This becomes even more challenging with the reducing fraction of dispatchable generation sources in the gird. Moreover, the location of renewable generation tends to be heavily defined by meteorological and geographical conditions, which makes the generation sites distant from load centres. Therefore, cost-efficient operation strategies must be analysed anew and designed to account for the heterogeneous nature of large variable RESs, for improved reliability and security. While the main challenge is to maintain the balance between supply and demand, this challenge can be further categorised according to controlled time scales, as follows:

1. **Frequency and voltage regulation and stability [9].** Challenges are brought by the variety of scattered RESs that create frequent power injections into the grid as well as possible reversed power flows. This problem is mainly regarded as in distribution networks [10], in the time scale of milliseconds to a second.

2. **Frequency inertia.** Conventional electricity networks mainly rely on synchronous generators with large inertia that are capable of providing key support in frequency and voltage stability. However, power electronics inverter-based distributed generation including RESs present a lack of frequency inertia. As a result, the stability of the grid and the quality of service might be affected as the voltage and frequency transient may become too large in a low mechanical inertia grid.

3. **Reliable and secure optimal power flow problem.** Although a relatively accurate forecast on load could be achieved by now, uncertainties brought by variable intermittent renewable sources normally induce a large-scale optimisation problem [11, 12], especially when security constraints are considered. Solution computation using a traditionally formulated deterministic problem might not be valid when the real generation of RESs deviates from the predicted value. This type of computation is normally done

in the minutes to hourly basis. Additionally, security and resilience of the electricity grid normally require a fast response from the disptachable generation that has been seen as a trend of reduction [13]. Therefore new and more efficient approaches need to be explored considering all aforementioned transitions in the network [14].

4. **Energy management system and scheduling.** Unit commitment [15] is normally adopted for day-ahead scheduling, where the uncertainties of the renewable generation could have a continuous impact on optimal decision-making, which normally leads to a stochastic problem. With constraints such as minimum running and shut down time for conventional large generators, the solution for long term scheduling could suffer even more due to the uncertain variables.

5. **Long-term operation and planning [16, 17].** The integration of RESs also urges the electricity network to experience a significant ongoing reconstruction and expansion in order to accommodate the heterogeneous nature of these sources as well as dynamic control and communication. Meanwhile, the grid also tends to be smaller, more resilient and less interdependent. Moreover, the locations of generation that used to be determined by the load centre become more diverse and could be remotely off shore.

A potential solution to these challenges is to find an efficient framework that is able to accommodate a high penetration level of RESs and is computationally efficient for operations in various time domains. In particular, diverse approaches should be exhausted for uncertainties of modelling and handling that correspond to different types of optimisation problems. In addition, mathematical approaches such as approximation and decomposition techniques are applied to the problem to alleviate the computational burden. Thus, this thesis aims to provide an efficient tool for modelling and analysing the steady state of the electricity grid with a high penetration of RESs. It aims to develop effective solving approaches so that variable RESs can be integrated smoothly into electricity networks.

1.2 Contribution

This PhD thesis presents the detailed steady-state modelling of the integration of renewable energy generation into the network for future electricity network operations and optimisation. Its contributions lie in its effectiveness in considering the intermittent renewable generation into the operation modelling and in developing efficient solving techniques. These contributions are summarised as follows:

- an efficient framework in modeling and optimising the electricity network operation by taking into account uncertainties, securities and new components;

- comparison, identification and analysis of various approaches are thoroughly conducted in considering uncertainties in the optimisation problem, based on which a robust optimal power flow approach is proposed for effectively considering random variables;
- in order to incorporate security measures against contingencies, the robust optimal power flow is elevated into a robust SCOPF problem, using decomposition techniques;
- a hierarchical SCOPF is then proposed for a meshed ac and dc grid. A two-level structure is investigated to effectively coordinate the offshore renewable generation with the in-land main grid optimal dispatch decision-making process;
- an incentive-based approach is designed and then tested to explore the potential of networked microgrids in supporting the main grid's security control actions in the post-contingency control scenario under uncertainties;
- an extended investigation of computation efficiency, optimisation approximation and convex relaxation is conducted. A semi-linearised SCOPF is proposed that could be computed fast without the loss of power system physical limitations; and
- finally, an efficient framework that could be applied to non-convex optimisation problems using distributed dual gradient algorithm is proposed to further alleviate the computation burden and to achieve better convergence.

1.3 Thesis Outline

Following this general introduction, this thesis is divided into the following chapters, including individual brief introductions.

Chapter 2 studies **the impact of renewable generation on the steady state** in the operation stage, in terms of an optimal dispatch decision-making process on an hourly basis. **It then introduces a framework to implement security requirements with uncertainties for hourly operation,** following a brief introduction of power flow modelling and optimal power flow models. Different approaches for accounting for uncertainties caused by random variables are carefully examined. Finally, after analysing various approaches, the chapter presents a new efficient approach to address the uncertain factors caused by load demand and renewable generation in power systems via a robust SCOPF model.

Chapter 3 studies **meshed ac and HVDC grid** connecting large-scale offshore wind farms in the scope of SCOPF. It provides background information on HVDC systems and proposes a hierarchical SCOPF model for a meshed ac/multi-terminal HVDC (MTDC) system with high wind penetration.

In **Chapter 4 multiple microgrids** are investigated in supporting main grid's security control. The chapter provides a detailed comparison of preventive control and corrective control in contingency control strategies. An incentive-based mechanism is designed to encourage the microgrids to actively cooperate with the main grid for post-contingency recovery.

Chapter 5 addresses **the computation efficiency and convergence analysis**. It describes concerns with regard to the computation efficiency and convergence in solving the SCOPF and analyses approaches used in proposed models. Furthermore, a double smoothing technique is introduced to improve the convergence performance in distributed optimisation in the DSM.

Chapter 6 presents **conclusion and outlook** draws the conclusion of this thesis and provides some information on future research possibilities.

Chapter 7 comprises the **list of publications.**

Chapter 2

Integration of Renewable Energy Source into Optimal Generation Dispatch

This chapter introduces an efficient framework to address both uncertain factors caused by load and renewable generation as well as security considerations in electricity network operations. To this end, the chapter first introduces the basic optimal power flow (OPF) principles by formulating a nonlinear optimisation problem and then simplifying it into a linearised OPF problem. Based on this, the chapter then introduces and compares various approaches to integrate random renewable sources generation into the OPF problem. Finally, it presents a robust SCOPF model [18], which consists of two steps. First, a robust OPF is realised through a minimum number of uncertainty scenarios selected from the Taguchi orthogonal array testing (TOAT) [19] method. Then, the security constraints are incorporated into the robust OPF using Benders Decomposition (BD) [20]. The obtained solution is robust against uncertain load and wind generation and secure against contingencies. The numerical simulation demonstrates the solution's effectiveness in accommodating RESs in hourly system operations. This chapter is based on [21].

2.1 Introduction

The challenges of integrating renewable generation sources into the electricity network operation exist at all different levels and in a range of time frames. The incorporation of renewable resources would significantly alter the traditional approach of economic dispatch. Moreover, the variability of renewable resources would require measures to accommodate fast generation changes. Although no short term marginal costs are associated with RESs, increased operational costs by utilizing other components in the grid to compensate for the

resources' intermittent nature would be incurred and need to be accounted for in the operation optimisation.

OPF determines the optimal control variables of a power system with regard to a predefined objective function and certain constraints [22]. The core of the economically efficient and reliable electricity network operation relies heavily on the OPF problem. The mathematical formulation of OPF was initially introduced in the 1960s [23] and was considered to be difficult to solve. The problem is complex economically, electrically and computationally. The development of the OPF has significantly benefited from the evolution of optimisation theory and computing technologies; an overview of the development can be found in [24] and [25].

Traditionally, the OPF problem only considers static physical and operating limits as the constraints. To protect the system against credible contingencies, however, there is an increasing interest in and necessity to take into account the security constraints corresponding to degraded conditions in the OPF, thus yielding SCOPF problems. The system therefore, gains immunity to the contingencies with a reasonable sacrifice of operation cost.

In recent years, with the increasing penetration of RESs, such as wind power, the system operating state tends to be more volatile and uncertain. Traditional deterministic SCOPF is able to determine the control variables of the system given information about load and non-controllable generation. However, given the intermittent nature of renewables, even with a highly accurate prediction of load and renewable resources, the solution of traditional deterministic SCOPF may not be valid, which may lead to overflows or even system failure should the contingency in fact occur. Therefore, SCOPF that is capable of adapting to uncertainties caused by the random load and renewable power injections has become considerably important for maintaining system reliability.

2.2 Optimal Power Flow Formulation

2.2.1 General Form of the Optimal Problem

The OPF problem is an optimisation problem, whose general form is given as follows,

$$\underset{u}{\text{minimise}}$$

$$f(\mathbf{x},\mathbf{u}) \tag{2.1}$$

subject to

$$h(\mathbf{x},\mathbf{u}) = 0 \tag{2.2}$$

$$g(\mathbf{x},\mathbf{u}) \leq 0. \tag{2.3}$$

Equation (2.1) is the objective function, where $\mathbf{x}$ denotes a n_x by 1 state vector, while $\mathbf{u}$ denotes the control vector in the size of n_u by 1 control variable. Equation (2.2) represents the equality constraints, and (2.3) the inequality constraints, which restrict the optimal solution space. Normally, a variable vector $\mathbf{z}$ can be defined to denote the combined variables of state variables $\mathbf{x}$ and control variables $\mathbf{u}$ with the length of n_z shown below:

$$\mathbf{z} = \begin{bmatrix} \mathbf{x} \\ \mathbf{u} \end{bmatrix} \tag{2.4}$$

2.2.2 Nonlinear Optimal Power Flow Formulation

Nonlinear OPF is also known as alternating current OPF(ACOPF), as it considers constraints on the variables related to the reactive power and voltages. This section first briefly introduced ac power flow, followed by the objective function, control variables, and state variables.

Ac power flow modeling

The power flow problem is a steady state computation problem of voltage magnitude and phase angle at each bus in a given power system network. Detailed modeling of the ac system can be found in [26]. Here, the unified nodal power and power flow equations are given as follows,

$$p_i = V_i \sum_{j=1}^{n_b} V_j(g_{ij}\cos(\theta_i - \theta_j) + b_{ij}\sin(\theta_i - \theta_j)) \tag{2.5}$$

$$q_i = V_i \sum_{j=1}^{n_b} V_j(g_{ij}\sin(\theta_i - \theta_j) - b_{ij}\cos(\theta_i - \theta_j)) \tag{2.6}$$

$$\begin{aligned} p_{ij} =& (tr_{ij}V_i)^2 g_{ij} - (tr_{ij}V_i)(tr_{ji}V_j g_{ij})\cos(\theta_{ij} + \varphi_{ij} - \varphi_{ji}) \\ & - (tr_{ij}V_i)(tr_{ji}V_j)b_{ij}\sin(\theta_{ij} + \varphi_{ij} - \varphi_{ji}) \end{aligned} \tag{2.7}$$

$$\begin{aligned} q_{ij} =& (tr_{ij}V_i)^2 (b_{ij} + b_{ij}^{sh}) - (tr_{ij}V_i)(tr_{ji}V_j g_{ij})\sin(\theta_{ij} + \varphi_{ij} - \varphi_{ji}) \\ & + (tr_{ij}V_i)(tr_{ji}V_j)b_{ij}\cos(\theta_{ij} + \varphi_{ij} - \varphi_{ji}) \end{aligned} \tag{2.8}$$

p_i and q_i are the real power and reactive power injections on the node i, while p_{ij} and q_{ij} denote the real and reactive power flows from bus i and bus j. The system series conductance, the series susceptance and the shunt susceptance between node i and node j are denoted by g_{ij}, b_{ij} and b_{ij}^{sh} respectively, while voltage angle difference and voltage angle shift between node i and j are denoted by θ_{ij} and φ_{ij} respectively. V_i, V_j are the voltage magnitudes of node i and j. Finally, t_{ij} is the controllable tap setting for tap changing transformers between nodes i and j.

Objective Function

Various objective functions could be formulated to achieve different goals, including minimising generation cost, losses, total generation, and maximising market surplus. Some examples are given in this section. The most widely used objective function for economical dispatching is to minimise the generation cost, which is closely related to the cost coefficients of each generator. The form of the objective function is normally in a quadratic model, shown below:

$$\underset{u}{\text{minimise}}\ f(\mathbf{x}, \mathbf{u}) \tag{2.9}$$

where

$$f(\mathbf{x}, \mathbf{u}) = \sum_{i=1}^{n_g} (a_i p_{g,i}^2 + b_i p_{g,i} + c_i) \tag{2.10}$$

To minimise the generation cost, the algorithm could minimise the quadratic cost model in (2.10), where a_i, b_i and c_i are the quadratic, linear and constant cost coefficients for generator i respectively. Therefore, (2.10) is normally the cost of conventional generators whose generation costs are the reflection of the fuel costs. While renewable generation is normally considered to have very low marginal costs, these costs are not considered in (2.10). Another cost function that is commonly adopted is shown in (2.11), which minimises the total losses.

$$f(\mathbf{x},\mathbf{u}) = \sum_{i=1}^{n_l}\sum_{j=1}^{n_l} g_{ij}(V_i^2 + V_j^2 - 2V_iV_j\cos(\theta_i - \theta_j)) \tag{2.11}$$

A similar approach to (2.11) is shown in (2.12), which minimises the total generation in the grid, leading to the minimum overall losses.

$$f(\mathbf{x},\mathbf{u}) = \sum_{i=1}^{n_g} p_{g,i} \tag{2.12}$$

Moreover, recent interests in regulating the voltage profile in the electricity network could also be achieved by reducing the difference between all of the node voltages to a predefined profile, for instance 1 p.u., as shown below,

$$f(\mathbf{x},\mathbf{u}) = \sum_{i=1}^{n_b}(V_i - V_{def,i})^2 \tag{2.13}$$

or

$$f(\mathbf{x},\mathbf{u}) = \sum_{i=1}^{n_b}(V_i - 1)^2 \tag{2.14}$$

Noticeably, the objective function of the OPF is variable and flexible. It could be an equation of control variables such as $p_{g,i}$ in (2.10), a function of the state variable V_i in (2.13), or a function of both as in (2.11). Therefore, before the chapter proceeds to the constraint, the state and control variables are defined in the next section.

Variables

The state variable vector $\mathbf{x}$ and the control variable vector $\mathbf{u}$ in the ACOPF problem can be normally defined as follows, and the parameters can vary depending on the operation model

and market decisions.

$$\mathbf{u} = [\mathbf{p}^{\mathbf{T}}, \mathbf{q}^{\mathbf{T}}, \mathbf{tr}^{\mathbf{T}}, \varphi^{\mathbf{T}}]^{\mathbf{T}} \tag{2.15}$$

Control variable vector $\mathbf{u}$ contains variables that can be controlled and alternated by the system operators. In general, the control variables can be determined to setpoints within their limits so that the objective function can be optimised. The first vector $\mathbf{p}$ in (2.15) includes a few sets of variables of $p_{g,i}\ \forall i = 1,...,n_g$, $p_{oth,i}\ \forall i = 1,...,n_{oth}$. $p_{g,i}$ normally refers to the conventional generator i whose generation setpoint can be determined and managed, while $p_{oth,i}$ refers to any other sources that can be controlled in the electricity network for real power injection, for example $p^{ac}_{vsc,i}$ which denotes the power injection from a voltage source converter [27] to the ac grid. On the other hand, RESs are normally treated as uncontrollable generations with uncertainties, and therefore output from renewable generations is not included in the control variable $\mathbf{u}$. By adopting different approaches, the OPF could be transformed into various types of optimisation problems, which is explained in details later in this chapter. The second vector $\mathbf{q}$ includes $q_{g,i}\ \forall i = 1,...,n_g$, $q_{svc,i}\ \forall i = 1,...,n_{svc}$. $q_{g,i}$, and $q_{oth,i}\ \forall i = 1,...,n_{oth}$, where $q_{g,i}$ refers to all reactive power generation from generators, $q_{svc,i}$ denotes the reactive power compensation from the static var compensators and $q_{oth,i}$ is all other reactive power injection from controllable sources. The third element $\mathbf{tr}$ in vector $\mathbf{u}$ includes all tapping transfers and tap ratios, while the last one φ contains all phase shifting transformers in the network. Their numbers are n_{tap} and n_{pha} respectively.

$$\mathbf{x} = [\mathbf{V}^{\mathbf{T}}, \theta^{\mathbf{T}}]^{\mathbf{T}} \tag{2.16}$$

The state variables of the system include voltage magnitude vector $\mathbf{V}$ and voltage angle θ, where $\mathbf{V}$ includes voltage magnitude $V_i,\ \forall i = 1,...,n_b$ on each bus n_b, and θ has the voltage angle $\theta_i,\ \forall i = 1,...,n_b$ on each bus.

Another set of variables, $\mathbf{r} \subseteq \mathbf{x}$, refers to random variables such as renewable generation $p_{r,i}\ \forall i = 1,...,n_{res}$ and real power and reactive power demand from load $p_{d,i}\ \forall i = 1,...,n_d$ and $q_{d,i}\ \forall i = 1,...,n_d$. For the deterministic OPF formulation, vector $\mathbf{r}$ becomes empty since the renewable energy generation and load can be treated as constant when the uncertainties are neglected. However, the deterministic approach becomes inadequate in handling decision making in an OPF problem with a high penetration of RESs. Therefore, the complete set of variables in this thesis is the following,

$$\mathbf{z} = [\mathbf{x}^\mathbf{T}, \mathbf{u}^\mathbf{T}, \mathbf{r}^\mathbf{T}]^\mathbf{T} \tag{2.17}$$

Constraints

There are two types of constraints in the formulated OPF problem: equality constraints and inequality constraints. The power balance equation is the first equality constraint that must be fulfilled for both real and reactive power balance, normally in the nodal balance equation for each bus $\forall i = 1, ..., n_b$:

$$p_{g,i} - p_{d,i} - p_i + p_{r,i} = 0 \; \forall i = 1, ..., n_b \tag{2.18}$$

$$q_{g,i} - q_{d,i} - q_i + q_{r,i} = 0 \; \forall i = 1, ..., n_b \tag{2.19}$$

It should be noted that all the variables in (2.18) are the power infeed on the bus i. If there is no generator on the bus i, then $p_{g,i} = 0$. Another equality constraint is purely for the purpose of computation, where the reference voltage angle is defined and fixed at the reference value, normally zero, on the slack bus:

$$\theta_{slack} = \theta_{ref} = 0 \tag{2.20}$$

The inequality sets normally correspond to the system operation limits on both control variables and state variables as follows:

$$p_{g,i}^{min} \leq p_{g,i} \leq p_{g,i}^{cap} \quad \forall i = 1, ..., n_g \tag{2.21}$$

$$q_{g,i}^{min} \leq q_{g,i} \leq q_{g,i}^{cap} \quad \forall i = 1, ..., n_g \tag{2.22}$$

$$V_i^{min} \leq V_i \leq V_i^{max} \quad \forall i = 1, ..., n_b \tag{2.23}$$

$$tr_{ij}^{min} \leq tr_{ij} \leq tr_{ij}^{max} \quad \forall i, j = 1, ..., n_b \tag{2.24}$$

$$\varphi_{ij}^{min} \leq \varphi_{ij} \leq \varphi_{ij}^{max} \quad \forall i, j = 1, ..., n_b \tag{2.25}$$

$$p_{ij}^{min} \leq p_{ij} \leq p_{ij}^{cap} \quad \forall i, j = 1, ..., n_b \tag{2.26}$$

$$q_{ij}^{min} \leq q_{ij} \leq q_{ij}^{cap} \quad \forall i, j = 1, ..., n_b \tag{2.27}$$

(2.21) and (2.22) are the inequality constraints on the active power and reactive power output for each generator. (2.24) and (2.25) are the tap ratio limits on the tap changing trans-

formers and phase shifting operation range on the phase shifting transformers respectively. The last two inequality constraints (2.26) and (2.27) are the real and reactive power line flow limits, and normally $p_{ij}^{min} = -p_{ij}^{cap}$, and therefore (2.26) is always written as:

$$-p_{ij}^{cap} \leq p_{ij} \leq p_{ij}^{cap} \quad \forall i, j = 1, ..., n_b \tag{2.28}$$

2.2.3 Linearised Optimal Power Flow

The nonlinear OPF can represent the real system operation, especially when voltage and reactive power are concerned. However, it is nonlinear and non-convex and therefore difficult to solve and heavy in computation. Powerful solvers, Bonmin [28], CPLEX [29], Gurobi [30], IPOPT [31], KNITRO [32], etc., could be applied to solve the nonlinear OPF in an iterative manor, but the iteration might not converge in time and the global optimal is difficult to prove. In contrast, linearised OPF is an approximation of the nonlinear OPF. It is often called dc OPF since it neglects the reactive power from the formulation. Linearised OPF has gained its popularity among system operators for several reasons, among which the most distinct advantage that the linearised OPF can be solved efficiently with solutions that are reliable and non-iterative.

Objective Function, Variables and Constraints

In linearised OPF, objective function such as minimisation of operating cost (2.11) and total generation (2.12) remain the same as in nonlinear OPF. However, since the reactive power is neglected, voltage profile optimisation (2.13) cannot be formulated in dc OPF. With the assumption that the voltage at each node is 1.0 p.u., as well as the elimination of reactive power in the control variable, the number of variables and system complexity are significantly reduced. The variables explicitly become:

$$\mathbf{u} = [\mathbf{p^T}, \boldsymbol{\varphi}^\mathbf{T}]^\mathbf{T} \tag{2.29}$$

$$\mathbf{x} = [\theta] \tag{2.30}$$

Consequently both equality constraints and inequality constraints are modified, and only those associated with the variables in (2.29) and (2.30) remain. The power flow equation (2.7) is also simplified with assumptions, such as that voltage magnitudes are constant at 1.0 p.u., the resistance of transmission line can be neglected, $\sin\theta = \theta$, etc.. It is transformed

into:

$$p_{ij} = -b_{ij}\theta_{ij} \; \forall i, j = 1, 2, ..., n_b \tag{2.31}$$

The detailed process of the linearised power flow is investigated in a sufficient amount of literature -see [33] and [26] and it is therefore omitted in this thesis.

2.2.4 Random Variables and Uncertainties

As discussed in the previous sections, variable vector **r** includes random variables that are caused by determinant renewable source generations and ever changing load demands. When the uncertainties of these random variables are considered, related constraints become equations containing random variables. In this thesis, $\widetilde{\bullet}$ is used to denote random variables. Considering renewable generation uncertainties as well as uncertainties in load demand, in a linearised OPF, constraints (2.18) and (2.26) become probabilistic constraints as follows,

$$p_{g,i} - p_{d,i} - \widetilde{p}_i + \widetilde{p}_{r,i} = 0 \quad \forall i = 1, ..., n_b \tag{2.32}$$

$$p_{ij}^{min} \leq \widetilde{p}_{ij} \leq p_{ij}^{cap} \quad \forall i, j = 1, ..., n_b \tag{2.33}$$

Normally, these uncertainties are captured using the probability density functions (PDF) [34] of the random variables, to obtain probabilistic characteristics. This requires presumptions of the knowledge of PDFs of the random variables, which are sometimes difficult to obtain. Alternatively, robust optimisation offers another method to deal with random variables in the optimisation problems with uncertainties.

2.3 Probability OPF Formulation and Solutions

A dc OPF model that aims to minimise the total cost can be summarised as follows, using the objective function, equality constraints, and inequality constraints described in the previous section:

Objective:

$$minimise \sum_{i=1}^{n_g} (a_i {p_{g,i}}^2 + b_i p_{g,i} + c_i) \tag{2.34}$$

Subject to:

$$\mathbf{p} = \mathbf{B}\theta = \mathbf{p_g} - \mathbf{p_d} + \mathbf{p_r} \tag{2.35}$$

$$\mathbf{p_g}^{min} \leq \mathbf{p_g} \leq \mathbf{p_g}^{cap} \tag{2.36}$$

$$p_{ij}^{min} \leq \frac{\theta_i - \theta_j}{x_{ij}} \leq p_{ij}^{max} \quad \text{or} \quad \mathbf{p_L}^{min} \leq \mathbf{p_L} \leq \mathbf{p_L}^{max} \tag{2.37}$$

Equations (2.35), (2.36) and (2.37) are the constraints (2.18), (2.21) and (2.26) in matrix form. Similarly, by replacing $\mathbf{p_r}, \mathbf{p_d}$ and $\mathbf{p_L}$ with the random variables $\widetilde{\mathbf{p}}_\mathbf{r}, \widetilde{\mathbf{p}}_\mathbf{d}$ and $\widetilde{\mathbf{p}}_\mathbf{L}$, the probabilistic problem is formulated as follows,

Objective:

$$minimise \sum_{i=1}^{n_g} (a_i {p_{g,i}}^2 + b_i p_{g,i} + c_i) \tag{2.38}$$

Subject to:

$$\widetilde{\mathbf{p}} = \mathbf{B}\widetilde{\theta} = \mathbf{p_g} - \widetilde{\mathbf{p}}_\mathbf{d} + \widetilde{\mathbf{p}}_\mathbf{r} \tag{2.39}$$

$$\mathbf{p}_g^{min} \leq \mathbf{p}_g \leq \mathbf{p}_g^{cap} \tag{2.40}$$

$$\mathbf{p}_L^{min} \leq \widetilde{\mathbf{p}}_\mathbf{L} \leq \mathbf{p}_L^{max} \tag{2.41}$$

Comparing the probabilistic formulations (2.38) to (2.41), the deterministic OPF formulations (2.34) to (2.37) take the traditional nonrenewable generation as controllable variable, while the renewables and loads are considered to be uncontrollable factors. The uncertainties within the uncontrollable parameters represents difficulties into the optimisation problem, as the optimised result in one scenario might cause constraint violation in another. A few different approaches are given in the following sections for the solution of OPF with random variables.

2.3.1 Formulation and Solution Methods

Various studies on the OPF problem under uncertainties have been proposed in the literature; they can generally be classified into probabilistic [35–37], stochastic [38, 39], and robust approaches [40, 41], depending on the way of integrating random variables into the problem formulation and computation process. The approaches can also be categorised according to the techniques of realisation of the random variables uncertainties: namely the scenario-based approach and interval optimisation.

In general, probabilistic OPFs target small systems and their solutions are also normally in the form of PDFs, and the system operators therefore need to further analyse these results to generate a short-term operation plan. Due to the stochastic nature of wind generation, stochastic OPF (S-OPF) has been widely used to accommodate uncertainties of both renewables and load in the optimal operation. Similarly to probability OPF (P-OPF), knowledge of PDFs of random variables is required for S-OPF formulation. Various solving techniques have been used in S-OPFs to reduce the computation burden. Chance constraints [39, 42, 43] are often used in S-OPF to study the uncertainties of load and renewables. Robust optimisation [44, 45] has also captured researchers' attention for determining control strategies under uncertainties.

The most significant difference of robust OPF compared to P-OPF or S-OPF is that it only requires the knowledge of the interval of variation of the random variables, but it is able to yield a solution that is robust within an uncertainties range [46, 47]. Moreover, it yields a solution that is immune to the effect of uncertainties within the given range. In terms of selecting solution approaches for formulated problems, the nscenario-based approach is the most straight forward method to uncertainty realisation [48–50]. With the knowledge of the PDFs of the random variables, the scenarios can be generated using sampling methods. The Monte Carlo Simulation (MCS)[51] has been popularly adopted to test scenario generations and is always used as a benchmark for solution accuracy. However, to ensure a full coverage of the probabilities, a large number of scenarios are normally generated, which can cause more computation burden, especially with large power system networks. In contrast, interval optimisation [52, 53] does not require the details of the PDFs of random parameters, and it is usually used in robust optimisation. In spite of having these merits, however, interval optimisation is argued to be conservative in certain circumstance. An overly wide confidence interval could lead to a narrowed solution region, resulting in the waste of system resources and losses of economic efficiency. On the other hand, an overly narrowed interval could lose the ability to represent significant probabilities.

Scenario-based Approach

The scenario-based OPF model aims to determine the optimal dispatch value of conventional generators to minimise the expected operation cost including operation cost and the penalties expected on an hourly basis caused by uncertainties brought by intermittent renewable generation and random load. The scheduled dispatch plan should allow the system to adjust from the previous state to any new state without violating any network constraints.

The Weibull probability distribution is well known for describing the distribution of wind velocity, while a normal distribution is normally used to describe photovoltaics energy generation. A large number of scenarios are ususally required for the selected samples to fully represent the probability distribution of the random variables. Each scenario is then associated with a probability whose total is one. Due to the large number of scenarios, the computation burden is normally high. Therefore, scenario reduction methods [54, 55] are usually applied in the scenario selection process.

By introducing the scenario-based S-OPF, the uncertainties of the renewable generation can be realised into n_s scenarios, where each scenario is assigned a probability equal to $\rho^s = 1/n_s \forall i = 1,2,...,n_s$. In addition, a number of n_s constraints associated with each scenario are added to the problem for uncertainties control, so that the optimised result can be valid under any probable wind generation. In this case, the number of variables is increased by n_s times, and so is the number of constraints. Therefore, the objective function of the P-OPF model adopting a scenario-based approach that aims to minimise the total operation cost can be expressed as:

$$f(\mathbf{x},\mathbf{u}) = \sum_{i=1}^{n_g}(a_i p_{g,i}^2 + b_i p_{g,i} + c_i) + \sum_{i=1}^{n_g}\sum_{s=1}^{n_s}\rho^s(p_{g,i} - p_{g,i}^s)^2 \tag{2.42}$$

and new constraint sets are created for each studied scenario n_s based on (2.35) to (2.37):

$$\mathbf{p} = \mathbf{p_g}^s - \mathbf{p_d}^s + \mathbf{p_r}^s \tag{2.43}$$

$$\mathbf{p_g}^{min} \leq \mathbf{p_g}^s \leq \mathbf{p_g}^{cap} \tag{2.44}$$

$$\mathbf{p_L}^{min} \leq \mathbf{p_L}^s \leq \mathbf{p_L}^{max} \tag{2.45}$$

$$\left|\mathbf{p_g}^s - \mathbf{p_g}\right| \leq \mathbf{p_g}^{s,max} \tag{2.46}$$

where the new constraint set (2.46) is the coupling constraint to prevent unrealistic movement of controllable generation in each scenario, and $\mathbf{p_g}^{s,max}$ is the vector defining maximum allowed adjustment of the control variables between the base case and all generated scenarios

in the allowed duration. It is clear that the scenario-based approach dramatically increases problem size and leads to long computation time, which makes it less suitable for frequency OPF computation.

Interval-based Approach

The interval optimisation approach is another way to deal with uncertainties. Unlike the scenario-based approach, interval optimisation does not need explicit PDFs of random variables. Instead, it selects the optimal intervals to represent the random variables so that the optimisation result can be valid with uncertainty to some extent. Another significant difference is that in the interval-based approach, the cost raised by uncertain wind generation is not applied to the objective function in the form of penalty costs. Instead, the uncertainty is embodied in the operation cost interval and reflected in the increased operation cost. This implies that the model based on the interval optimisation usually exhausts all available RES instead of locating an optimally scheduled value. The problem derives the power confidence interval on the power generation control variables, in this case $[p_{g,i}^{-}, p_{g,i}^{+}]$, and its corresponding cost interval$[\sum_{i=1}^{n_g}(a_i(p_{g,i}^{-})^2+b_i p_{g,i}^{-}+c_i), \sum_{i=1}^{n_g}(a_i(p_{g,i}^{+})^2+b_i p_{g,i}^{+}+c_i)]$, according to the interval of renewable generation $[p_{r,i}^{-}, p_{r,i}^{+}]$. The unique feature of the interval optimisation is that it uses confidence interval numbers to describe uncertainty, without any presumptions on PDFs, and derives optimistic and pessimistic solutions to satisfy the operational and economic requirements of power systems. Therefore, the objective function of the interval-based OPF model can be expressed as:

$$f(\mathbf{x},\mathbf{u}) = \sum_{i=1}^{n_g}(a_i(p_{g,i}^{\pm})^2 + b_i p_{g,i}^{\pm} + c_i) \tag{2.47}$$

and new constraint sets are created for each studied scenario n_s based on (2.35) to (2.37):

$$\mathbf{p} = \mathbf{p_g}^{\pm} - \mathbf{p_d}^{\pm} + \mathbf{p_r}^{\pm} \tag{2.48}$$

$$\mathbf{p_g}^{min} \leq \mathbf{p_g}^{\pm} \leq \mathbf{p_g}^{cap} \tag{2.49}$$

$$\mathbf{p_L}^{min} \leq \mathbf{p_L}^{\pm} \leq \mathbf{p_L}^{max} \tag{2.50}$$

$$\mathbf{p_r}^{\pm} \in [\mathbf{p_r}^{-}, \mathbf{p_r}^{+}] \tag{2.51}$$

from (2.47) to (2.51), the optimised cost is closely related to $[p_{g,i}^{-}, p_{g,i}^{+}]$, which is the confidence interval derived from given information in (2.51). The derivation of the representative interval on $P_{g,i}$ can be subjective and difficult. Moreover, the optimised results tend to have more value in analysis than in decision-making.

2.4 Security Constrained OPF

Contingencies are inevitable in electricity grid operations. Without appropriate control actions, these contingencies may result in catastrophic consequences such as cascading failures and/or widespread blackouts. In general, the security control strategies can fall into the preventive control (PC) and corrective control (CC) categories.

2.4.1 Security Constrained OPF General Form

The general optimisation problem (2.1) to (2.3) is transformed into SCOPF by adding variables and constraints for contingencies.

$$\underset{u}{\text{minimise}}$$

$$f(\mathbf{x_0}, \mathbf{u_0}) \tag{2.52}$$

subject to

$$h_k(\mathbf{x_k}, \mathbf{u_k}) = 0 \quad k = 0, 1, ...n_k \tag{2.53}$$

$$g_k(\mathbf{x_k}, \mathbf{u_k}) \leq 0 \quad k = 0, 1, ...n_k \tag{2.54}$$

$$|\mathbf{u_k} - \mathbf{u_0}| \leq \Delta\mathbf{u_k} \quad k = 0, 1, ...n_k \tag{2.55}$$

The index $k = 0$ indicates that this problem is posed for the pre-contingency condition,while $k > 0$ corresponds to the post-contingency states. Although the objective function remains to minimise the operation cost only involving controllable generators, a complete new set of equality constraints (2.53) and inequality constraints (2.54) for $\forall k = 1, 2, ..., n_k$ is created. In addition, equality constraint set (2.55) is created to couple variables at the pre-contingency($k = 0$) state with post-contingency($k > 0$) states.

2.4.2 Preventive Control versus Corrective Control

The security control strategies can generally fall into the PC and CC categories. PC involves preparing a system operating state that is able to withstand a set of credible but not yet occurring contingencies. The instantaneous cost of PC is relatively low, but its aggregate cost over the long term can be considerable. In contrast, CC seeks to recovery actions after a fault back to a normal state, and its actions include post-contingency generation rescheduling and load/generation shedding. The instantaneous cost of CC can be high, but its long-term cost is relatively low, due to the fact that contingencies are high impact/low probability

events. Mathematically,the difference between PC and CC remains in the allowed deviation of control variable **x** between pre-contingency states and post-contingency states. The PC SCOPF and CC SCOPF are formulated as follows, PC SCOPF:

$$\underset{u}{\text{minimise}}$$

$$f(\mathbf{x_0}, \mathbf{u_0}) \tag{2.56}$$

subject to

$$h_k(\mathbf{x_k}, \mathbf{u_0}) = 0 \quad k = 0, 1, ...n_k \tag{2.57}$$

$$g_k(\mathbf{x_k}, \mathbf{u_0}) \leq 0 \quad k = 0, 1, ...n_k \tag{2.58}$$

CC SCOPF:

$$\underset{u}{\text{minimise}}$$

$$f(\mathbf{x_0}, \mathbf{u_0}) \tag{2.59}$$

subject to

$$h_0(\mathbf{x_0}, \mathbf{u_0}) = 0 \tag{2.60}$$

$$g_0(\mathbf{x_0}, \mathbf{u_0}) \leq 0 \tag{2.61}$$

$$h_k(\mathbf{x_k}, \mathbf{u_k}) = 0 \quad k = 1, ...n_k \tag{2.62}$$

$$g_k(\mathbf{x_k}, \mathbf{u_k}) \leq 0 \quad k = 1, ...n_k \tag{2.63}$$

$$|\mathbf{u_k} - \mathbf{u_0}| \leq \Delta\mathbf{u_k} \quad k = 1, ...n_k \tag{2.64}$$

By comparing (2.56)-(2.63) to (2.59)-(2.64), it is clear that the PC approach has more restrictions on the control variable $\mathbf{u_0}$, which needs to satisfy all constraint sets in both pre- and post-contingency states. In contrast, control variable $\mathbf{u_0}$ only needs to be considered in the pre-contingency state, while a new control variable $\mathbf{u_k}$ is created for each contingency k for the post-contingency action, provided that it is coupled with $\mathbf{u_0}$ by (2.64). Since the cost only concerns $\mathbf{x_0}, \mathbf{u_0}$, CC SCOPF (2.59)-(2.64) normally results in a lower operation cost.

2.4.3 Improved Combined Control Strategy

Both formulations in (2.56)-(2.63) and (2.59)-(2.64) only consider the operation cost for the pre-contingency state, neglecting the cost associated with corrective actions, such as generation redispatch in CC. There are two major drawbacks to these formulations. First, mathematically, since the decision variable $\mathbf{u_k}$ is not included in the objective function, multiple sets of solutions might exist. Economically, the optimal solution from SCOPF (2.59)-

(2.64) might result in a considerable cost for post-contingency control actions. Therefore, it is crucial to incorporate the cost associated with corrective actions into the objective function, and a mixed preventive- and post-contingency control SCOPF is formulated as follows to achieve a minimised overall operation cost,

$$\underset{u}{\text{minimise}}$$

$$f(\mathbf{x},\mathbf{u}) - f(\hat{\mathbf{x}},\hat{\mathbf{u}}) + \sum_{k=1}^{n_k} \rho^k C_k(\mathbf{x},\mathbf{u}) \tag{2.65}$$

subject to

$$h_0(\mathbf{x},\mathbf{u}) = 0 \tag{2.66}$$

$$g_0(\mathbf{x},\mathbf{u}) \leq 0 \tag{2.67}$$

$$h_k(\mathbf{x_k},\mathbf{u_k}) = 0 \quad k = 1,...n_k \tag{2.68}$$

$$g_k(\mathbf{x_k},\mathbf{u_k}) \leq 0 \quad k = 1,...n_k \tag{2.69}$$

$$|\mathbf{u_k} - \mathbf{u}| \leq \Delta\mathbf{u_k} \quad k = 1,...n_k \tag{2.70}$$

The objective function (2.65) has two parts: the first element $f(\mathbf{x},\mathbf{u}) - f(\hat{\mathbf{x}},\hat{\mathbf{u}})$ measures the cost imposed by modified PC actions, while the other element $\sum_{k=1}^{n_k} \rho^k C_k(\mathbf{x},\mathbf{u})$ is the sum of CC costs. It is noticeable that $\mathbf{x_0}$ and $\mathbf{u_0}$ are replaced, since there is no longer a purely preventive control action. Instead, $\mathbf{x}$ and $\mathbf{u}$ are the variable for calculating the operation cost, which is adjusted in a hybrid way considering both CC and PC actions. $\hat{\mathbf{x}},\hat{\mathbf{u}}$ represents the optimal operating state determined by a conventional OPF solution without security considerations. ρ_k corresponds to the probability of the contingency k and $C_k(\mathbf{x},\mathbf{u})$ is the CC cost function of the contingency for the operating point $\mathbf{x},\mathbf{u}$, normally modeled as a quadratic function of deviation on controllable variables, taking generation difference as an example:

$$C_k(\mathbf{x},\mathbf{u}) = \sum_{i=1}^{n_g} \alpha_{g,i}(p_{g,i} - p_{g,i}^k)^2 \tag{2.71}$$

$\Delta\mathbf{u_k}$ is the vector defining maximal allowed adjustment of the control variables between the pre-contingency and the post-contingency state. Taking generation redispatch as an example for corrective generation rescheduling, $\Delta\mathbf{u_k}$ is the generation ramping rate in response to contingency k in the allowed time.

2.5 Robust Security Constrained Optimal Power Flow Formulation and Solving Method

Traditional deterministic SCOPF introduced in section2.4 is able to determine the control variables of the system given information on load and non-controllable generation. However, given the intermittent nature of renewables, even with a highly accurate prediction of load and renewable resources, the solution of traditional deterministic SCOPF may not be valid. Therefore, a SCOPF that is capable of adapting to uncertainties caused by the random load and renewable power injections has become considerably important for maintaining system reliability. However, the work that has been done to incorporate the uncertainties into SCOPF is limited. The major difficulty lies in a huge problem size caused by the combination of the contingencies and variable uncertainties. After the introduction of P-OPF and SCOPF in sections2.3 and 2.4 respectively, the complexity of the SCOPF under uncertainties could be foreseen. Therefore, this section introduces a new efficient approach to address the uncertain factors caused by load demand and renewable generation in the power system, via a robust SCOPF model. The presented robust SCOPF algorithm is not only capable of satisfying the security requirements, but is also robust against uncertain renewable generation output and load demand. To get a balance between representativeness, economic efficiency and computation efficiency, a combination of scenario-based and interval-based optimisation method is used. This is achieved by adding the uncertainties directly back to the OPF problem using TOAT for selecting a minimum number of representative uncertainty scenarios. Moreover, security requirements are checked and satisfied by the using PC, to fortify the reliability of the network. The BD technique is employed to convert the original optimisation problem into a master problem corresponding to a base operation case and N sub-problems each representing contingency scenarios. Finally the modified robust SCOPF can be seen as a deterministic equivalent OPF model that considers the uncertainty and security with high scalability.

2.5.1 Robust Constraint Formulation using the Taguchi Orthogonal Array Testing Technique

In the OPF formulation, the traditional nonrenewable generation is taken as controllable variable, and the renewables and loads are considered as uncontrollable factors. The uncertainties within the uncontrollable parameters represent difficulties in the optimisation problem, as the optimised result in one scenario might cause constraint violation in another. The presented robust OPF problem aims to minimise the cost of all conventional generation with the load

and renewable generation of the largest probability to appear, and the optimised result is robust against all other probabilities that are caused by uncertainties of renewables and loads. Here the TOAT is adopted for the derivation of the modified OPF constraints, so that the uncertainties of the uncontrollable parameters are reflected in the optimisation problem as a narrowed feasible region of the controllable variables. In this study, the loads are modelled as a normal distribution, and the renewables' intermittent power output varies from zero to their capacities. Inherit the P-OPF formulated in (2.38) to (2.41). The dc power flow model can also describe the changes of the branches flows due to changes of the nodal real power injections by using injection shift factors [56]. When the sensitivities are organised into n_l by n_b matrices, matrices called power transfer distribution factors (PTDFs) can be achieved, which are denoted as H. The element in row i and column j, denoted as h_{ij} , represents the changes of real power flow on branch i caused by the changes in the real power injection on node j. Therefore for branch L in the matrix form:

$$\Delta\widetilde{\mathbf{p}}_L = H\Delta\widetilde{\mathbf{p}} \tag{2.72}$$

and,

$$\widetilde{\mathbf{p}}_L = H\tilde{\mathbf{p}} \tag{2.73}$$

Substituting (2.39) into (2.73),

$$\tilde{\mathbf{p}}_L = H(\mathbf{p}_g - \tilde{\mathbf{p}}_d + \tilde{\mathbf{p}}_r) \tag{2.74}$$

Now substituting (2.74) into (2.41), the constraints for control variable $\mathbf{p}_g$ that include the uncertainties can be described as follows:

$$-\mathbf{p}_L^{max} - H\tilde{\mathbf{p}}_r + H\tilde{\mathbf{p}}_d \leq H\mathbf{p}_g \leq \mathbf{p}_L^{max} - H\tilde{\mathbf{p}}_r + H\tilde{\mathbf{p}}_d \tag{2.75}$$

The above constraint (2.75) is a probabilistic constraint since the uncertain variables $\tilde{\mathbf{p}}_r$ and $\tilde{\mathbf{p}}_d$ are included. The aim is to transfer this probabilistic constraint into an equivalent deterministic constraint that is easy to solve and also guarantees a solution that is robust against uncertainties caused by the random load and renewable power injections.

TOAT Application and Uncertainty Aggregation

The transformation of constraints for the active power line flow limit provides a starting point for the robust operation formulation. As discussed in the previous section, the goal here is

to transform this probabilistic constraint (2.75) into a deterministic equation. There are two reasons for this:

- The first reason, as previously mentioned, is that the equivalent deterministic constraint is easy to solve and also guarantees a solution that is robust against uncertainties caused by the random load and renewable power injections.
- The second reason is that this approach can be well incorporated into the decomposition technique well, which is used later for security constraints formulation.

Given a system $\mathbf{Z}$ that is depicted by $\mathbf{z} = \mathbf{Z}(\mathbf{u}, \tilde{\mathbf{r}})$, where $\mathbf{u} = [u_1, u_2, ...u_{n_u}]$, are n_u controllable factors and $\tilde{\mathbf{r}} = [\tilde{r}_1, \tilde{r}_2, ..., \tilde{r}_{n_{rad}}]$ are n_{rad} uncontrollable uncertain factors. By optimising the controllable factors $\mathbf{u}$ in such a way that the system Z can be immune to the uncertainties caused by vector $\mathbf{r}$, roust formulation can be achieved. The uncertain variations of $\mathbf{r}$ can be represented by a series of scenarios. Since it is impractical to consider all possible scenarios, only the most representative scenarios are selected to guide the optimisation.

To represent a full operation state of random variable $\tilde{r}_i = \tilde{r}_1, \tilde{r}_2, ..., \tilde{r}_{n_{rand}}$, assuming that each random variable $\tilde{r}_i$ can be represented by M levels, a total number of combinations $M^{n_{rand}}$ is generated. This is still of a large size and computationally expensive. Therefore, TOAT is adopted for scenario selection. Specifically, for a given problem, once the number of uncertainty parameters and representative level are determined, an orthogonal array (OA) that contains a number of testing scenarios, can be selected from the OA library. These testing scenarios from the OA library are proven to be uniformly distributed over the uncertain operating space. An OA can normally be expressed in the form of $L_S(M^{n_{rand}})$, meaning that this experiment testing has $n_r and$ variables at M different settings. By searching in the OA library, the number of tests can then be determined. For example, given a system with $n_{rand} = 4$ random variables x1, x2, x3 and x4 at $M = 3$ different levels, a full factorial testing would require $3^4 = 81$ experiments. However, based on the OA library, only 9 testing experiments can be used from $L_9(3^4)$ array to represent the whole space, where xi(m) denotes value for the level m random xi in table 2.1:

For a given problem $\mathbf{Z}$, the appropriate OA is determined from OA libraries according to the following two considerations: number of random variables $n_{rand}$and the level M for each random variable $\tilde{r}_i$.

1. **Number of random variables** n_{rand} is easy to determine. However, since the number of experiments exponentially increases with n_{rand}, a lower number of random variables is preferred. Therefore, the aggregation rule [57] for normally distributed random variables and deterministic variables is given to reduce the total number of random variables.

Table 2.1 $L_9(3^4)$ OA Array

Experiment number	Random variable x1	Random variable x2	Random variable x3	Random variable x4
1	x1(1)	x2(1)	x3(1)	x4(1)
2	x1(1)	x2(2)	x3(2)	x4(2)
3	x1(1)	x2(3)	x3(3)	x4(3)
4	x1(2)	x2(1)	x3(2)	x4(3)
5	x1(2)	x2(2)	x3(3)	x4(1)
6	x1(2)	x2(3)	x3(1)	x4(2)
7	x1(3)	x2(1)	x3(3)	x4(2)
8	x1(3)	x2(2)	x3(1)	x4(3)
9	x1(3)	x2(3)	x3(2)	x4(1)

(a) If a random variable $\tilde{r}_i$ is normally distributed with mean $\mu(\tilde{r}_i)$ and variance $\sigma^2(\tilde{r}_i)$, then a linear transformation $\tilde{r}' = a\tilde{r}_i + b$ is still a normal distribution with mean $a\mu(\tilde{r}_i) + b$ and variance $a^2\sigma^2(\tilde{r}_i)$.

(b) If another random variable $\tilde{r}_j$ is normally distributed with mean $\mu(\tilde{r}_j)$ and variance $\sigma^2(\tilde{r}_j)$,then a linear transformation $\tilde{r}'' = a_1\tilde{r}_i + a_2\tilde{r}_j$ is still a normal distribution with mean $a_1\mu(\tilde{r}_i) + a_2\mu(\tilde{r}_j)$ and variance $a_1^2\sigma^2(\tilde{r}_i) + a_2^2\sigma^2(\tilde{r}_j)$.

2. **Number of levels M for each random variable**. When designing testing experiments for the studied system $\mathbf{Z}$, the number of levels M for each random variable $\tilde{r}_i$ and the value at each level need to be properly defined, so that the selected testing experiments can cover the random space. Normally, if a random variable $\tilde{r}_i$ has a quadratic effect on $\mathbf{Z}$, then $M = 3$ levels are selected for $\tilde{r}_i$, and the corresponding values for these levels are $\mu(\tilde{r}_i) - \sqrt{3/2}\sigma(\tilde{r}_i)$, $\mu(\tilde{r}_i) + \sqrt{3/2}\sigma(\tilde{r}_i)$, and $\mu(\tilde{r}_i)$ provided that $\tilde{r}_i$ is symmetrically distributed. Moreover, if a random variable $\tilde{r}_i$ has a linear relation on $\mathbf{Z}$, then $M = 23$ levels are selected for $\tilde{r}_i$, and the corresponding value for these levels are $\mu(\tilde{r}_i) - \sigma(\tilde{r}_i)$, $\mu(\tilde{r}_i) + \sigma(\tilde{r}_i)$, provided that $\tilde{r}_i$ is symmetrically distributed.

Transformation of Probabilistic Constraint by TOAT

Now looking back at (2.75), it is clear that both random variable vector $\tilde{\mathbf{p}}_d$ and $\tilde{\mathbf{p}}_r$ have a linear effect on (2.75). Therefore two levels are selected for $\tilde{\mathbf{p}}_d$ and $\tilde{\mathbf{p}}_r$. By eliminating zero elements in $\mathbf{p}_g$, $\tilde{\mathbf{p}}_d$ and $\tilde{\mathbf{p}}_r$, the equation (2.75) can be transformed into:

$$
\begin{aligned}
&-\begin{bmatrix} p_{L,1}^{max} \\ p_{L,2}^{max} \\ \vdots \\ p_{L,n_l}^{max} \end{bmatrix} - H_R \begin{bmatrix} \tilde{p}_{r,1} \\ \tilde{p}_{r,2} \\ \vdots \\ \tilde{p}_{r,n_r} \end{bmatrix} + H_D \begin{bmatrix} \tilde{p}_{d,1} \\ \tilde{p}_{d,2} \\ \vdots \\ \tilde{p}_{d,n_d} \end{bmatrix} \leq H_G \begin{bmatrix} p_{g,1} \\ p_{g,2} \\ \vdots \\ p_{g,n_g} \end{bmatrix} \\
&\leq \begin{bmatrix} p_{L,1}^{max} \\ p_{L,2}^{max} \\ \vdots \\ p_{L,n_l}^{max} \end{bmatrix} - H_R \begin{bmatrix} \tilde{p}_{r,1} \\ \tilde{p}_{r,2} \\ \vdots \\ \tilde{p}_{r,n_r} \end{bmatrix} + H_D \begin{bmatrix} \tilde{p}_{d,1} \\ \tilde{p}_{d,2} \\ \vdots \\ \tilde{p}_{d,n_d} \end{bmatrix}
\end{aligned} \tag{2.76}
$$

where H_R, H_D and H_G are the selected columns from PTDFs that correspond to the non-zero element of $\tilde{\mathbf{p}}_d$, $\tilde{\mathbf{p}}_r$ and $\mathbf{p}_g$. Therefore, H_R, H_D and H_G have the same number of rows but different number of columns. If the constraint for the $l_t h$ line is considered using the newly formulated equitation 2.76, then:

$$
\begin{aligned}
&-p_{L,l}^{max} - h_r^{l,1}\tilde{p}_{r,1} - \cdots - h_r^{l,n_r}\tilde{p}_{r,n_r} + h_d^{l,1}\tilde{p}_{d,1} + \cdots + h_d^{l,n_d}\tilde{p}_{d,n_d} \\
&\leq h_g^{l,1}p_{g1} + h_g^{l,2}p_{g,2} + \cdots + h_g^{l,n_g}p_{g,n_g} \\
&\leq p_{L,l}^{max} - h_r^{l,1}\tilde{p}_{r,1} - \cdots - h_r^{l,n_r}\tilde{p}_{rn_r} + h_d^{l,1}\tilde{p}_{d,1} + \cdots + h_d^{l,n_d}\widetilde{p}_{d,n_d}
\end{aligned} \tag{2.77}
$$

where $h_r^{i,1}, h_r^{i,2}, \cdots, h_r^{i,n_r}$, $h_d^{i,1}, h_d^{i,2}, \cdots, h_d^{i,n_d}$ and $h_g^{i,1}, h_g^{i,2}, \cdots, h_g^{i,n_g}$ are the elements in the ith row of H_R, H_D and H_G respectively. Applying the linear aggregation rule for normally distributed variables earlier since the load is considered to be normally distributed, here the variables $\tilde{P}_{a,l}^{min}$ and $\tilde{P}_{a,l}^{max}$ are introduced and used to describe the aggregation for the normally distributed load with PTDF transformation of branch $l = 1, 2, ..., n_l$. The equations are the followings,

$$
\tilde{P}_{a,l}^{min} = -p_{L,l}^{max} + h_d^{l,1}\tilde{p}_{d,1} + \cdots + h_d^{l,n_d}\tilde{p}_{d,n_d}, \forall l = 1, 2, ..., n_l \tag{2.78}
$$

$$
\tilde{P}_{a,l}^{max} = p_{L,l}^{max} + h_d^{l,1}\tilde{p}_{d,1} + \cdots + h_d^{l,n_d}\tilde{p}_{d,n_d}, \forall l = 1, 2, ..., n_l \tag{2.79}
$$

Therefore, according to the linear aggregation rule for normally distributed variables, $\tilde{P}_{a,l}^{min}$ and $\tilde{P}_{a,l}^{max}$ are also normally distributed. Substituting (2.78) and (2.79) into (2.77) yields:

$$
\begin{aligned}
\tilde{p}_{a,l}^{min} - h_r^{l,1}\tilde{p}_{r,1} - \cdots - h_r^{l,n_r}\tilde{p}_{r,n_r} \leq h_g^{i,1}p_{g,1} + h_g^{l,2}p_{g,2} + \cdots \\
+ h_g^{i,n_g}p_{g,n_g} \leq \tilde{p}_{a,l}^{max} - h_r^{l,1}\tilde{p}_{r,1} - \cdots - h_r^{l,n_r}\tilde{p}_{r,n_r}
\end{aligned} \tag{2.80}
$$

It should be noted that $\tilde{P}_{a,l}^{min}$ and $\tilde{P}_{a,l}^{max}$ are a linear combinations of real power limitation of branch l and the line flow associated with all of the loads. This transformation effectively reduces the number of random variables down to 1, instead of number of loads n_d. By comparing (2.80) and (2.77), it is clear that the number of random variables n_{rand} for each branch i has been reduced from $n_r + n_d$ to $n_r + 1$. Finally, TOAT can be used to create representative testing scenarios. In (2.80), every random variables has a linear effect on the inequality. Therefore, 2 is selected as the level number. For normally distributed $\tilde{p}_{a,l}^{min}$ and $\tilde{p}_{a,l}^{max}$, each two representative values are selected, described by the aggregated mean and variance. Due to the intermittent nature of renewables' output, it is considered to vary from zero to its capacity. Therefore, zero and capacity are selected as representative values for renewables. Then according to TOAT, the testing scenarios can be created in a few steps as follows,

Step 1: According to the discussion above, the representative values for all the random values are:

$$p_{a,l}^{min}(1) = \mu(\tilde{p}_{a,l}^{min}) - \sigma(\tilde{p}_{a,l}^{min}), \quad \forall l = 1,2,...,n_l \tag{2.81}$$

$$p_{a,l}^{min}(2) = \mu(\tilde{p}_{a,l}^{min}) + \sigma(\tilde{p}_{a,l}^{min}), \quad \forall l = 1,2,...,n_l \tag{2.82}$$

$$p_{a,l}^{max}(1) = \mu(\tilde{p}_{a,l}^{max}) - \sigma(\tilde{p}_{a,l}^{max}), \quad \forall l = 1,2,...,n_l \tag{2.83}$$

$$p_{a,l}^{max}(1) = \mu(\tilde{p}_{a,l}^{max}) + \sigma(\tilde{p}_{a,l}^{max}), \quad \forall l = 1,2,...,n_l \tag{2.84}$$

$$p_{r,i}(1) = 0, \quad \forall i = 1,2,...,n_r \tag{2.85}$$

$$p_{r,i}(2) = p_{r,i}^{Cap}, \quad \forall i = 1,2,...,n_r \tag{2.86}$$

Step 2: From (2.80), it can be seen that all of the random variables have a linear relation to inequality. Therefore, two level factors are selected. For a system with n_r renewables and n_d loads, the total random variable for each branch is reduced from $n_{rand} = n_r + n_d$ to $n_{rand} = n_r + 1$. Thus, $L_S(2^{n_{rand}})$ from the OA library is selected to generate S number of testing scenarios, shown in equation (2.87). Now the probabilistic constraint (2.80) is transformed into a deterministic constraint set (2.87) as follows,

$$\begin{cases} p_{a,l}^{min,(1)} - h_r^{l,1} p_{r,1}^{(1)} - \cdots - h_r^{l,n_r} p_{r,n_r}^{(1)} \leq h_g^{l,1} p_{g,1} + h_g^{i,2} p_{g,2} + \\ \quad \cdots + h_g^{l,n_g} p_{g,n_g} \leq p_{a,l}^{max,(1)} - h_r^{l,1} p_{r,1}^{(1)} - \cdots - h_r^{l,n_r} p_{r,n_r}^{(1)} \\ p_{a,l}^{min,(2)} - h_r^{l,1} p_{r,1}^{(2)} - \cdots - h_r^{l,n_r} p_{r,n_r}^{(2)} \leq h_g^{l,1} p_{g,1} + h_g^{l,2} p_{g,2} + \\ \quad \cdots + h_g^{l,n_g} p_{g,n_g} \leq p_{a,l}^{max,(1)} - h_r^{l,1} p_{r1}^{(2)} - \cdots - h_r^{l,n_r} p_{r,n_r}^{(2)} \\ \vdots \\ p_{a,l}^{min,(S)} - h_r^{l,1} p_{r,1}^{(S)} - \cdots - h_r^{l,n_r} p_{r,n_r}^{(S)} \leq h_g^{l,1} p_{g,1} + h_g^{l,2} p_{g,2} + \\ \quad \cdots + h_g^{l,n_g} p_{g,n_g} \leq p_{a,l}^{max,(S)} - h_r^{l,1} p_{r,1}^{(S)} - \cdots - h_r^{l,n_r} p_{r,n_r}^{(S)} \end{cases} \tag{2.87}$$

Step 3:Finally, the (2.87) can be simplified by interval optimisation concepts. If the maximum value of all S experiments on the left of $\leq$ is selected as the lower bound for $h_g^{l,1} p_{g,1} + h_g^{l,2} p_{g,2} + \cdots + h_g^{l,n_g} p_{g,n_g}$, while the minimum of the maximum value of all S experiment on the right side of $\leq$ is selected as the upper bound for $h_g^{l,1} p_{g,1} + h_g^{l,2} p_{g,2} + \cdots + h_g^{l,n_g} p_{g,n_g}$, then the equation (2.87) for each branch l could be simplified into:

$$p_{h,l}^{min} \leq h_g^{i,1} p_{g1} + h_g^{i,2} p_{g2} + \cdots + h_g^{i,n_g} p_{gn_g} \leq p_{h,l}^{max} \tag{2.88}$$

where,

$$p_{h,l}^{min} = \max \begin{cases} p_{a,l}^{min,(1)} - h_r^{l,1} p_{r,1}^{(1)} - \cdots - h_r^{l,n_r} p_{r,n_r}^{(1)} \\ p_{a,l}^{min,(2)} - h_r^{l,1} p_{r,1}^{(2)} - \cdots - h_r^{l,n_r} p_{r,n_r}^{(2)} \\ \vdots \\ p_{a,l}^{min,(S)} - h_r^{l,1} p_{r,1}^{(S)} - \cdots - h_r^{l,n_r} p_{r,n_r}^{(S)} \end{cases} \tag{2.89}$$

and,

$$p_{h,l}^{max} = \min \begin{cases} p_{a,l}^{max,(1)} - h_r^{l,1} p_{r,1}^{(1)} - \cdots - h_r^{l,n_r} p_{r,n_r}^{(1)} \\ p_{a,l}^{max,(2)} - h_r^{l,1} p_{r,1}^{(2)} - \cdots - h_r^{i,n_r} p_{r,n_r}^{(2)} \\ \vdots \\ p_{a,l}^{max,(S)} - h_r^{l,1} p_{r,1}^{(S)} - \cdots - h_r^{l,n_r} p_{r,n_r}^{(S)} \end{cases} \tag{2.90}$$

Thus, a robust constraint is created for the active power limitation for branch i. All of the testing scenarios that were generated by TOAT are now simplified into two cases $p_{h,l}^{max}$ and $p_{h,l}^{min}$. Applying this for all branches $i = 1,2,...,n_l$, the final constraint for $H_G\mathbf{p}_g$ in matrix form is achieved,

$$\mathbf{p}_H^{min} \leq H_G\mathbf{p}_g \leq \mathbf{p}_H^{max} \tag{2.91}$$

The inequality constraint (2.88) and (2.91) are deterministic constraints that are without any random variables. Therefore, in three steps, the probabilistic constraint (2.75) is approximated into a deterministic constraint (2.91).

Robust OPF Transformation and Formulation

Finally, after the transformation according to constraint (2.41), the robust OPF is formulated as follows,

Objective:

$$minimise \sum_{i=1}^{n_g} (a_i {p_{g,i}}^2 + b_i p_{g,i} + c_i) \tag{2.92}$$

Subject to:

$$\mathbf{p} = \mathbf{p}_g - \mathbf{p}_d^{\rho^{max}} + \mathbf{p}_r^{\rho^{max}} \tag{2.93}$$

$$\mathbf{p}_g^{min} \leq \mathbf{p}_g \leq \mathbf{p}_g^{cap} \tag{2.94}$$

$$\mathbf{p}_H^{min} \leq H_G\mathbf{p}_g \leq \mathbf{p}_H^{max} \tag{2.95}$$

where $\mathbf{p}_d^{\rho^{max}}$ and $\mathbf{p}_r^{\rho^{max}}$ are the most probable values for load and renewable generation respectively, and generally forecast values can be used.

The above formulated OPF is an equivalent deterministic OPF that can be solved easily. Compare (2.92)-(2.95) to (2.34) and to (2.37), the most significant change is the consideration of constraint (2.95). Another noticeable change is the way in which the renewable generation output and load are considered in both problems. In (2.34) to (2.37), P_R and P_D are taken as deterministic values, for instance as the most probable value. The optimised result $\mathbf{p}_g^*$ from such formulation would most likely lead to overflows on branches, if there was an offset between the real output and renewables from the predicted value. It should be noted that the solution space from (2.95) is the common solution space from (2.37) for probable scenarios.

Therefore the robust solution can also be seen as the common solution space of traditional OPF.

2.5.2 Robust SCOPF by Benders Decomposition

This section presents a robust SCOPF, which is a security reinforcement of the robust OPF formulated in (2.5.1). Due to the complexity of the electric power system, the SCOPF problem usually creates a large-scale optimisation problem; BD is an effective method to solve this problem. The merit of BD is its ability to reduce the complexity and the large size of the original problem into a master problem and several sub-problems. In the presented robust SCOPF, the master problem corresponds to the robust OPF formulated in (2.92)-(2.95) in section 2.5.1 by adopting TOAT, which only considers of the operation cost under the uncertainties. Therefore, the master problem for robust SCOPF can be formulated as follows,

Objective:

$$minimise \sum_{i=1}^{n_g} (a_i {p_{g,i}}^2 + b_i p_{g,i} + c_i) \tag{2.96}$$

Subject to:

$$(2.93) - (2.95)$$

$$Benders\ infeasibility\ cut \tag{2.97}$$

The solution from (2.96)-(2.97) is then tested against each contingency case in sub-problems. By doing this, the result from the master problem is feasible for all of the operational constraints. For each contingency k, the positive slack variable $r_{l,k}$, $l = 1,2,...,n_l$, $k = 1,2,...,n_k$ is introduced for the optimisation problem below,

Objective:

$$min\omega = \sum_{l=1}^{n_l} r_{l,k} \tag{2.98}$$

Subject to:

$$\mathbf{p}^k = \mathbf{p}_g^k - \mathbf{p}_d^{\rho^{max}} + \mathbf{p}_r^{\rho^{max}} \tag{2.99}$$

$$\mathbf{p}_L^k = \mathbf{Hp} \tag{2.100}$$

$$p_{L,l}^{min} - r_{l,k} \leq p_{L,l}^k \leq p_{L,l}^{max} + r_{l,k} \tag{2.101}$$

$$r_{l,k} \geq 0 \tag{2.102}$$

$$\mathbf{p}_g^k = \mathbf{p}_g^* : \lambda_k \tag{2.103}$$

In the subproblem for each contingency, the Lagrangian coefficient λ_k and corresponding value $\mathbf{p}_g^k$ are calculated. If $\omega > 0$, the Benders cut is formed according to the λ_k and added back to the master problem (2.97). The sub-problem then is updated in each iteration which leads to adjustments on the controllable variables in the master problem, until the procedure converge. The Benders cut can be given as:

$$\omega^* + \lambda_k(\mathbf{p}_g - \mathbf{p}_g^*) \leq 0, \tag{2.104}$$

The whole robust SCOPF computation is illustrated in figure 2.1 The above SCOPF formulation is based on the robust OPF formulated in section 2.5.1. Therefore, the robustness against the uncertain variables is first given from the master problem, and then tested against each contingency using N-1 contingency analysis, as shown in figure 2.1. Since the linearised model is adopted to approximate the power flow model, the whole robust SCOPF is convex and able to converge efficiently. This chapter mainly focuses on the structure of robust SCOPF formulation, where only the PC action is considered for security control. Numerical simulations are conducted on the modified IEEE 14-bus system and IEEE 118-bus system to demonstrate the effectiveness of the presented approach.

2.6 Numerical Simulation

The robust SCOPF model is verified on the modified IEEE 14-bus and IEEE 118-bus systems. The algorithm is programmed in MATLAB and the system data is from MATPOWER package. The simulations were carried out on a Intel Core I5 CPU at 3.20GHz with 4.00GB of RAM. The OPF and power flow are solved using the MATPOWER package. The result of the robustness SCOPF is compared tothe traditional OPF in terms of the robust degree and generation cost. The testing scenarios are generated by MCS with 50000 scenarios.

The interior point method is adopted to solve the OPF problem. The renewable resources are assumed as wind farms, installed in selected nodes. The Weibull distribution has been used to describe the wind speed in various studies, usually with the parameters of using $\beta_w = 11.0086$ and k_w=1.9622. For $v > 0$ the wind speed PDF model is as follows:

$$f(v, \beta_w, k_w) = \frac{k_w}{\beta_w}(\frac{v}{\beta_w})^{k_w - 1} e^{-\frac{v}{\beta_w}^{k_w}} \tag{2.105}$$

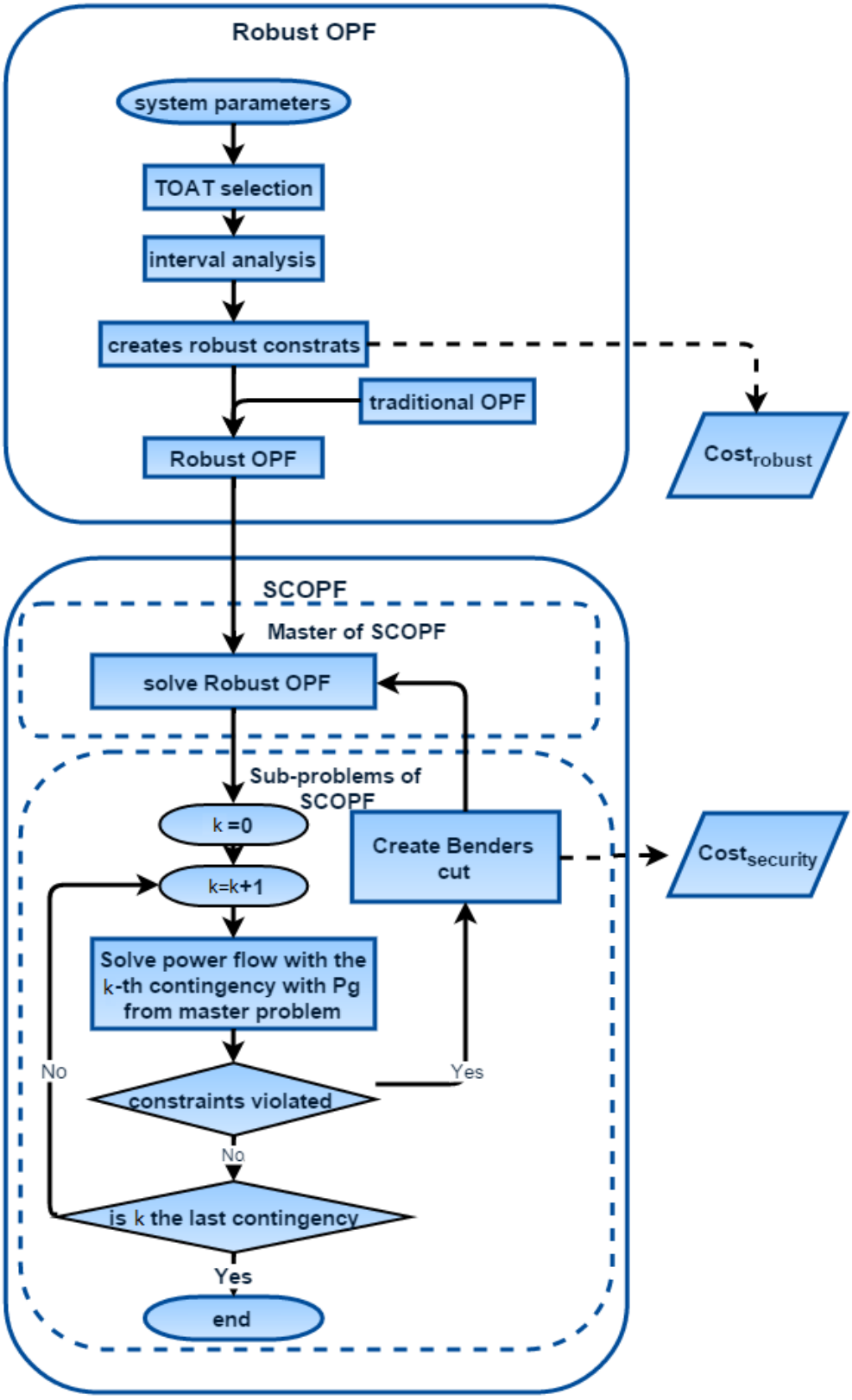

Fig. 2.1 Computation flowchart of the robust SCOPF

and the wind turbine power is simulated using:

$$p_r = \begin{cases} p_{rate}(v - v_{ci})/(v_{rate} - v_{ci}) & v_{ci} \leq v \leq v_{rate} \\ p_{rate} & v_{rate} \leq v \leq v_{co} \\ 0 & otherwise \end{cases} \tag{2.106}$$

During the simulation, the load is treated as normally distributed with the mean value of the original load value from the given system, whose deviation is assume to be 5% of the mean.

2.6.1 Simulation on the IEEE 14-bus System

This system consists of n_b =14 buses, n_g =5 generation units, n_d =11 loads and n_l =20 branches; therefore the 'N-1' security checks contain k =25 scenarios. The traditional generators are taken as controllable variables, whose generation limits and cost functions are the default values from the MATPOWER case14. The maximum branch active power flow for branches 1 and 7 are 80MW; for branches 3 and 6 are 50MW; for branches 17 to 20 are 20 MW; and rest 40MW. Two wind farms ($n_r = 2$) rated at 40MW are connected to bus 2 and bus 3, respectively. The total number of uncertainties of this system is $n_{ran} = n_d + n_r$, which is 13. Applying the linear aggregation rule for normal distributed variables (2.78) and (2.79), the number of uncertainties is reduced to $n_r + 1 = 3$. Therefore $L_4(2^3)$ is selected, which leads to $S = 4$ scenarios, as follows,

$$L_4(2^3) = \begin{bmatrix} 1 & 1 & 1 \\ 1 & 2 & 2 \\ 2 & 1 & 2 \\ 2 & 2 & 1 \end{bmatrix} \tag{2.107}$$

Therefore, taking the lower bound for example, four testing experiments can be constructed using variables $\tilde{p}_{a,l}^{min}$, $\tilde{p}_{r,1}$, and $\tilde{p}_{r2}$, and each of two levels:

$$p_{a,l}^{min}(1) = \mu(\tilde{p}_{a,l}^{min}) - \sigma(\tilde{p}_{a,l}^{min}) \tag{2.108}$$
$$p_{a,l}^{min}(2) = \mu(\tilde{p}_{a,l}^{min}) + \sigma(\tilde{p}_{a,l}^{min}) \tag{2.109}$$
$$p_{r,1}(1) = 0 \tag{2.110}$$
$$p_{r,1}(2) = 40MW \tag{2.111}$$
$$p_{r,2}(1) = 0 \tag{2.112}$$
$$p_{r,2}(2) = 40MW \tag{2.113}$$

Table 2.2 Results for the IEEE14-Bus System

Robust SCOPF	Cost (10^3\$/h)	5.657
	Robust Degree (%)	99.47
	No. Security Constraints for PC	4(L_{4-5}, L_{4-9} L_{5-6}, G_4)
Traditional OPF	Cost (10^3/h)	5.17
	Robust Degree(%)	4.48

and therefore the OA used to create the lower bound for branch i for the given simulation is:

$$L_4(2^3) = \begin{bmatrix} p_{a,l}^{min}(1) & 0 & 0 \\ p_{a,l}^{min}(1) & 40 & 40 \\ p_{a,l}^{min}(2) & 0 & 40 \\ p_{a,l}^{min}(2) & 40 & 0 \end{bmatrix} \tag{2.114}$$

The constraints (2.88) can then be created for robust OPF once the values of $p_{h,l}^{min}$ and $p_{h,l}^{max}$ are determined.

Next, 25 'N-1' security tests are conducted in addition to the robust OPF, where Benders infeasibility cuts are created as PCs if there is a violation of branch flow limits. The results tested against 50000 MCS scenarios are shown in table 2.2. where the robust degree η is defined as,

$$\eta = \frac{S_{feasible}}{S} \times 100\% \tag{2.115}$$

where $S_{feasible}$ is the number of scenarios without violations, and S is the total number of scenarios.

It can be observed that the minimum operation cost of robust OPF is higher than that of traditional OPF by $487\$/h$, 84% of which is from the robust requirement and the rest from the security constraints. However, the results demonstrate the significance of the robust degree, as the solution from traditional OPF only has 4.48 % feasibility against uncertainties.

2.6.2 Simulation on the IEEE 118-Bus System

The IEEE 118-bus system consists of n_b =118 buses, n_g =54 generation units and n_l =186 branches, therefore the 'N-1' security checks contain k =240 scenarios. The maximum branch active power flow limit from node 8 to node 9 and node 9 to node 10 is set as 550MW; from node 8 to node 5 as 500MW; and for the rest as 280 MW. Five wind farms ($n_r = 5$) rated at 200MW are connected to bus 16, bus 37, bus 48, bus 75 and bus 83

Table 2.3 $L_8(2^7)$ OA for IEEE 118-Bus System

Experiment	Column						
Number	1	2	3	4	5	6	7
1	$p_{a,l}^{min}(1)$	0	0	0	0	0	0
2	$p_{a,l}^{min}(1)$	0	200	200	200	200	0
3	$p_{a,l}^{min}(1)$	200	0	0	200	200	0
4	$p_{a,l}^{min}(1)$	200	200	200	0	0	0
5	$p_{a,l}^{min}(2)$	200	0	200	0	200	0
6	$p_{a,l}^{min}(2)$	200	200	0	200	0	0
7	$p_{a,l}^{min}(2)$	0	0	200	200	0	0
8	$p_{a,l}^{min}(2)$	0	200	0	0	200	0

respectively. The number of random variable is reduced to $n_r + 1 = 6$ after aggregating all loads. Therefore,$L_8(2^7)$ are selected for testing scenario generation. Similarly, eight experiments are created for the lower bound of branch i for the given simulation, as shown in table 2.3. it should be noted that the elements in the last column in table 2.3 are all zero. This is because the number of random variable for this simulation is 6, but there is no matrix in the OA library corresponding to experiments with 6 variables. Therefore, the closest OA with more variable is selected. The simulation result is shown in table 2.4.

Table 2.4 Results for the IEEE118-Bus System

Robust SCOPF	Cost (10^3\$/h)	99.114
	Robust Degree (%)	99.88
	No. Security Constraints for PC	$4(L_{4-5})$
Traditional OPF	Cost (10^3/h)	88.85
	Robust Degree(%)	28.60

2.6.3 Discussion

Tables 2.2 and 2.4 show the comparison between results of robust SCOPF and traditional OPF. It is clear that robust SCOPF outperforms the traditional OPF in terms of the robust degree. This means that the optimal solution from robust SCOPF performs better in accommodating the uncertainties that are brought by high renewable penetration and load uncertainties, although with some sacrifices in terms of the operation cost, consisting of robust cost and security cost.

The main goal of OPF is to determine the controllable variables in order to achieve a minimal operation cost. Therefore, the generators with lower cost are normally scheduled

with higher output. However, constraints such as branch flow limit affect the results, so that the generator with the lowest cost does not normally operate at its full capacity. The presented robust SCOPF actually incorporates the uncertainties into the branch flow limitation using PTDF and approaches such as scenario reduction and interval optimisation.

2.7 Conclusion

Using a robust SCOPF model, this chapter has presented a new efficient approach to address the uncertain factors caused by load demand and renewable generation in power system is presented in this chapter, via a robust SCOPF model. The robust SCOPF algorithm is not only capable of satisfying the security requirements, but is also robust against uncertain renewable generation output and load demand. The algorithm is able to achieve a balance between representativeness, economic efficiency, and computation efficiency. Moreover, the uncertainties are incorporate into the OPF problem in such a way that the formulated model can be seen as a deterministic equivalent OPF model. Furthermore, the approach could be a useful tool to estimate the relative costs to secure a given system against uncertainties from RESs and load, costs to secure the system from contingencies, or both. The numerical simulations have demonstrated the effectiveness of the presented algorithm. In addition, the computational burden can be further alleviated by facilitating the grid computation techniques since the problems can easily be decomposed. In conclusion, this chapter has introduced a general framework to efficiently integrate the uncertainties from the RESs into a steady state analysis in the forms of SCOPF. However, a few more points need to be further analysed. First, the linearised OPF model in this chapter neglects some system operating constraints such as voltage and reactive power limits, which needs to be addressed in the following chapters. Second, new large-scale RESs tend to be built remotely and expansion on existing transmission network is worth considering in the modelling. Moreover, RESs exist in the electricity grid in various forms and different levels. Therefore, it is also worth examining recent developments of RESs in sub-transmission systems and on the demand side. Finally, only PC is considered in the contingency control in this chapter, which is considered to be conservative in the long term. The following chapters investigate the competition between CC and PC actions as well.

Chapter 3

Hierarchical SCOPF Considering Wind Energy Integration through Multi-Terminal VSC-HVDC Grids

This chapter discusses two topics. First, in addition to its intermittent nature, renewable generation is also affected by high meteorological and geographical impacts, which means that large-scale renewable generation farm away from load centres and expansion on existing transmission are needed. High-voltage direct current (HVDC) transmission systems offer unique benefits in terms of economy, capacity and distance, and this is why HVDC has been used as a new form to transmit power from off shore large-scale renewable energy generation. Therefore this chapter first examines the question of how an operation and control structure of a meshed ac and HVDC grid is designed and constructed. Second, it then discusses how to efficiently coordinates the offshore renewable generation into the inland ac electricity grid operation, via a hierarchical SCOPF model considering large scale offshore wind energy integration through multi-terminal voltage source converter-HVDC(VSC-HVDC) grids. This chapter is based on [58, 59].

3.1 Introduction

With the development of large scale offshore wind farms and floating photovoltaics farms, MTDC systems have drawn significant attention in interconnecting the renewable energy to the main ac grid. It is becoming increasingly important to consider the injection of the off shore renewable generation into the main ac power system in the economic operation. In the meantime requirements such as making the control strategies robust against the uncertainties

caused by the intermittency of renewables, have been considered to be of great significance to the electricity network reliability.

Although HVDC technology has traditionally been restricted to the transmission of power between two points on the ac grid, connecting wind farms through MTDC grids offers several advantages, such as increased reliability of power transmission, improved balance service across ac interconnections and reduced generation variability. Given that MTDC grids offer unique capability in terms of regulating power flow, the meshed ac/HVDC systems can be operated more flexibly and cost effectively. Currently, wind is treated as a negative load, and supply is tailored to match the random demand [60]. Therefore, many technical issues must be addressed [61, 62] to connect offshore wind farms using MTDC grids. To take advantage of applying MTDC grids to support ac system operation and wind energy integration, extensive research has been directed towards the modelling, control and operation of mixed ac/dc systems [63], in terms of system modelling, power flow modelling, wind power integration and optimal dispatching computation.

The previous chapter two introduced a framework to incorporate renewable energy generation into the security constrained OPF with efficient computation approach. However, two aspects need further review. First, the renewable generation is assumed to be installed within the existing transmission infrastructure, and connected directly back to the electricity grid, which is also assumed to be operated by the transmission system operators. In this chapter, this assumption is examined by modelling offshore wind farms that are connected by VSCs. Each wind farm is operated by an individual energy plant owner, which would have an effect on the problem formulation structure. Second, the chapter also examines the contingency control strategies. For simplicity, PC was the only strategy adopted in the previous chapter, in contrast, the present chapter investigates how to coordinate CC effectively with PC under the structure of SCOPF model considering large-scale offshore wind farms through a multi-terminal VSC-connected ac/HVDC system. Finally, although the dc power flow or linearised power flow model has its advantage in computation efficiency, neglecting constraints on variables such as voltage and reactive power might lead the solution from linearised power flow model to be infeasible in real-world operations. This chapter describes the approach of using dc OPF combined with an ac power flow check via BD for improved computation efficiency and better security.

3.2 Combined Ac and Multi-Terminal HVDC Grids

3.2.1 Ac versus Dc

The devision between ac and dc systems began in the late 19^{th} century, when it was not feasible to integrate both systems with the technology available at the time. The ac system dominated the industry for a long time, and it was not until the early 20^{th} century that the dc system started to come back. The first commercial dc link was initially operated in 1954 to connect the island of Gotland with mainland Sweden. This inspired much dc system research and many projects. With the developmemnt of converter technologies, today numerous MTDC grid projects connecting offshore floating renewable generations are observed all around the world. There has been offshore wind generation with an operating capacity of 3,813MW in total in relatively shallow waters around the United Kingdom, Germany, Denmark, Belgium and so on [64, 65]. Similar growth has also been seen in China, Canada, and the United States (US) in recent years.

One important concern associated with the deployment of offshore wind generation is the cost of building the long distance of transmission lines to deliver the generated energy to the load centres. In recent years, there has been an increasing interest in building MTDC [66–68] systems driven by the grid integration of remotely located wind energy. The total cost of building dc cable connections is cheaper, with around 300-600 miles' breakeven distance [69] for overhead lines. Therefore, HVDC systems are significantly beneficial for large amount power transmission at large distances. However, existing transmission systems are HVAC dominant, and it is therefore crucial to study approaches to increase the transmission efficiency of existing HVAC networks with newly added HVDC systems. One approach is to find a proper modification of HVAC systems and connected remote renewable generations in the HVDC system through converters, so that this meshed interconnection can effectively share the diverse portfolio of intermittent resources and increase operational flexibility. However expanding renewable energy such as wind power mainly from wind resources poses a number of unique challenges because its generation output is inherently intermittent. Uncertainties raised by with RESs due to their intermittent nature threaten the system's reliable operation. As more wind resources are brought online, it is becoming increasingly critical to consider the integration of offshore RESs into the economic operation of main grids. Therefore requirements such as making the control strategies robust against the uncertainties caused by the intermittency of renewables have been considered to be of great significance to the electricity network reliability.

3.2.2 Operation Schemes

In general, HVDC systems connecting the offshore renewable generation are expansions on top of existing transmission systems. Normally, transmission systems operators are responsible for operating the grids and coordinating with other adjacent transmission systems. The new HVDC transmission in the electricity grid not only provides power injections to the entire grid, but might also have a significant impact on the power flow directions in whole network, causing difficulties in operation and the possibility of violating network constraints. A well-designed coordination strategy and a clearly defined responsibility for different types of operators could be beneficial to reduce such risks.

Three operating schemes are introduced in [70] for a mixed HVAC-HVDC system. These are the supper independent system operator, the technology separated independent system operator and the geographically separated independent system operator. In this thesis, the operating schemes are categorised into two types according to the information accessibility of each system operator, namely centralised operation scheme and the distributed operation scheme. This in turn shapes the formulation of the system power flow problem.

Centralised Scheme

The centralised scheme requires that a system operator have the knowledge of the whole system, including both ac and HVDC systems. In this scenario, data are sent to a central authority that is able to conduct an optimisation based on all of the system's requirement information. The control signal can then reach all components in the entire system.

The advantage of such a scheme is clear: since information over the entire ac and dc grid is known, an optimisation problem can be easily formulated such as OPF problem to minimise operation costs, or to minimise overall losses. However, the drawback of such a scheme is the formulated problem size and complexity, especially when both uncertainties and security requirements are considered.

Distributed Scheme and Independent System Operator

Alternatively, different system operators can be responsible for ac and dc grids. For a new HVDC system, a new system operator can be organised so that it operates and controls the information of the HVDC system and only shares partial knowledge with the ac system operators for coordination purposes. In this case, the optimisation problem such as the OPF problem needs to be carefully formulated, and the limitation on the control signals needs to be addressed. The computation complexity is reduced and the solution is normally achieved iteratively by using the repeated exchange of information.

3.3 Hierarchical SCOPF Considering Wind Energy Integration through Multi-Terminal VSC-HVDC Grids

3.3.1 Mixed HVAC and Multi-Terminal VSC-HVDC System Modelling

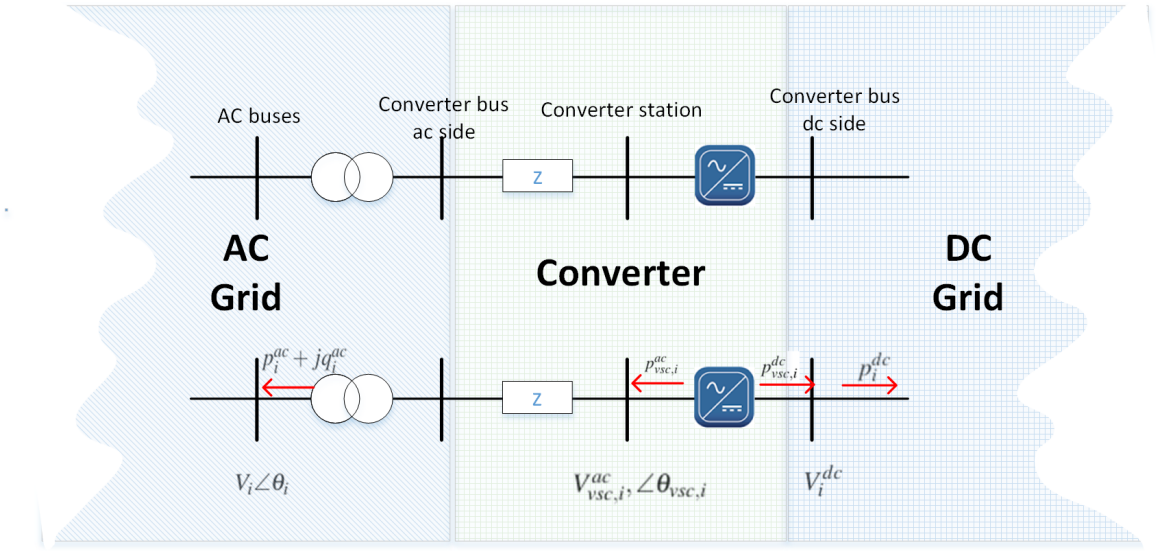

Fig. 3.1 General configuration of an ac grid (left side) with an embedded VSC-MTDC system connected to the dc grid (right side)

The entire grid can be split into a few sections; namely dc grid, ac grid and the connecting converters. The following introduces models for each of these three sections.

DC Grid

The power flow in the dc system is determined mainly by the node voltage. according to Kirchhoff's current law,the steady state relationship between the dc voltages and currents can be written as follows,

$$\mathbf{I^{dc}} = \mathbf{Y}\mathbf{V^{dc}} \tag{3.1}$$

where $\mathbf{Y}$ is the admittance matrix of the dc network. In the literature, the dc transmission lines are modelled only as resistive elements. Therefore, the steady state power flows over

the lines from node i and node j can be calculated as follows,

$$p_{ij}^{dc} = \frac{V_i^{dc} - V_j^{dc}}{r_{ij}} \tag{3.2}$$

where V_i^{dc} and V_j^{dc} are the voltage deviation from the reference bus and r_{ij} denotes the line resistance between node i and j. The active power injection on node i in the MTDC system can be written as,

$$p_i^{dc} = V_i^{dc} \sum_{j=1}^{n_b^{dc}} Y_{ij} V_j^{dc}. \tag{3.3}$$

and the active power flow on the branch from node i to node j is

$$p_{ij}^{dc} = V_i^{dc} Y_{ij} (V_j^{dc} - V_i^{dc}) \tag{3.4}$$

Ac System

The modelling of the ac system was described in Chapter 2, and is therefore not repeated here.

Converter Modelling

The VSC is modelled as an ac voltage source that is connected to a dc voltage source. The converter can be modelled by an ac side and a dc side. For the ac side, the active power $p_{vsc,c}^{ac}$ and reactive power $q_{vsc,c}$ can be controlled by controlling the voltage magnitude $V_{vsc,c}^{ac}$ and the voltage angle $\theta_{vsc,c}$. On the dc side, the voltage V_{vsc}^{dc} can be controlled within its limits to control the power flow. For a lossless VSC, the power balance equation couples the ac and dc systems together, as follows:

$$p_{vsc,c}^{ac} = \eta_t p_{vsc,c}^{dc}, \forall c = 1, 2, ..., n_{vsc} \tag{3.5}$$

where η_t indicates transmission and conversion efficiency and thus for a system neglects losses $\eta_t = 1$.

3.3.2 Security Constrained Optimal Power Flow with Two Levels

PC and CC SCOPF are two types of control strategies to deal with credible contingencies to ensure that the system can either withstand or recover from faults. Although PC can secure the system against all contingencies, the strategy is normally viewed as conservative in that it leads to a higher operational cost. Various approaches focus on CC actions to alleviate post-contingency overloads, such as generation redispatch and load curtailment. The objective of a SCOPF algorithm is to minimise the total generation cost in addition to the security control cost, which includes both PC and CC costs. PC costs may be included in the SCOPF objective function during the initial scheduling stage. On the other hand, CC costs normally refer to the expected costs, for they are probably related. Moreover, PC costs can be predetermined using known information regarding generator cost coefficients, whereas CC costs vary with selected actions during the post-contingency period. A cost-efficient and readily available CC strategy, such as adopting MTDC to coordinate terminal power injections by redistributing wind power generated in the system, offers great potential for efficient CC actions. The operation scheme for the HVAC and MTDC system in this chapter adopts a distributed structure, as described in the previous section. The introduced scheme makes use of the power flow control capability of MTDC grids to provide support for ac systems, so that the ac/dc system can be operated in a cost-effective way. A two-layer interaction is designed for the SCOPF so that limited information is exchanged between two system operators. The hierarchical dispatch scheme is a particularly attractive method of problem decomposition as it provided a highly intuitive system redispatch architecture.

Security Constrained Optimal Power Flow in Ac System

The SCOPF in the ac system adopts the structure of (2.59)-(2.64), which promotes post-contingency control strategy. The control variables vector **u** and state variables vector **v** in the SCOPF for the ac system are given as follows,

$$\mathbf{z_k} = \begin{bmatrix} \mathbf{u_k} \\ \mathbf{v_k} \end{bmatrix} \tag{3.6}$$

$$\mathbf{u_k} = \begin{bmatrix} \mathbf{p_{g,k}} \\ \mathbf{q_{g,k}} \\ \mathbf{p^{ac}_{vsc,k}} \\ \mathbf{q^{ac}_{vsc,k}} \\ \mathbf{tr_k} \\ \varphi_\mathbf{k} \end{bmatrix} \tag{3.7}$$

$$\mathbf{v_k} = \begin{bmatrix} \theta_\mathbf{k} \\ \mathbf{V_k} \end{bmatrix} \tag{3.8}$$

Normally, the tapping transformers tap-changing vector **tr** and phase shifting φ are set as constant. Given that the focus is on the utilisation of flexibility in MTDC for CC actions, by optimising $p^0_{g,i}$ to minimise system generation costs as in (2.10), the objective function in the ac system is subject to network constraints for all contingencies, which are as follows,

Subject to:

$$p^{ac,k}_{vsc,i} + p^k_{g,i} - p_{d,i} = V^{ac,k}_i \sum_{j=1}^{n^{ac}_b} V^{ac}_j (g_{ij}\cos\theta^k_{ij} + b_{ij}\sin\theta^k_{ij}) \tag{3.9}$$

$$q^{ac,k}_{vsc,i} + q^k_{g,i} - q_{d,i} = V^{ac,k}_i \sum_{j=1}^{n^{ac}_b} V^{ac}_j (g_{ij}\cos\theta^k_{ij} - b_{ij}\sin\theta^k_{ij}) \tag{3.10}$$

$$\sum_{i=1}^{n_{vsc}} p^{ac,k}_{vsc,i} = \sum_{j=1}^{n_w} p^{\rho^{max}}_{w,j} \tag{3.11}$$

$$p^{min}_{g,i} \le p^k_{g,i} \le p^{cap}_{g,i} \quad \forall i = 1,2,...,n_g \tag{3.12}$$

$$q^{min}_{g,i} \le q^k_{g,i} \le q^{cap}_{g,i} \quad \forall i = 1,2,...,n_g \tag{3.13}$$

$$V^{min}_i \le V^k_i \le V^{cap}_i \quad \forall i = 1,2,...,n^{ac}_b \tag{3.14}$$

$$-s^{max}_{ij} \le s^k_{ij} \le s^{max}_{ij} \quad \forall i,j = 1,2,...,n^{ac}_b \tag{3.15}$$

$$p^{ac,min}_{vsc,c} \le p^{ac,k}_{vsc,c} \le p^{ac,cap}_{vsc,c} \quad \forall c = 1,2,...,n_{vsc} \tag{3.16}$$

$$\left| p^0_{g,i} - p^k_{g,i} \right| \le \Delta p^{max}_{g,i} \quad \forall i = 1,2,...,n_g \tag{3.17}$$

$$\left| p^{ac,0}_{vsc,c} - p^{ac,k}_{vsc,c} \right| \le \Delta p^{ac,max}_{vsc,c} \quad \forall c = 1,2,...,n_{vsc} \tag{3.18}$$

Equality constraints (3.9) and (3.10) are nodal power balance constraints on each ac buses $i = 1,2,...,n^{ac}_b$. Constraint (3.11) indicates the constraint on the VSCs ac side power

injections, for which the sum of the power injection equals the forecast converter wind power generation delivered from the HVDC system to VSCs. $p_{w,j}^{p^{max}}$ denotes the most probable wind generation. The inequality constraints (3.12) to (3.16) are the operation limits on active power generation limits, reactive generation limits, voltage limits, branch line flow limits in the ac system, and VSCs' power ratings, respectively. (3.17) and (3.18) are coupling constraints on $p_{g,i}^{k}$ and $p_{vsc,c}^{k}$ to avoid unrealistic movements in CC actions. (3.17) and (3.18) correspond to coupling constraint (2.55). Normally, the problem can be considered a PC-CC SCOPF by selecting different $\Delta\mathbf{u_k}$, where $\Delta\mathbf{u} = T_k d\Delta\mathbf{u_k}/dt \; \forall k = 1,2,\ldots,n_k$. The coupling constraint (2.55) indicates that the controllable variable $\mathbf{u_0}$ can be moved from $\mathbf{u_0}$ to $\mathbf{u_k}$ within bounds to satisfy the post-contingency constraints. Therefore, by setting $\Delta\mathbf{u} = 0$, the problem becomes a pure PC-OPF. It should be noted that CC costs are not included in the objective function, as post-contingency control variable $\mathbf{u_k}$ is not included in the objective function. Therefore, the formulated objective function can maximise the number of post contingency control actions, and the ability of MTDC in post-contingency control can then be evaluated. Furthermore, as CC costs are incurred when contingency happens, there is a slight possibility that this approach may lead to a higher overall estimated control cost. The formulation of the SCOPF in the ac grid is able to determine the optimised values of $p_{g,i}^{ac,0}$ and $p_{vsc,c}^{ac,0}$ using the given forecast information on remote wind farm generation, and $p_{vsc,c}^{ac,0}$ is the reference information announced to the HVDC system operator for OPF computation in the HVDC system.

Optimal Power Flow in the Dc System

In this thesis, a distributed operation scheme is assumed, where the HVDC system is managed and operated by the HVDC system operator. Therefore, the ac system operation only has limited information from the HVDC system operator to coordinaten the optimal dispatch decision-making process. The HVDC system power dispatching is then regulates the power transmitted to the VSC terminals by determining the converter dc sides' droop gains with a fixed active power set point, according to the reference power injection required from the ac grid. Wind farms are assumed to be connected to the HVDC system with wind voltage source converter (WVSC), which is regulated as a voltage source.

Assuming that the loss through WVSC is neglected and the power injected from the wind farm side is based on the real wind power generation, the active power from the WVSC injected into the MTDC grid $p_i^{dc}, i = 1,2,...,n_w$ equals to the wind power generation $p_{w,i}, i = 1,2,...,n_w$. Then using dc voltage droop control, the active power flow at each grid-side voltage source converter(GVSC) $p_i^{dc}, i = n_w+1, n_w+2,...,n_b^{dc}$ can be controlled

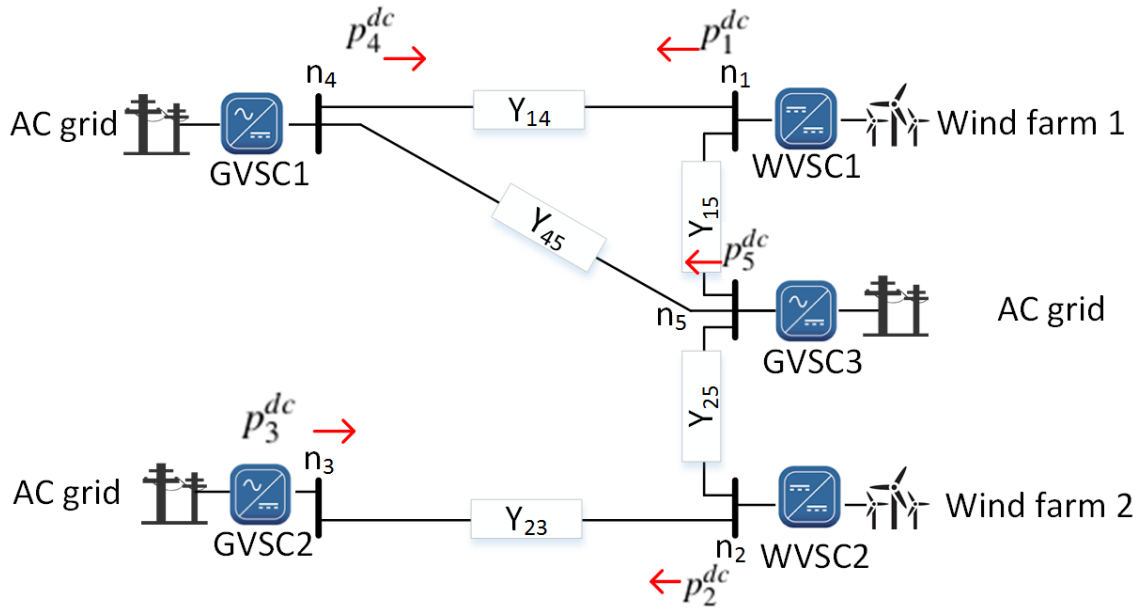

Fig. 3.2 Single-line diagram of the offshore wind farm connected with a VSC-MTDC system

as follows,

$$p_i^{dc} = p_i^{dc,0} + K_i(V_i^{dc} - V_i^{dc,0}) \tag{3.19}$$

where $p_i^{dc,0}$ is the active power injection initial set point of the node i in the HVDC system. Therefore, the dc voltage at each node in the HVDC system can be calculated in an iterative manner, introducing the Jacobian matrix for the MTDC grid $\mathbf{J_{DC}}$ as follows,

$$\mathbf{V}_{m+1} = (\mathbf{J_{DC}}^{(m+1)})^{-1}[\mathbf{P} - \mathbf{P}(\mathbf{V^{DC}}^{(m)})] + \mathbf{V^{DC}}^{(m)} \tag{3.20}$$

where active power vector $\mathbf{P^{DC}} = [p_1^{dc}, p_2^{dc}, ..., p_{n_w}^{dc}, p_{n_{w+1}}^{dc}, ..., p_{n_b^{dc}}^{dc}]^T$, and the vector of dc voltage on each dc bus $\mathbf{V} = [V_1^{dc}, V_2^{dc}, ..., V_{n_w}^{dc}, V_{n_w+1}^{dc}, ..., V_{n_b^{dc}}^{dc}]$ Therefore, an optimisation problem is formulated to minimise the difference between the reference power to the actual

power injection at each MTDC GVSC terminal as follows,

Objective:

$$minimise \sum_{i=n_w+1}^{n_{dc}} \left| p_{vsc,i}^{dc} - p_{vsc,i}^{dc,ref} \right| \tag{3.21}$$

Subject to:

$$\underline{K_i} \leq K_i \leq \overline{K_i} \tag{3.22}$$

$$\underline{V_i} \leq V_i \leq \overline{V_i} \tag{3.23}$$

$$-\overline{i_{ij}^{dc}} \leq i_{ij}^{dc} \leq \overline{i_{ij}^{dc}} \tag{3.24}$$

By optimising (3.24), the actual power output p_i^{dc} can be set close to the required value, within limitations on the droop constants (3.22), converter dc voltage level limits (3.23) and the cable rating on the dc cables (3.24).

3.3.3 Benders Decomposition for N-1 Contingency Analysis in the Two Level Framework

In this study, both PC and CC are computed through BD as introduced in Chapter 2. This approach has been successfully applied to take advantage of underlying problem structures for various optimisation problems. Master problem as base case $k = 0$:

Objective:

$$minimise \sum_{i=1}^{n_g} (a_i (p_{g,i}^{ac,0})^2 + b_i p_{g,i}^{ac,0} + c_i) \tag{3.25}$$

Subject to:

$$p_{vsc,i}^{ac,0} + p_{g,i}^{0} - p_{d,i} = p_i^0 \quad \forall i = 1,2,...,n_b^{ac} \tag{3.26}$$

$$\sum_{c=1}^{n_{vsc}} p_{vsc,c}^{ac,0} = \sum_{j=1}^{n_w} p_{w,j}^{p^{max}} \tag{3.27}$$

$$p_{g,i}^{min} \leq p_{g,i}^{0} \leq p_{g,i}^{cap} \quad \forall i = 1,2,...,n_g \tag{3.28}$$

$$-p_{ij}^{max} \leq p_{ij}^{0} \leq p_{ij}^{max} \quad \forall i,j = 1,2,...,n_b^{ac} \tag{3.29}$$

$$p_{vsc,c}^{ac,min} \leq p_{vsc,c}^{ac,k} \leq p_{vsc,c}^{ac,cap} \quad \forall i = c,2,...,n_{vsc} \tag{3.30}$$

$$Benders\ infeasibility\ cut \tag{3.31}$$

Subproblem:

Objective:

$$minimise \omega = \sum_{i=1}^{n_l} r_{i,k} \tag{3.32}$$

Subject to:

$$p_{vsc,i}^{ac,k} + p_{g,i}^{k} - p_{di} = V_i^{ac,k} \sum_{j=1}^{n_b^{ac}} V_j^{ac} (G_{ij} \cos\theta_{ij}^{k} + B_{ij} \sin\theta_{ij}^{k}) \tag{3.33}$$

$$q_{vsc,i}^{ac,k} + q_{g,i}^{k} - q_{di} = V_i^{ac,k} \sum_{j=1}^{n_b^{ac}} V_j^{ac} (G_{ij} \cos\theta_{ij}^{k} - B_{ij} \sin\theta_{ij}^{k}) \tag{3.34}$$

$$\sum_{c=1}^{n_{vsc}} p_{vsc,c}^{ac,k} = \sum_{j=1}^{n_w} p_{w,j}^{p^{max}} \tag{3.35}$$

$$p_{g,i}^{min} \leq p_{g,i}^{k} \leq p_{g,i}^{cap} \qquad \forall i = 1,2,...,n_g \tag{3.36}$$

$$q_{g,i}^{min} \leq q_{g,i}^{k} \leq q_{g,i}^{cap} \qquad \forall i = 1,2,...,n_g \tag{3.37}$$

$$V_i^{min} \leq V_i^{k} \leq V_i^{cap} \qquad \forall i = 1,2,...,n_b^{ac} \tag{3.38}$$

$$-p_{L,l}^{max} - r_l^{k} \leq p_{L,l}^{k} \leq p_{L,l}^{max} + r_l^{k} \qquad \forall l = 1,2,...,n_l^{ac} \tag{3.39}$$

$$-q_{L,l}^{max} \leq q_{L,l}^{k} \leq q_{L,l}^{max} \qquad \forall l = 1,2,...,n_l^{ac} \tag{3.40}$$

$$p_{vsc,c}^{ac,min} \leq p_{vsc,c}^{ac,k} \leq p_{vsc,c}^{ac,cap} \qquad \forall i = 1,2,...,n_{vsc} \tag{3.41}$$

$$\left| p_{g,i}^{0} - p_{g,i}^{k} \right| \leq \Delta p_{g,i}^{max} \quad \forall i = 1,2,...,n_g \tag{3.42}$$

$$\left| p_{vsc,c}^{ac,0} - p_{vsc,c}^{ac,k} \right| \leq \Delta p_{vsc,c}^{max} \quad \forall c = 1,2,...,n_{vsc} \tag{3.43}$$

$$r_{i,k} \geq 0 \tag{3.44}$$

$$\mathbf{p}_g^{k} = \mathbf{p}_g^{*} : \lambda_{g,k} \tag{3.45}$$

$$\mathbf{p}_{vsc}^{ac,k} = \mathbf{p}_{vsc}^{ac,*} : \lambda_{c,k} \tag{3.46}$$

The original optimisation problem is decomposed into a master problem corresponding to a base operation case $k = 0$ and n_k sub-problems $k = 1, 2, ..., n_k$, each corresponding to one of the contingency scenarios from the N-1 contingency analysis. As the aim is to maximise the MTDC's ability in post-contingency control, a two-stage BD is adopted to promote the CC actions supported by MTDC. For both stages, the BD includes a master problem and corresponding sub-problems. The first stage determines the feasibility of CC. In this stage, the solution from the master problem is tested in the subproblems that are with coupling constraints (3.17) and (3.18). If a solution can be obtained in the first stage, the contingency will be recorded as post-contingency controlled, and no Benders cut will be created or added back to the master problem. However, if no solution can be achieved, the second stage BD will be triggered and the coupling constraint (3.17) and (3.18) will be removed before Benders cuts are added back to the master problem as constraints, so that the optimised result is valid against the remaining contingencies, and this process is normally regarded as PC actions.

The N-1 security check is traditionally considered when determining the optimal setting for controllable generation dispatch against credible contingencies. This refers to the case in which the created constraints in the second stage of BD need to be fulfilled and the rest are supported by CC. The decomposition process can be formulated as shown in (3.25) to (3.46), If there is a solution for contingency k, then contingency k is rated as post-contingency controlled with CC action, and the corresponding cost is calculated according to the decision variables of rescheduled generation and grid-side VSCs injections. If no feasible CC solution is found for contingency k, vectors of the dual variables $\lambda_{g,k}$ and $\lambda_{c,k}$ and corresponding value $\mathbf{p}_g^k$ and $\mathbf{p}_{vsc}^{ac,k}$ are calculated. If $\omega > 0$, Benders cut is formed according to the $\lambda_{g,k}$ and $\lambda_{c,k}$ and then added back to the master problem as a constraint (3.31). The sub-problem is then updated in each iteration which leads to adjustments to the control variables in the master problem until they converge. In this case, the contingency is classified as a preventive controlled contingency. The Benders cut can be given as follows,

$$\omega^* + \boldsymbol{\lambda}_{\mathbf{g},\mathbf{k}}(\mathbf{p}_g^k - \mathbf{p}_g^*) + \boldsymbol{\lambda}_{\mathbf{c},\mathbf{k}}(\mathbf{p}_{vsc}^{ac,k} - \mathbf{p}_{vsc}^{ac,*}) \tag{3.47}$$

It should be noted that the BD approach for the hierarchical SCOPF problem has some unique features:

1. **The master problem** (3.25) **to** (3.47) **is a linearised approximation of the original ac OPF problem** by removing variables such as the reactive power and voltage, and it is used as the base case to compute the optimal dispatch decisions on $\mathbf{p}_g$.

2. **The reactive power and voltage are then checked in the subproblems** based on the solution of $\mathbf{p}_g^*$ from the master problem.

3. The master problem adopts a linearised power flow model for optimisation, which is convex and easy to solve, while the solution is handed over to the subproblem as an input for the N-1 contingency analysis. A nonlinear power flow is adopted in the subproblem, which attempts to find a feasible solution given the restriction on reactive power generation and voltage limits. This process does not aim to further optimise the system, but is instead used as a feasibility check realised by the BD approach.

4. **Although there are concerns that BD may fail to converge to either a global optimal or a local optimal** when applied to nonlinear SCOPF exist, the approach of adopting a linearised OPF in the master problem that is convex helps to reduce such risk, and the computation experience with the ac power flow in the subproblems has been encouraging. Moreover, convex relaxation [71, 72] techniques that are discussed in Chapter 5 could be applied to further alleviate such concerns.

5. **In general, the additional security constraints introduced on top of the OPF problem do lead to a more complicated optimisation problem** since the solution needs to satisfy not only the system's physical limits, but also all of the contingency cases, which poses challenges in real-time operation. However the computation time can be alleviated by checking all contingencies at the same time, since all sub-problems are not interdependent. Moreover, to further reduce the computation burden, the contingency filter technique could be applied, which only includes the most severe contingencies into the feasibility check.

.

3.3.4 SCOPF Framework for the Meshed Ac/MTDC Grids

After introducing each part of the system, this section introduces the overall dispatch algorithm, which is able to make use of the power flow control capability of MTDC grids to provide support for ac systems, so that the ac/dc system can be operated in a cost-effective way. The presented hierarchical dispatch scheme, where two layers interact, is a particularly attractive method of problem decomposition, as the layers provide a highly intuitive system redispatch architecture.

The two-layer BD SCOPF dispatch algorithm (TLDSCOPF algorithm)is described as follows,

TLDSCOPF Algorithm

iteration $m = 1$

high level dispatch

- Receive $p_{w,i}^{p^{max}}$ wind forecast.
- Compute $\mathbf{p}_g$ and $\mathbf{p}_{vsc}^{ac}$ from master problem (3.25) to (3.47).
- **for** $k = 1, 2, ..., n_k$
- feasibility check by BD in subproblem k

Receive final result on $\mathbf{p}_g$ and $\mathbf{p}_{vsc}^{ac}$

Check if following criteria(s) is(are) **TRUE**

- $\left| \mathbf{p}_{vsc}^{ac,m-1} - \mathbf{p}_{vsc}^{ac,m} \right| \leq \tau$, or
- $m > m^{max}$

if: YES, Dispatch and **END**

Else: m=m+1 and

Continue to low level dispatch, set $p_{vsc,c}^{dc,ref}$ by $p_{vsc,c}^{ac}$;

Low level dispatch:

- **Run:** (3.21) to (3.24) with given reference value $p_{vsc,c}^{dc,ref}$ by adjusting droop coefficients and active power set points.
- Go back to high level

A flow chart in figure 3.3 illustrates this process.

3.4 Case Study

The case study includes two sections. The first section demonstrates the performance of the TLDSCOPF algorithm on the modified IEEE 14-bus and 118-bus systems, which shows the effectiveness of TLDSCOPF in coordinating meshed ac/dc systems in contingency controls, leading to an overall lower operation cost. The second section shows the advantage of the droop control used in TLDSCOPF over a fixed droop in terms of accommodating renewable generations, under the scenario of a distributed operation scheme.

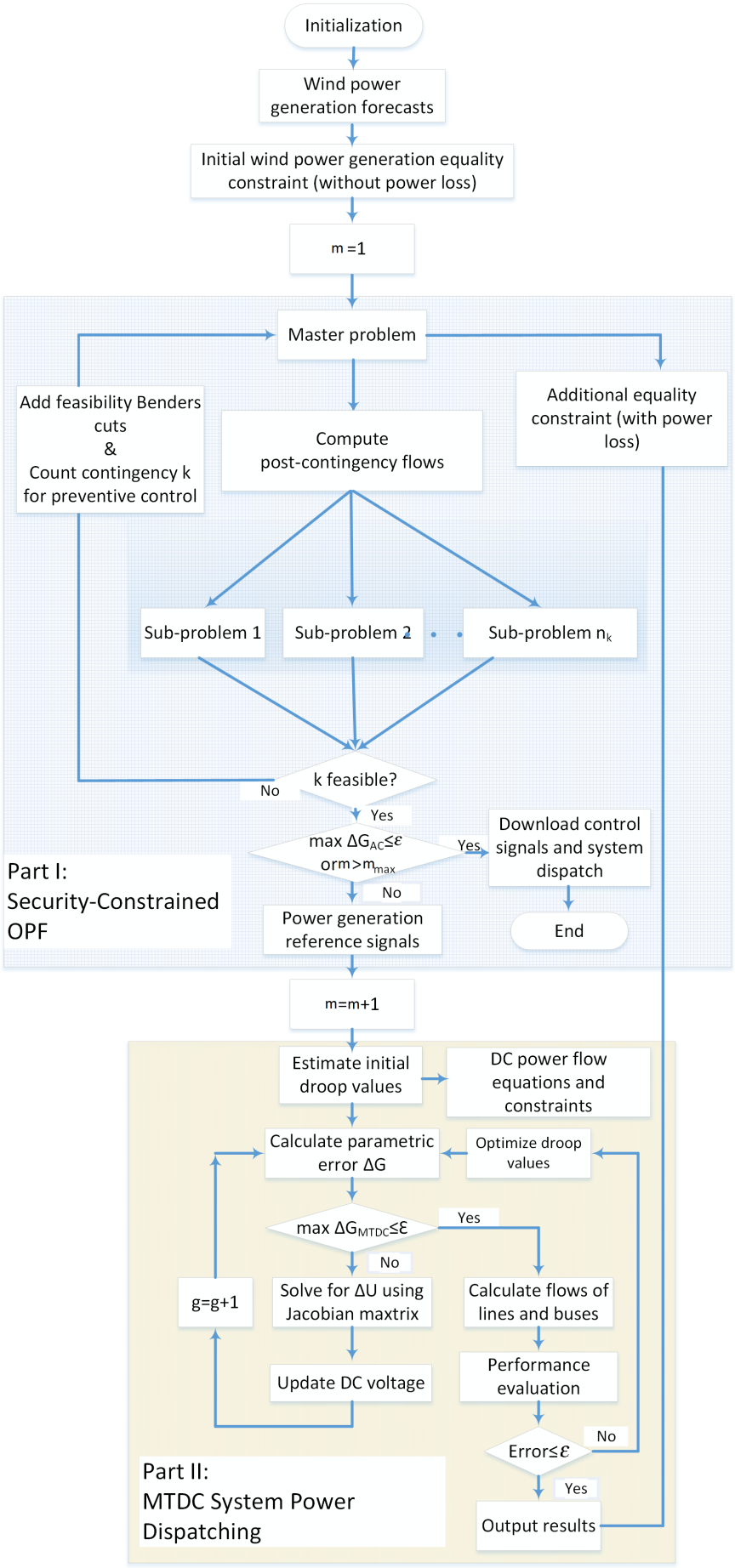

Fig. 3.3 Hierarchical system dispatch scheme for meshed ac/MTDC grids

3.4.1 SCOPF Results

Integrating multiple wind farms into the MTDC grid allows for effective sharing of renewable resources and cost-effective electricity supply. Two modified meshed ac/dc systems, the IEEE 14-bus and the IEEE 118-bus systems, are used to demonstrate the presented strategy's performance. To quantitatively evaluate the performance of the presented method, the Expected Security Control Cost (ESCC) index is selected, given the probabilistic nature of contingencies, which can be expressed as follows,

$$ESCC = \overbrace{\sum_{k=1}^{n_k} \rho^k \sum_{i=1}^{n_g} \alpha_{g,i}(p_{g,i}^k - p_{g,i}^*)^2}^{CC\ Cost} + \overbrace{\sum_{i=1}^{n_g} f(p_{g,i}^*) - f(\hat{p}_{g,i})}^{PC\ Cost} \tag{3.48}$$

where $\hat{p}_{g,i}$ denotes the conventional OPF result for generator i without considering any security constraints, and $f(p_{g,i})$ is the associated OPF cost. (3.48) shows that the CC cost is the sum of all probable post-contingency control costs, where ρ^k is the probability of contingency k, while the PC cost of a given state variable is the cost difference between OPF problems with and without security constraints.

IEEE 14-Bus System

A ±400 kV five-terminal dc grid has been added to the system, which provides the interconnection of two wind farms to three buses at a benchmark ac system through VSC converters. The one-line diagram is shown in figure 3.4. The maximum power flow limits for branches 1 and 7 are 80 MVA; for branches 3 and 6, 50 MVA; for branches 17-20, 20 MVA; and for the rest 40 MVA. The two wind farms, each consisting of 30 Vestas 2 MW wind turbines, are located at bus 18 and bus 19.

In this study, a wind power generation overestimation scenario is selected to demonstrate the ability of the MTDC to coordinate with generator rescheduling in the CC stage, where the available wind power generation is 20% less than the estimated value. To accommodate the base loading level, the load profile and unit parameters of the original system are adjusted accordingly. The rate of generator redispatch is set at \$30/MW/h. In total, 25 N-1 contingencies are analysed in this study, including loss of transmission lines l1, l2,..., l20 and generators G1, G2,...,G5. The simulation results are given in table 3.1.

IEEE 118-Bus System

A modified version of the IEEE 118-bus system is used, which contains three VSC converters and a dc grid with five buses and four dc lines. Thus, the system consists of 123 buses, 54

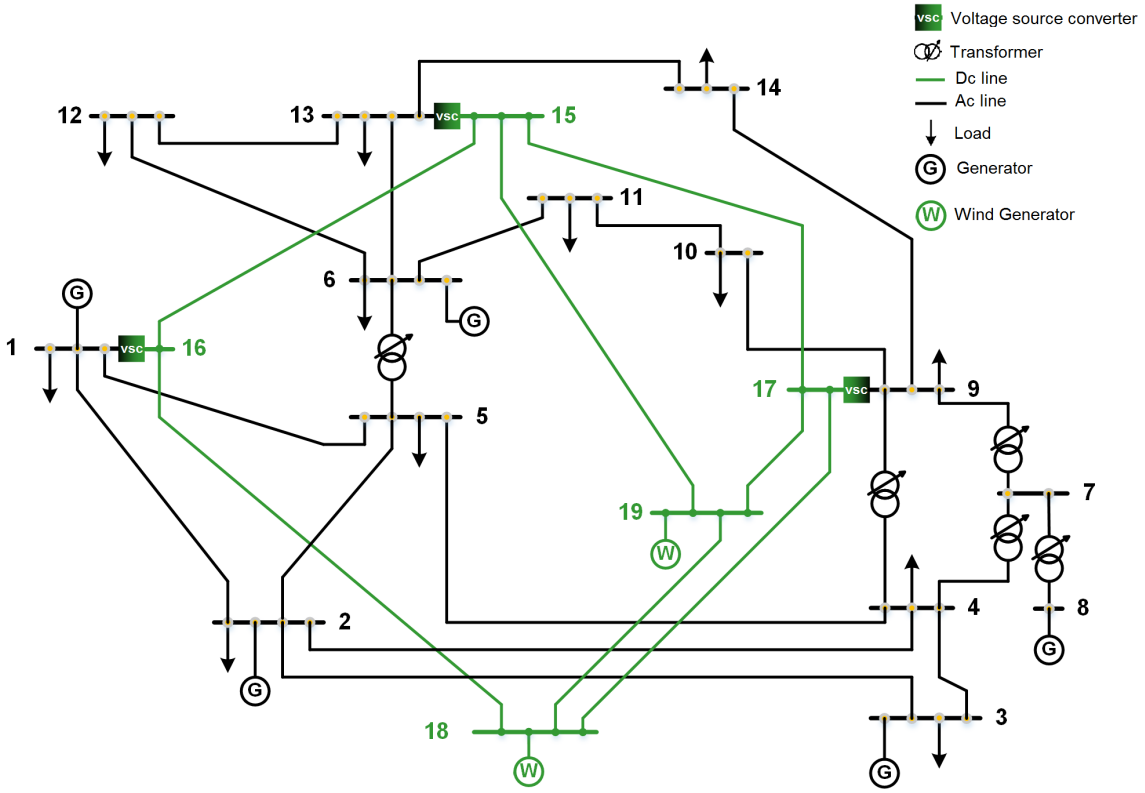

Fig. 3.4 Single-line diagram of the offshore wind farm connected with a VSC-MTDC system

Table 3.1 SCOPF Result for IEEE14-Bus System

Algorithm	Total Cost ($/h)	3800.80	
	Total Cost Breakdown		
	OPF Cost ($/h)	CC Cost ($/h)	PC Cost ($/h)
	3567.18	233.62	0
	Contingencies that need to be controlled		
	Number of PC	Number of CC	
	0	13(L1, L2, L3, L4. L5, L6, L7, L8, L11, L13, L15, L18, G1)	
Fixed Droop Constant	Total Cost ($/h)	4640.64	
	Total Cost Breakdown		
	OPF Cost ($/h)	CC Cost ($/h)	PC Cost ($/h)
	3567.18	0	1073.46
	Contingencies that need to be controlled		
	Number of PC	Number of CC	
	13(L1, L2, L3, L4. L5, L6, L7, L8, L11, L13, L15, L18, G1)	0	

traditional generators, 2 wind farms, and 186 branches. Therefore the n-1 security checks 240 scenarios. The maximum branch power flow limits are set at 280 MVA. Two wind farms rated at 200 MW each are connected to bus 4, bus 8 and bus 10 through VSCs. A case study considering wind farm connections through an MTDC network is simulated to show the reduced cost of utilising MTDC in the network, with available wind generation 20% greater than the estimated value. It should be noted that the MTDC in this study not only connects two buses with wind farms but also connects three other buses in the ac system, such that the renewables may be shared more effectively. In the study, the cost of generator redispatch is set at \$20/MW/h. The results are shown in table 3.2.

Table 3.2 SCOPF Result for IEEE118-Bus System

Algorithm	Total Cost (10^3\$/h)	92.60	
	Total Cost Breakdown		
	OPF Cost (10^3\$/h)	CC Cost (10^3\$/h)	PC Cost (10^3\$/h)
	92.60	1.41	0
	Contingencies that need to be controlled		
	Number of PC	Number of CC	
	0	8(L8, L9, L20, L36, G28, G29, G37, G40)	
Fixed Droop Constant	Total Cost (10^3\$/h)	95.76	
	Total Cost Breakdown		
	OPF Cost (10^3\$/h)	CC Cost (10^3\$/h)	PC Cost (10^3\$/h)
	92.66	0	3.12
	Contingencies that need to be controlled		
	Number of PC	Number of CC	
	8(L8, L9, L20, L36, G28, G29, G37, G40)	0	

Simulation of A Centralised Control Operation Scheme on IEEE 14-Bus System

A unified and linearised SCOPF formulation is simulated in this section. The modelling is done on the AMPL platform and the problem is solved using the Gurobi solver. The system's numerical data are the same as the data used in Section 3.4.1. In total, 25 n-1 tests are analysed in this study, including loss of transmission lines L1, L2, ..., L20 and generators G1, G2, ..., G5. It should be noted that $n_k = n_g + n_b + n_m + 2n_{vsc} + n_l)$ additional variables are added for the centralised SCOPF formulation, with additional $n_k = (2n_g + n_b + n_m + 4n_{vsc} + n_l)$ constraints, and the exact SCOPF solution is shown in table 3.3.

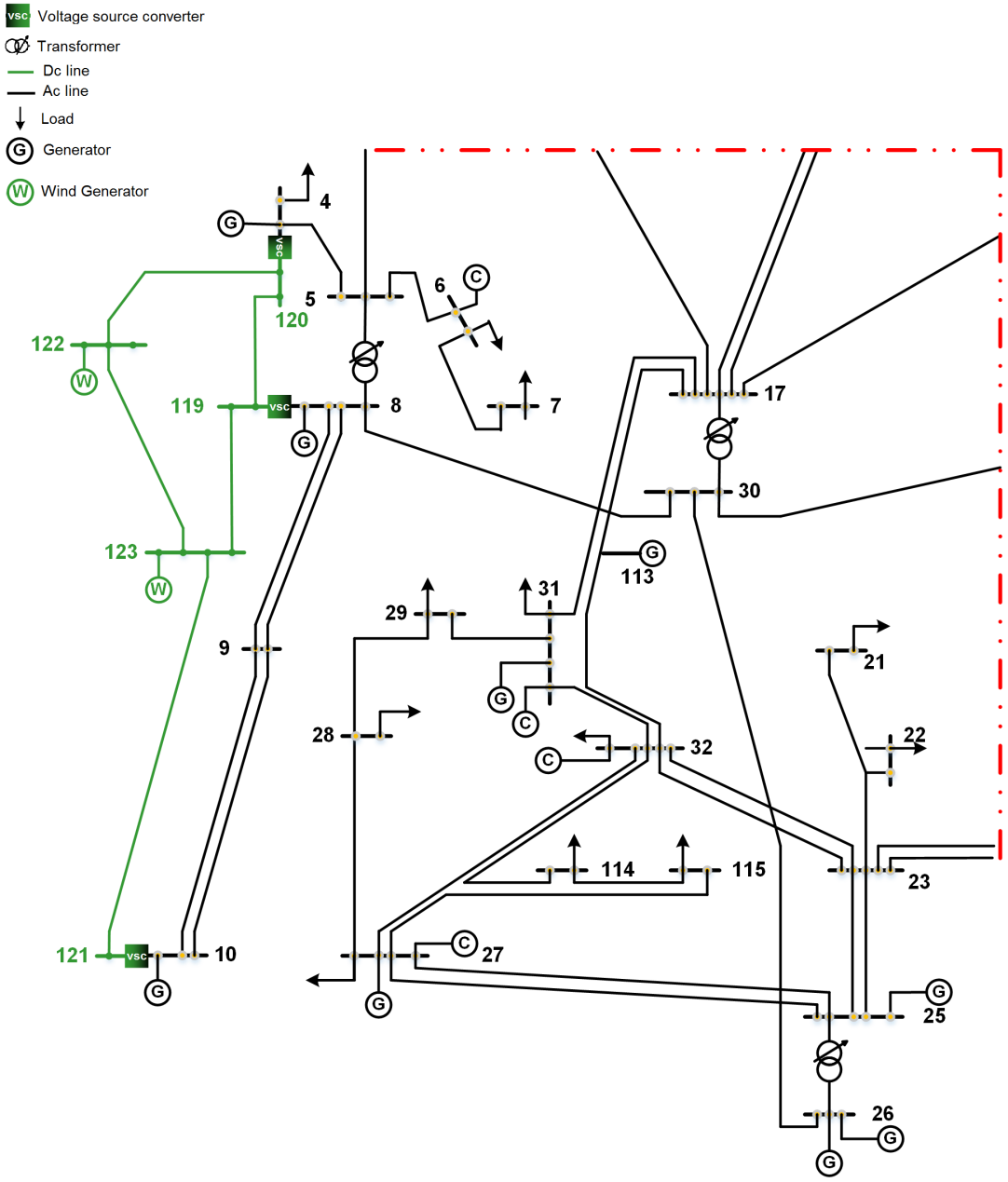

Fig. 3.5 Single-line diagram of the offshore wind farm connected with a VSC-MTDC system

Table 3.3 Centralised Scheme Simulation on Linearised SCOPF on IEEE 14-Bus System

Centralised Scheme	Total Cost ($/h)	3,774.33	
	Total Cost Breakdown		
	OPF Cost ($/h)	CC Cost ($/h)	PC Cost ($/h)
	3,541.65	232.68	0
	Contingencies that need to be controlled		
	Number of PC	Number of CC	
	0	13(L1, L2, L3, L4. L5, L6, L7, L8, L11, L13, L15, L18, G1)	

3.4.2 Redispatch Wind Generation in the MTDC System

The results in table 3.4 and 3.5 compare the performance of a dynamic droop control to that of a fixed or predefined droop scheme when available wind generation deviates from its forecast, in the distributed operation scheme.

Table 3.4 Rescheduling Result Due to Wind Generation Deviation on IEEE 14-Bus System

Systems	14-Bus System	
Droop control scheme	With dynamic power dispatching droop control	Without dynamic power dispatching droop control (fixed droop)
Redispatch solution	available	not available
Cost for redispatch ($/h)	8.65	NA

3.4.3 Analysis and Discussion

Operation Cost

First, the simulation results show that the presented method can reduce the total cost by 12.5% and 3% in the IEEE14-bus and 118-bus systems, respectively. Due to higher wind penetration and a lower demand level, the performance of the TLDSCOPF approach has a more significant advantage in the IEEE 14-bus system. The solution of the CC is computed by exploring all possible adjustments to the power injection at all buses. Although the presented method is shown to be less effective in a large-scale power system, e.g. the 118-bus system, MTDC grids can still contribute to regulating the power flow and reducing power loss.

Table 3.5 Rescheduling Result Due to Wind Generation Deviation in the IEEE118-Bus System

Systems	118-Bus System	
Droop control scheme	With dynamic power dispatching droop control	Without dynamic power dispatching droop control (fixed droop)
Redispatch solution	available	not available
Cost for redispatch ($/h)	77.1	NA

CC vs. PC

As shown in tables 3.1 and 3.2, with the TLDSCOPF approach, some pre-contingency actions can be shifted to post-contingency control and the corresponding PC cost can be eliminated. Compared to CC, which relies solely on redispatching traditional generators, integrating wind energy through MTDC grids is economically efficient as there is no extra cost incurred by redistributing renewable units in the MTDC system.

Accommodating Intermittent Generation

Another advantage of adopting dynamic droop control when dealing with random generation from the off-shore wind farms in the MTDC system is observed in tables 3.4 and 3.5. Systems with fixed or predefined droop constants have difficulty achieving a solution when faced with variations in wind power generation. However, by optimising the droop values in the presented method, MTDC grids can provide corrective support to ac systems by redistributing power flow across grids, thereby reducing control costs. It should be noted that the CC cost and PC cost shown in the tables only consider the redispatching costs that are intended to alleviate security constraint violations. The redispatching costs for covering losses of generation that do not cause system constraint violations are not included.

Centralised Operation vs. Distributed Operation

To compare the adopted distributed operation scheme with a centralised one, a centralised SCOPF is formulated and simulated. The computation results shown in tables 3.4 and 3.5 use the solution from the previous SCOPF as the reference value, and the simulation only serves to mitigate the imbalance caused by the mismatch between forecast wind generation and real wind generation in the allowed period. Also it should also be noted that the presented

algorithm does not need to consider the uncertainties of off-shore wind farm generation at the SCOPF stage. As shown in the tables 3.4 and 3.5, with fixed droop constants, the available wind energy cannot be redistributed across the entire system, which leads to infeasible solutions in the initial OPF results. The presented method shows capability in accommodating the intermittence of the renewables even though randomness is not considered in the SCOPF stage, which could contribute to mitigating operational challenges.

When comparing the hierarchically distributed method with the centralised unified method, it is observed that both approaches have their own advantages and disadvantages.

1. In the hierarchical method, the mixed ac/dc system is decomposed into an ac subsystem and a multi-terminal dc subsystem, where each level is solved individually during each step of the iterations. The structure of the problem becomes simpler, and communication and computation requirements are reduced compared to the unified approach.

2. If the MTDC subsystem and the ac subsystem are owned and operated independently by different organisations, the hierarchical method provides more flexibility to system operations in terms of communication, computation, control, etc.

3. In practical situations, for a super-large-scale interconnected power system, the dispatch interval may be insufficient for the computation time required for convergence in the presented iterative algorithm. In such situations, the algorithm has to be terminated prior to convergence. To allow intermediate termination, all iterates generated by the hierarchical method must be feasible system-wide.

4. The case study shows that, the results of the hierarchical method are almost identical to these of the unified approach. In fact, sub-optimal inputs are allowed due to computational limits. As a result, the presented formulation, though sub-optimal, achieves desired operational objectives.

3.5 Conclusion

In this chapter, the SCOPF model has been extended to incorporate a dc grid with several renewable generations. Two operation schemes were introduced for system operators, and a system redispatch scheme was proposed to facilitate wind power integration through MTDC grids. Moreover, the contingency control strategy was extended: CC and PC were compared, and a hierarchical structure was employed to promote post-contingency control in the mesh ac/dc grid.

Through a hierarchical structure where two layers (the high level is a traditional SCOPF problem and the low level is a dynamic MTDC grid power dispatching problem.) interact, an highly intuitive system redispatch scheme can be achieved. This is advantageous compared to other approaches in that it 1) takes advantage of MTDC grids' power flow regulating capability, which ensures that the meshed ac/dc systems can be operated more flexibly and cost-effectively; 2) isolates ac and dc systems, which simplifies computation procedures; and 3) makes wind power integration technically and economically available for system operations, which indicates high potential for practical applications. Moreover, despite the fact that an increasing number of MTDC systems will be commissioned in the future, the technology is still under development. Future work should focus on network topology, converter outage, and delayed information exchange, among others. Thus, the successful implementation of MTDC systems relies heavily on planning.

This chapter has also attempted to adopt a linearised OPF (dc-OPF) model and nonlinear power flow (ac power flow) check in the n-1 contingency analysis via BD techniques. Such an approach typically finds a dispatch solution from DC-OPF that does not violate any constraints in the ac power flow in contingencies. This has become a common practice widely employed by system operators.

In the next chapter, the advantages and disadvantages of adopting post-contingency controls are studied in details, and these controls are compared to pre-contingency approaches. The chapter also introduces microgrids, which are another effective method for integrating of RESs, and it presents an incentive-based mechanism to encourage the use of microgrids in contingency recovery supports.

Chapter 4

Robust SCOPF Using Multiple Microgrids for Corrective Control under Uncertainties

RESs penetrate the electricity networks at various levels and in all different forms. After introducing concepts such as power flow models and OPF, Chapter 2 introduced a framework to incorporate intermittent renewable energy generation into the electricity network operation under security consideration, via a robust SCOPF model, which adopts preventive control as the security control strategy. Given the significant growth in microgrid (MG) deployments across the world and appealing merits of CC strategies, this chapter explores the potential of using multiple MGs in supporting the main grid's security control. CC is employed to relieve post-contingency overflows by effectively coordinating system generators and multiple MGs. In addition, an incentive based mechanism is designed to encourage the MGs to actively cooperate with the main grid for post-contingency recovery in order to enhance both the reliability of supply and the security of the connected power system. This chapter is based on[73, 74].

4.1 Introduction

Power system operations require the system to stay within its security and economic constraints, and the system operator consistently manages the system to achieve an optimal balance in operations. Power blackouts are a serious problem, especially for modern societies. During a blackout event in South Australia in 2016, thousands of households were affected due to an outage affecting an interstate connector. Pre-contingency control, which

was introduced in Chapter two, is generally regarded as conservative, since contingencies are high-risk/low-probability events. Therefore, reliable and economically efficient post-contingencies have attracted enormous amount of research interest. Among all of the proposed elements, generation re-dispatch is the most direct method of post-contingency control. Several solution techniques are proposed in [75] to solve CC problems by using generation re-dispatch. The performance of the presented iterative approach is compared to other techniques and claimed to be more computationally efficient. The authors in [76] presented an optimal coordination strategy between PC and CC so that the overall estimated expected security control cost is minimised. The proposed control strategy mainly focuses on steady state overflow security and solving post-contingency with generation re-dispatch.

These aforementioned security controls rely heavily on the traditional thermal generation re-dispatch. However, relying on generation re-dispatch only as CC actions is inadequate. First, the solution region of this approach is overly tightened by slow generators ramping rate in allowing time, which leads to a limited number of CC solutions. Moreover, due to the complexity of electricity networks, the coupling constraint is normally not capped by the generator with the slowest ramping, making it difficult to determine the feasibility of the CC without studying the electric network structure. Moreover, another concern is that frequent generator ramping could lead to an increased cycling cost and a reduced lifetime of generators. To overcome these disadvantages, new elements with fast response, such as distributed energy sources , energy storage [77] and DSM [78, 79], high voltage dc, and multi-terminal high voltage dc grid [80] that was introduced in Chapter 3, have recently been explored for post contingency control actions.

Among various new methods, direct load control provides an equivalent approach to post-contingency control action, when others are not sufficient. It is usually used as a backup plan to avoid causing dramatic inconvenience for the electricity consumers. An approach using voluntary load shedding to remove the overload after contingencies is proposed in [79]. The approach manages to seek the optimal point between security and operation costs. However, the paper only focuses on the feasibility of using the voluntary load reduction as CC actions, and neglects the design of a proper incentive mechanism. Apart from direct load control and load shedding, energy storage also shows potential in remedying the overflow caused by contingencies. In [77], a CC strategy is proposed coordinating both bulk and distributed energy storage for SCOPF. Different types of energy storage are selected and then analyzsed. However, the energy storage devices are still expensive for large-scale installation. Besides these strategies, other techniques, such as high voltage dc [81] and FACT devices [82], are also used in the application of control strategies in the SCOPF. However, due to the

complex nature of electricity networks and the large size of the SCOPF problem, the existing studies normally use only single method to achieve contingency control.

Moreover, these studies only aim to propose the feasible post-contingency control solutions without discussing on the cost or incentive associated with adopting such methods, thereby posing difficulties in real execution.

In the meantime, traditional deterministic SCOPF does not consider uncertainty, thus assuming that the load is deterministic and that all generations are controllable. However, large-scale RESs such as wind and solar power are integrated into today's power grid. Various methods have been introduced to model the uncertainty into the problem, among which robust optimisation has gained popularity, as it does not require the details of the probability distribution functions of random parameters.

However, uncertainties in load demand and renewable power generation for the security control are not systematically addressed. In addition, each element in the electricity network is closely related, and it is unrealistic for system operator to make decisions regarding individual components. These considerations motive the search for alternatives, such as using multiple MGs as CC actions in post-contingency recovery. Therefore, this chapter introduces a new model to illustrate and compute the incentives and costs of multi-MGs to participate in the post-contingency control actions under uncertainty.

MG technology is recognised as a crucial platform for accommodating a high level of renewables, considering not only energy management but also instantaneous power. An MG is a cluster of interconnected loads, distributed energy resources and storage within clearly defined electrical boundaries that acts as a single controllable entity with regard to the grid [83]. MGs are an attractive solution to facilitate the most efficient utilisation of RESs, and they have enormous potential to enhance both the reliability of supply and the security of the connected power system. MGs have seen a significant growth in industrial investments in the last decade. In the US, around 124 MGs were in operation by 2015, with a total capacity of 1,169 MWs [84]. It is expected that a higher number number of MGs will be deployed in future power systems. According to a report titled 'North American Microgrids 2015: Advancing Beyond Local Energy Optimization', industry experts predict that the nation-wide MG capacity in the US will exceed 2,850MW. Not only does this incentivise a boom in the MG market, but also provides opportunities for MGs to support grid operations. In this Chapter, multiple MGs are integrated as an entity and connected to the main ac transmission grid via substations as a collected controllable connection of controllable demand, conventional demand, and energy storage. Furthermore, from the MG operator's point of view, as a whole, MGs are capable of acting as an entity that is able to provide incentive based [85] post-contingency control action when needed.

4.2 Post-Contingency Robust SCOPF with Multiple Microgrids

This chapter elevates the robust SCOPF model from Chapter 2 by examining differences between PC and CC, and focusing on using post-contingency control to alleviate overflow caused by contingencies. In addition, multiple MGs in the network are investigated to aid in the CC actions. Moreover, an ac power flow model is used to check whether the solutions are within the system operation limits, combined with a linearised power flow model in the optimal dispatch decision making stage.

4.2.1 Post-Contingency Robust SCOPF Formulating and Contingency Control Categorising

The general form of the robust SCOPF is given in (2.59)-(2.64). In particular, the coupling constraint (2.64) corresponds to the ramping limitation of the conventional generators and upper and lower limits on adjustable power injection from MGs during the allowed response time so that unrealistic changes during the post-contingency can be avoided. However, one point is slightly different in the present chapter and Chapter 3 in terms of the sub-problems formulation. In Chapter 2, the power flow model in the sub-problems uses the linearised model, so that limitations on reactive power or voltages are neglected. In this chapter and Chapter 3, ac power flow model is adopted in the sub-problem so that the solution from the master problem can be verified against voltage limits and reactive power. These considerations of more parameters also lead to a higher operation cost. This implementation will be discussed in detail in the next chapter in terms of computation efficiency, convergence and effectiveness. The variables are given as follows, where linearised power flow is adopted to formulate the optimisation problem,

$$\mathbf{z} = \begin{bmatrix} \mathbf{u} \\ \mathbf{v} \end{bmatrix} \tag{4.1}$$

$$\mathbf{u} = \begin{bmatrix} \mathbf{p_g} \\ \mathbf{p_m} \end{bmatrix} \tag{4.2}$$

$$\mathbf{v} = \begin{bmatrix} \theta \end{bmatrix} \tag{4.3}$$

where $\mathbf{p_m}$ is the vector of active power injection of MGs. The original problem (2.59)-(2.64) is decomposed into a master problem, corresponding to a base operation, and several sub-problems each representing contingency scenarios. Furthermore, during the computation, contingencies can be grouped into three different classifications, which are S_K^C, S_K^P and S_K^{Nil} respectively. Therefore, the master problem for robust SCOPF can be formulated as follows to represent the base operation.

$$\underset{u}{\text{minimise}}$$

$$f(\mathbf{x_0}, \mathbf{u_0}) \tag{4.4}$$

subject to

$$h_0(\mathbf{x_0}, \mathbf{u_0}) = 0 \tag{4.5}$$

$$g_0(\mathbf{x_0}, \mathbf{u_0}) \leq 0 \tag{4.6}$$

$$Benders\ infeasibility\ cut \tag{4.7}$$

The solution from (4.4)-(4.7) is then tested against each contingency case in the sub-problems. For each contingency k, the positive variable $r_{l,k}$ is introduced for the optimisation problem below,

Objective:

$$minimise \omega = \sum_{l=1}^{n_l} r_{l,k} \tag{4.8}$$

Subject to:

$$h(\mathbf{x_k}, \mathbf{u_k}) = 0 \tag{4.9}$$

$$g(\mathbf{x_k}, \mathbf{u_k}) \leq 0 \tag{4.10}$$

$$|\mathbf{u} - \mathbf{u_k}| \leq \Delta \mathbf{u_k} \tag{4.11}$$

$$\mathbf{u} = \mathbf{u}^* : \lambda_\mathbf{k} \tag{4.12}$$

In the each sub-problem, the dual variable $\lambda_\mathbf{k}$ and corresponding variables $\mathbf{u_k}$ and $\mathbf{x_k}$ are calculated based on the given decision regarding $\mathbf{u}^*$ from the master problem. If $\omega > 0$, a Benders cut is formed according to $\lambda_\mathbf{k}$ and added back to the master problem (4.4)-(4.7). The sub-problem then is updated in each iteration which leads to adjustments to the variables $\mathbf{u}$ and $\mathbf{x}$ in the master problem. The Benders cut can be given as follows:

$$\omega^* + \sum_{i=1}^{n_u} (u_i - u_i^*) \leq 0 \tag{4.13}$$

where n_u is the number of control variables u_i. The processes (4.4)-(4.13) are used not only to decompose a complex problem into several sub-problems for computational efficiency, but also to categorise different types of contingencies. The application of the BD into the SCOPF for contingency action determination is shown in flowchart in figure 4.1. As shown in Figure 4.1, the feasibility of S_K^C is analysed first. If a feasible solution set $(\mathbf{u_k}, \mathbf{x_k})$ exists in the sub-problem k by taking the decision variable set $(\mathbf{u_0}, \mathbf{x_0})$ from the master problem, then the contingency k can be solved by CC, thus $k \in S_k^c$. If no feasible solution is found, the Benders cuts are created and taken into the master problem for PC solutions. As shown in (4.2), the control variables include two sets of vectors. Apart from conventional generation $\mathbf{p_g}$, the active power injections $\mathbf{p_m}$ from multiple microgrids are taken into consideration as control variables, where both positive and negative power injections can be made according to the requirements for the contingency control. Therefore, in MGs' normal operation mode, each MG's energy management system (EMS) optimises the schedule of the generation and consumption within itself. If a contingency occurs, microgrids operators can offer support to the upper-level grid to alleviate the overflow caused by contingencies. Mathematically, control variables $\mathbf{p_m}$ are not considered in PC actions, and only in CC actions. Alternatively, $\mathbf{p_m}$ can be treated in the same way as $\mathbf{p_d}$ in the normal operation mode.

4.2.2 Incentive Based Post-Contingency Controls with Multiple MGs

In the post-contingency situation, the main grid system operator needs to take actions to resolve the overflow. As the active power flow on the transmission line can be seen as the composed contribution of each node injection [56], overflow caused by contingencies could traditionally be resolved by quickly changing the generation output. Various methods have been investigated for CC actions to replace relying solely on generation re-dispatch. In this section, aggregated multiple MGs are used to support CC along with conventional generators.

MG Architecture

A typical MG architecture [86] is presented in figure 4.2, including the key components uncontrollable and flexible loads, dispatchable units (e.g. diesel generator), non-dispatchable units (e.g. wind turbine and photovoltaics), and energy storage (e.g. batteries, fuel cells and electric vehicles).

A centralised EMS control through the communication system by the MG controller is adopted to perform the optimal scheduling for the entire MG. In a normal operation state, a MG provides reliable power to loads, manages the renewable generations, and coordinates all dispatchable units, flexible loads, and energy storage to achieve certain objectives, such as

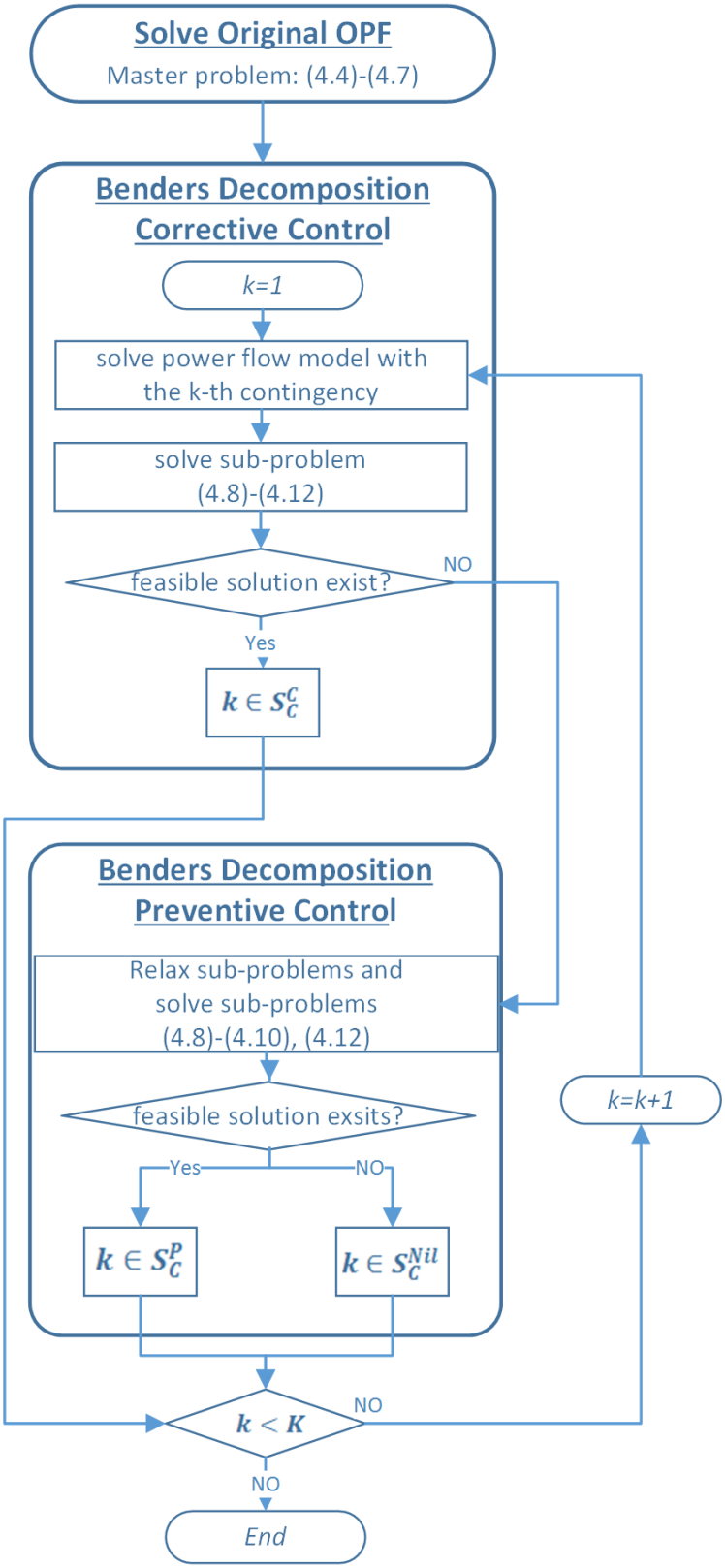

Fig. 4.1 Flowchart of the decomposition algorithm for SCOPF

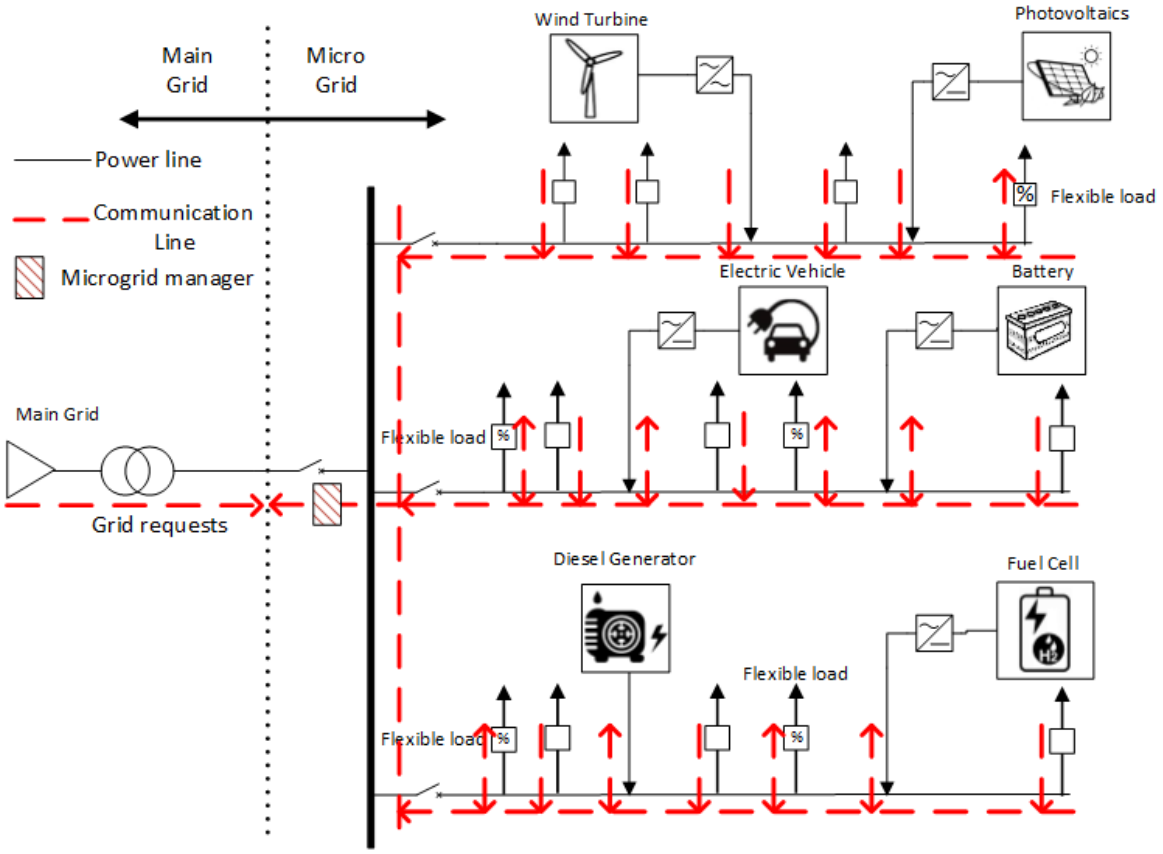

Fig. 4.2 MG architecture

minimising the operation costs or optimising social welfare. Meanwhile, the MG controller can assist the main grid, then support HV network for requested control actions. An MG can be as small as a commercial building; that is connected within a local electricity network and distribution network with one battery storage, an array of photovoltaics(PV) panels and a dedicated EMS , as shown in figure 4.3. On the other hand, it can also be the whole distribution network after the connection point from the upper-level main grid, as shown in figure 4.4. In this study, multiple MGs are aggregated to participate in providing incentive-based post-contingency control actions. It should be noted that the main grid in the figure 4.2 refers to the distribution network. However, with multiple MGs connected in each distribution network, the amount of the controllable power aggregated granularly to the transmission network is adequate to participate in security control actions. Given this consideration, this chapter develops an innovative coordinated operation methodology for networking multiple MG, optimally controlling these together with all associated power system components, including generator units, capacitor banks and on-load tap changers. The methodology intends to prevent overflow caused by current grid contingencies.

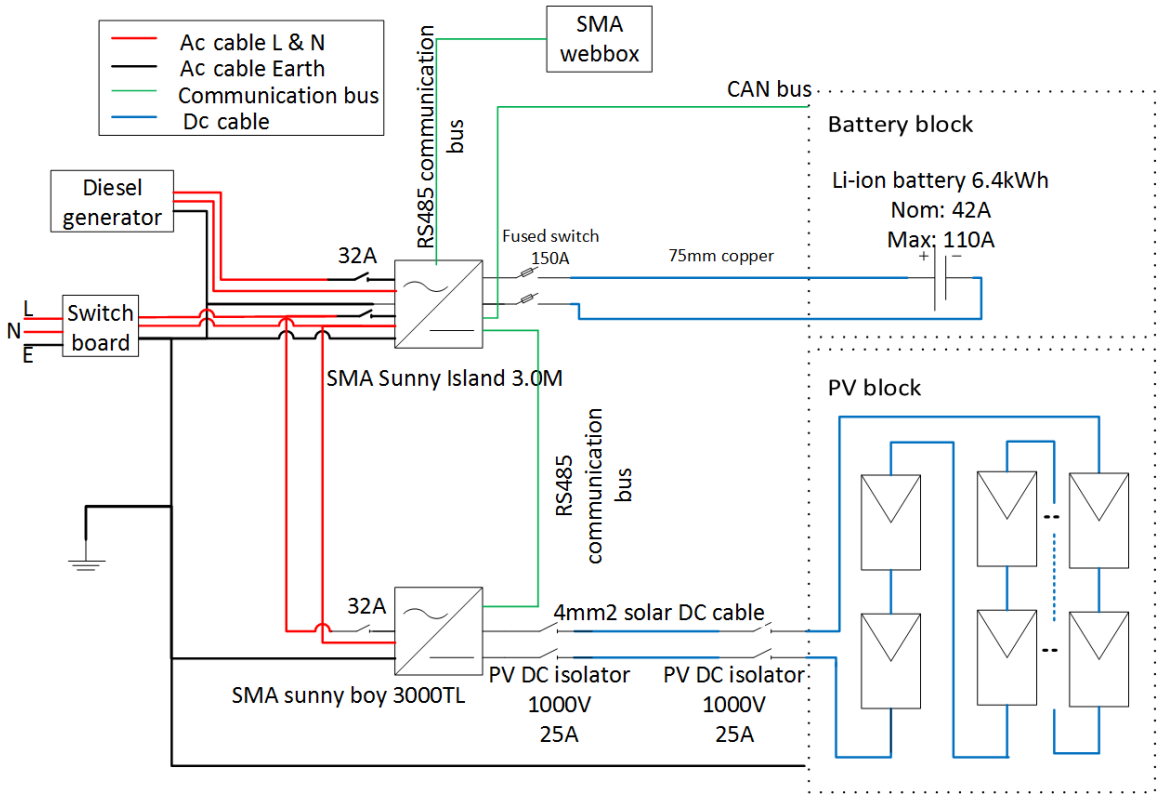

Fig. 4.3 A small household-sized MG

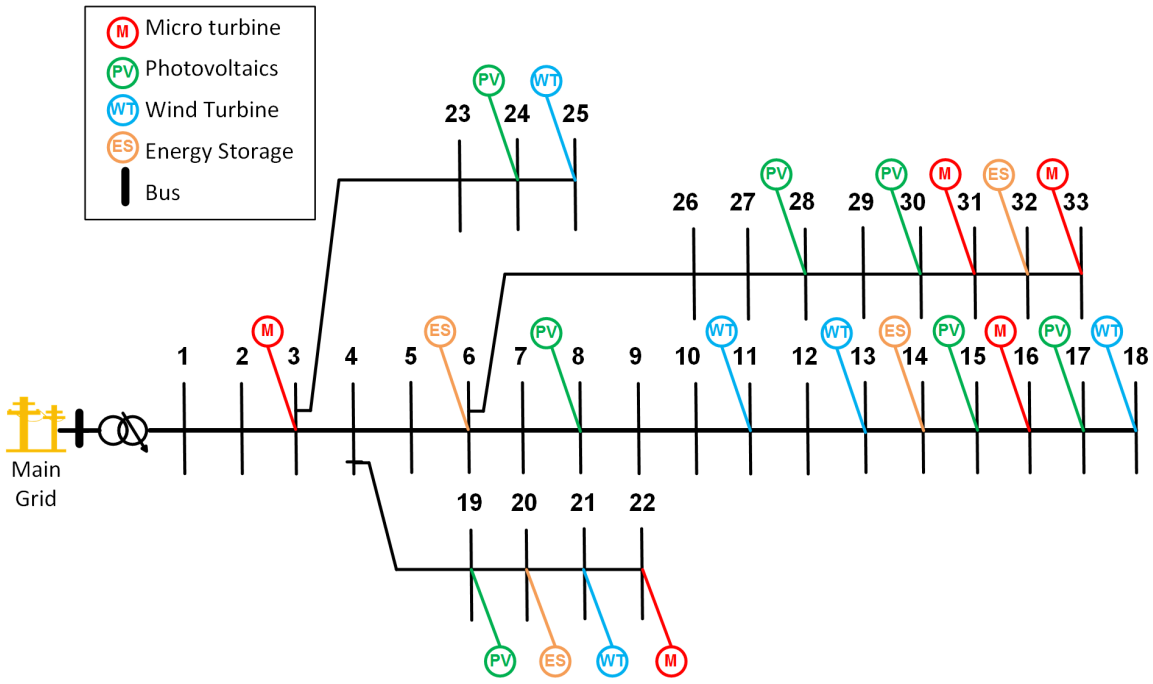

Fig. 4.4 IEEE 33-bus grid regarded as a whole MG

Incentive-Based MG Control Action

Aggregated multiple MGs provide a comprehensive yet sophisticated solution that is able to provide both reductions and increments on the connected load when required from the main grid. The interaction of coordinating multiple MGs for post-contingency control with the main grid is illustrated in figure 4.5, and its detailed mathematical model is given in this section. As illustrated in figure 4.5, if a feasible solution is found, the contingency $k \in S_K^C$, otherwise $k \in S_K^P \cup S_k^{Nil}$. For $k \in S_K^C$, the associated cost C_{cc}^k is calculated, which is the sum of the generators redispatch cost $C_{cc,g}^k$ and MGs control action cost $C_{cc,m}^k$ for each contingency $k \in S_K^C$, defined as,

$$C_{cc,g}^k = p_k \sum_{i=1}^{n_g} \alpha_{g,i} \Delta p_{g,i}^2 \tag{4.14}$$

$$C_{cc,m}^k = p_k \sum_{i=1}^{n_m} \alpha_{m,i} \Delta p_{m,i}^2 \tag{4.15}$$

The ESCC of SCOPF considering MGs for CC action is denoted as $C_{ESCC}^m = C_{cc,m} + C_{pc}^m$, where $C_{cc,m}$ is the sum of each individual CC cost by MGs actions, and C_{pc}^m is the total cost of all remaining credible contingencies can only be controlled by PC when using MGs for CC, as shown below,

$$C_{cc}^{m\&g} = \sum_{k \in S_k^c} (C_{cc,g}^k + C_{cc,m}^k) \tag{4.16}$$

$$C_{pc}^{m\&g} = \sum_{i=1}^{n_g} f(p_{g,i}) - f(\hat{p}_{g,i}) \tag{4.17}$$

where $\hat{p}_{g,i}$ denotes the conventional OPF result for generator i without considering security constraints, and $f(p_{g,i})$ is the OPF cost function, which can be in the form of (2.10). Moreover, the main grid is able to compute the ESCC of securing all credible contingencies at the generation dispatch stage, assuming that all MGs are at normal operation. In this case, only conventional generators are required for contingency controls, and all connected MGs are no allowed to participate. Therefore, from the main grid system operator's perspective, the aggregated multiple MGs are treated as load. In this case, the cost associated with contingency control can be easily computed by removing variable $p_{m,i}$ from control variable $\mathbf{u}$, and the cost can be denoted as the base case scenario cost at $C_{ESCC}^{base} = C_{cc}^{base} + C_{pc}^{base}$.

From the main grid system operator's perspective, the approach that has a lower total ESCC and more CC actions is preferred. In other words, if the $C_{ESCC}^m \leq C_{ESCC}^{base}$, the main grid system operator will accept the support from MGs and then coordinate the generators together

with MGs for post-contingency actions to achieve an overall lower contingency control cost. Regarding the MGs, when the contingency k occurs, the MG controller can determine the upper and lower limits of the power adjustment by checking the states of the available energy storage level, flexible demand, controllable generators and RESs. MGs can then provide post-contingency control actions by adjusting their power injection within the limit for contingency control support and to be paid by the main grid system operator. In equations (4.14)-(4.17), the probability of contingencies ρ_k and cost coefficients of conventional generators $\alpha_{g,i}$ are both known by the main grid system operator. The algorithm then needs to iterate on $(\Delta p_{g,i}, \Delta p_{m,i})$ while updating the cost coefficient $r_{m,i}$ in each iteration, until the criterion of $C^m_{ESCC} \leq C^{base}_{ESCC}$ is satisfied.

It should be noted that the individual MG operator defines not only the upper and lower bounds of power injection adjustments of MG i $\Delta p_{m,i}$ but also the limits on $\alpha_{m,i}$. This means that at certain stage of the iteration, any MG can refuse further reduction on the cost coefficients $\alpha_{m,i}$. Noticeably, compared to the direct load control method, the incentive-based scheme includes economic aspects in its formulation. The scheme can dynamically look into the current situation and make the economically optimal solution based on the current situation. Moreover, the incentive-based scheme enables active participation of MGs in the contingency control, and the burden of taking post-contingency control actions is shared by almost all entities in the electricity networks. In addition, as shown in figure 4.5, $\Delta p_{m,i}$, which means that changes in power injection from MG i in the post contingency control are computed by MG i. Therefore, the upper and lower limits on $\Delta p_{m,i}$ do not need to be acknowledged by the upper level grid system operator. This makes the overall incentive-based CC strategy computationally efficient.

The problem can be generalised into a quadratic problem with linear constraints as follows, assuming that branch flow adjustment vector $\Delta p_{L,l}$ is computed from the BD in SCOPF for any contingency $k \in S^C_K$. Iterate on the problem (4.18)-(4.22) and update

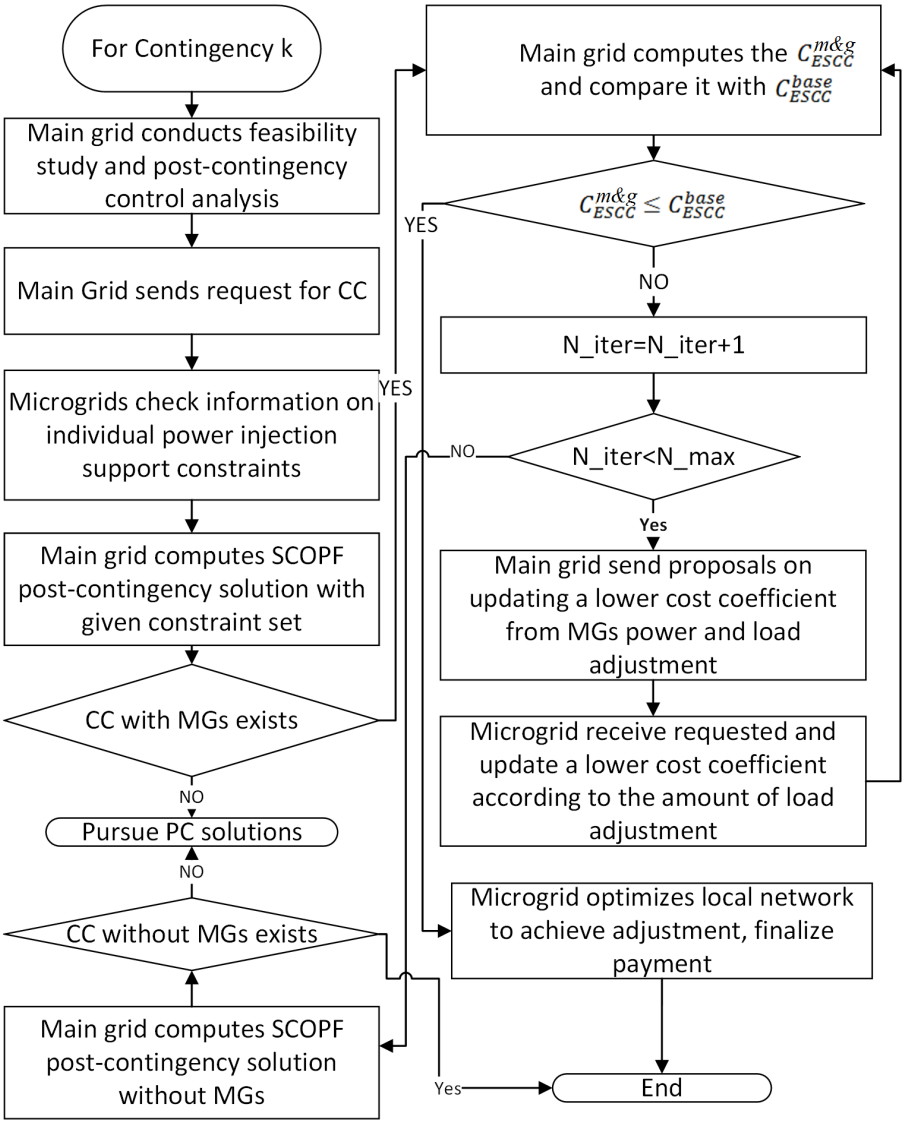

Fig. 4.5 Process of post-contingency control with MGs

$r_{m,i}, \quad \forall i = 1,2,...,n_m$ until criterion (4.23) is satisfied,

Objective:

$$min \sum_{i=1}^{n_g} \alpha_{g,i} \Delta p_{g,i}^2 + \sum_{i=1}^{n_m} \alpha_{m,i} \Delta p_{m,i}^2 \tag{4.18}$$

Subject to:

$$\sum_{i=1}^{n_g} \Delta p_{g,i} + \sum_{i=1}^{n_m} \Delta p_{m,i} = 0 \tag{4.19}$$

$$\mathbf{H}(\Delta \mathbf{p}_g + \Delta \mathbf{p}_m) = \Delta \mathbf{p}_L \tag{4.20}$$

$$p_{g,i}^{dn} \leq \Delta p_{g,i} \leq p_{g,i}^{up} \quad \forall i = 1,2,...,n_g \tag{4.21}$$

$$p_{m,i}^{dn} \leq \Delta p_{m,i} \leq p_{m,i}^{up} \quad \forall i = 1,2,...,n_m \tag{4.22}$$

and the criteria is defined as follows,

$$C_{ESCC}^{m} \leq C_{ESCC}^{base} \tag{4.23}$$

where C_{ESCC}^{base} can be pre-determined by SCOPF analysis and $\alpha_{m,i}$, C_{ESCC}^{m} are updated during each iteration. Furthermore, $\mathbf{p}_g$ and $\mathbf{p}_m$ are vectors of $\Delta p_{g,i}$ and $\Delta p_{m,i}$. $\Delta p_{g,i}$ denotes the control variable as generation ramping in the allowed time period, constrained by ramping limits or generation reserve.

4.3 Case Study

The formulated SCOPF is tested on modified IEEE 14-bus and IEEE 118-bus systems. The simulation is divided into two sub-sections. Section 4.3.1 presents the simulation results in terms of robust degree, contingency sets, and total SCOPF cost. Then based on the simulation results in that section, the incentives and cost coefficients are simulated and determined for MGs to participate in the post-contingency control actions in section 4.3.2.

4.3.1 Robust Degree, Contingency Set Categorisation and Cost Calculation

First, the results of traditional SCOPF and robust SCOPF with supports from MGs are verified and compared for the modified IEEE 14-bus and IEEE 118-bus systems, in terms of the robust degree and generation cost. The testing scenarios are generated by MCS with

50000 scenarios. The Weibull distribution is adopted for wind speed PDF, whose parameters are the same as those shown in Chapter 2.

IEEE 14-Bus System

The modified IEEE 14-bus system adopts the same configuration as in Chapter 2. Furthermore, additional information for the simulation is described. To account for the probability effect of the contingency in the problem, the probability of each contingency and the generation ramping cost of each generator are assumed to be 1% and 30 $/MW/h, respectively. The original load buses in the IEEE14-bus system are modified into nodes connected to multiple MGs. The capacity of the aggregate flexible load in the MGs on load bus $i \in n_b$ is assumed to be at 10% of the original load on bus i. Similarly, the capacity of the total dispatched energy unit is assumed to be at 10% of the original load and energy storage is 10% as well. First, the robust SCOPF and traditional SCOPF are compared in terms of operation cost and robust degree, as shown in table 4.1.

Table 4.1 IEEE 14-Bus System Robust SCOPF vs. Traditional SCOPF

Robust SCOPF	Cost ($/h)	6067.01
	Robust Degree (%)	99.47
Traditional SCOPF	Cost ($/h)	5947.11
	Robust Degree (%)	94.09

The SCOPF in table 4.1 has a higher cost compared with the SCOPF model in Chapter 2. This increase reflects making the solution more secure by considering more system constraints. Since the subproblems in this chapter adopt an ac power flow model, some solutions that were feasible with only linearised power flow become infeasible when constraints such as reactive power and voltage are taken into consideration.

The SCOPF simulation results are shown in table 4.2. The SCOPF without MG CC actions only relies on generation redispatch for post-contingency control. It is obvious that number of contingencies that can be remedied by CC actions is much lower without MG support. Since the cost coefficients for generator redispatch are known by the system operator, the cost associated with CC actions without MGs can be determined, as shown in table 4.2, where the CC cost with MG support needs to be determined, taking the CC cost without MGs as a reference.

Table 4.2 IEEE14-Bus System Contingency Control and Cost

SCOPF (with MG CC action)	SCOPF cost ($/h)	4,863.08 $+C^m_{ESCC}$		
	Cost ($/h)	S^P_K 0	S^C_K To be determined	
	Number of contingencies in each set	S^P_K Nil	S^C_K 13	S^{Nil}_K Nil
		Nil	L1, L2, L3, L4, L5, L6, L7, L8, L9, L10, L15, L16, L17, G2	Nil
SCOPF (without MG CC actions)	SCOPF cost ($/h)	5,947.11		
	Cost ($/h)	S^P_K 1,084.03	S^C_K 5.26	
	Number of Contingencies in each set	S^P_K 12	S^C_K 1	S^{Nil}_K Nil
		L1, L2, L3, L4, L5, L6, L7, L8, L9, L10, L15,L17, G2	L16	Nil

IEEE 118-Bus System

The modified IEEE 118-bus system adopts the same configuration as in Chapter 2. In addition, the probability of each contingency and the generation ramping cost of each generator are assumed to be 1% and 20$/MW/h, respectively. As for the IEEE14-bus system, the modification is applied to original load buses in the IEEE118-bus system. The capacity of aggregate flexible load in the MGs connected within the same load bus is assumed to be 10% of the original load, 20% for dispatchable energy units and 10% for energy storage devices. For the purpose of comparisons, traditional SCOPF is simulated with wind power generations equal to their capacity; the same is done for robust SCOPF, and load is the base case value.

Table 4.3 IEEE118-Bus System Robust SCOPF vs. Traditional SCOPF

Robust SCOPF	Cost ($/h)	97,340
	Robust Degree (%)	99.88
Traditional SCOPF	Cost ($/h)	108,993
	Robust Degree (%)	78.46

Table 4.4 IEEE118-Bus System Contingency Control and Cost

SCOPF (with MG CC action)	SCOPF cost ($/h)	93,280 +C^m_{ESCC}		
	Cost ($/h)	S^P_K 4,060	S^C_K To be determined	
	Number of contingencies in each set	S^P_K 3 L32, L38, G40	S^C_K 26 L8, L20, L31,L36, L71, L96, L100, L103, L105, L106, L108, L119, L129, L185; G5, G6, G11, G12, G21, G22, G25, G26, G28, G29, G37, G45	S^{Nil}_K 9 L7, L9, L113, L133, L176, L177, L183, L184
SCOPF (without MG CC actions)	SCOPF cost ($/h)	108,993		
	Cost ($/h)	S^P_K 19,770	S^C_K 0	
	Number of contingencies in each set	S^P_K 29 L8, L20, L31, L32, L36, L38, L71, L96, L100,L103, L105, L106,L108, L119, L129, L185; G5, G6, G11, G12, G21, G22, G25, G26, G28, G29, G37, G40 G45	S^C_K 0 Nil	S^{Nil}_K 9 L7, L9, L113, L133, L176, L177, L183, L184

4.3.2 Incentive of MG CC Simulation and Analysis

The simulation results of the robust SCOPF structure were presented in the section 4.3.1. It is evident that it is possible to shift contingencies from PC to CC utilising MGs as control support in the network. The incentives of the MGs to participate in the CC actions are simulated and presented in this section. As described in the section 4.2.2, the aim is to find the marginal value of the incentive price α_m \$/(MWh), at which the total ESCC can be less or equal to the ESCC of SCOPF purely relying on generators redispatch for CC actions, or $C^m_{ESCC} \leq C^{base}_{ESCC}$. The total ESCC for SCOPF is 1,089.29\$/h for the IEEE14-bus system, corresponding to 1,084.03\$/h PC cost and 5.26\$/h CC cost, while it is 19,766.42\$/h for the IEEE 118-bus system, which is entirely contributed by PC cost. Therefore, the incentive price α_m \$/MWh, at which the main grid operator would be willing to use the MG CC action,

Table 4.5 IEEE14-Bus System With MG CC Cost for Each Corresponding Contingency with Given Incentive Rate

Incentive rate ($/MWh)		247.88	
Total: ($/h)		1,040.95	
Contingency k	$C_{cc}^{m\&g}$ ($/h)	Contingency k	$C_{cc}^{m\&g}$ ($/h)
L1	202.9	L9	36.1
L2	137.5	L10	59.4
L3	106.1	L15	80.8
L4	39.7	L16	3.6
L5	47.7	L17	34.8
L7	105.3	G2	123.1
L8	63.9		

is calculated based on these values. The results of both systems are presented in tables 4.5 and 4.6 respectively.

Tables 4.5 and 4.6 indicate that as long as the cost coefficient of MG is less than 247.9$/MWh and 90.1$/MWh in the IEEE 14-bus and 118-bus systems respectively, the support from multiple MGs will be accepted and the costs are C_{ESCC}^{m}=1,040.95$/h and 9,810$/h for the IEEE14-bus and 118-bus systems respectively. Tables 4.5 and 4.6 show that for each contingency that occurs and is correctively controlled by MGs' response, MGs receive payment for their support actions. The costs listed in the tables 4.5 and 4.6 are the CC cost aggregated by the cost of generation redispatch and the cost of all MGs' actions for each contingency. It should be noted that the incentive rates given in the tables are the rates at which the main grid starts to benefit from MGs participation in terms of obtaining a reduced ESCC. The value can be used as an indicator to make pricing decisions. For the main grid, a reduced generation ramping is observed, as the generation redispatch becomes less desirable when the MGs can provide equivalent service at lower costs.

Tables 4.1 and 4.3 compare the results of robust SCOPF and traditional SCOPF. It is evident that robust SCOPF outperforms the traditional OPF in terms of robust degree, indicating that the optimal solution for robust SCOPF performs better in accommodating the uncertain-ties caused by high renewable penetration and flexible load, though with some sacrifices regarding the operation cost. Tables 4.2 and 4.4 contain information on the SCOPF cost for a system that uses MGs as CC actions and a system that does not. The costs are also broken down into costs for different types of control actions, namely CC and PC. The clearest observation is that the former system results in an increased number of CC actions, which is highly desired. Furthermore, this results in an overall reduced operating cost, because, compared to PC cost, CC cost can be determined and minimised by coordinating all possible

Table 4.6 IEEE118-bus system with MG CC cost for each corresponding contingency with given incentive rate

Incentive rate ($/MWh)		90.07	
Total: ($/h)		5754.82	
Contingency k	$C_{cc}^{m\&g}$ ($/h)	Contingency k	$C_{cc}^{m\&g}$ ($/h)
L8	490.1	L185	58.2
L20	74.2	G5	272.8
L31	63.1	G11	192.6
L71	82.6	G12	296.7
L96	56.5	G21	126.8
L100	53.5	G21	126.8
L103	260.3	G25	406.5
L105	80.7	G26	423.9
L106	69.8	G28	1196.1
L108	45.3	G29	862.3
L119	126.4	G45	204.3
L129	67.3		

mechanisms, e.g. MG, in the post-contingency stage. Based on the results from section 4.3.1, the cost coefficients for MGs in CC are determined in section 4.3.2. The incentive rates for both systems are shown in tables 4.5 and 4.6, below which the total ESCC of using MG in post-contingency control is cost efficient. Compared to the predetermined ramping cost coefficients of 30$/MW/h and 20$/MW/h for IEEE14- and 118-bus systems, respectively, 247.9$/MW/h and 90/MW/h are reasonable and appealing.

4.4 Conclusion

This chapter has presented a robust SCOPF method to facilitate MG in post-contingency control and to address the uncertain factors caused by demands and renewable generations in the system. The problem has been formulated in such a way that it can benefit from BD in the sense not only of reducing the problem size but also taking advantages of the underlying problem structure. The feasibility of using MG in post-contingency control was first studied, and then based the results a model was designed to illustrate the interaction between the main grid operator and multi-MG operators. The cost coefficient value was then determined in an iterative approach. The model and computational strategy were verified on the IEEE 14-bus and 118-bus systems. The numerical simulations have demonstrated the effectiveness of the algorithm. In addition, the computational burden can be further alleviated by facilitating the grid computation techniques since the problems can be easily decomposed. For industrial

application, as a dispatch tool, the formulated robust SCOPF method can help the system operator to enhance the system security while optimising the system's economic performance under large-scale intermittent renewable power integration and MG deployments.

Chapter 5

Computation Efficiency and Convergence Analysis

This chapter comprises two parts. The first concerns computation efficiency and convergence, which are of significant importance in the optimal dispatch decision-making process. However the SCOPF problem is normally computationally expensive if a full ac power flow model is implemented with large number of contingencies. Adding uncertainties to a complex problem makes it more complicated. A bottleneck here is not only due to the large number of variables and contingencies, but also to the scale of the problem by implementation of the uncertainties. Approaches can normally be exploited. First the issue can be tackled by applying decomposition techniques. Second, the computational burden can be eased by identifying the most efficient method for uncertainties realisation. Finally, since SCOPF with a full ac power flow model is non-linear, and non-convex, an approximation can be made so that the problem can be solved easily for global optimal. This chapter initially discusses these approaches, some of which have been employed in this thesis, while others might be beneficial in future implementation. Next, the second part discusses the issue of some convex optimisation problems requiring further smoothing when a distributed algorithm is employed. Using demand side flexibility to compensate for the uncertainties caused by the generation side is another effective method to accommodate the growing fraction of RESs in the grid, and a DSM model using social welfare optimisation is demonstrated using a fast distributed dual gradient method to improve the convergence of the algorithm. This chapter is based on [21, 58, 59, 73, 87].

5.1 Problem Complexity Analysis of SCOPF Under Uncertainties and Its Solutions

The OPF problem is the essential part of the power system, which underlines various applications in economic dispatch, unit commitment, loss minimisation, voltage regulation, planning, etc. The basic structure and several types of formulation were introduced in Chapter 2.

The SCOPF problem under uncertainties brings the scale of the OPF problem to a even higher level. Its fundamental structure is generally non-convex and NP-hard, with an enormous number of constraints and variables. The difficulties in solving the SCOPF problem can be summarised into the following three points.

1. The core of SCOPF is the ac OPF problem, which is nonconvex and NP-hard, and may have local solutions. Ongoing research on OPF solution techniques has been conduced for as long as the OPF problem has existed [88–90]. Several techniques have been applied, such as successive quadratic programs, Lagrangian relaxation, the interior points methods (IPM), and artificial intelligence. Although IPM has been widely adopted in the power system analysis for its advantages in terms of good convergence and robustness, when the scale of the problem becomes large, the method has difficulty to initialising a feasible solution, and the iteration can grow. Therefore, approximation and relaxation approaches have been proposed. The most popular approximation is the DC-OPF model or linearised OPF model, introduced in Chapter 2. Although the DC-OPF problem becomes convex and the constraints are linear, however, the disadvantages in neglecting some system and engineering constraints make it less adequate for certain tasks.

2. Another factor that makes the SCOPF under uncertainties a large-scaled problem is the large amount of security constraints and variables in an N-1 contingency analysis for security considerations. One approach to reduce the computation load is to apply the contingency filter techniques [91], since contingencies are low-probability/high-impact events. In this case, only the most severe contingencies are selected for study, so that the number of constraints and variables can be significantly reduced. However, determining the severity of a contingency for a given network can be arbitrary, applying the contingency filter therefore might avoid some high impact contingencies. Another approach is to apply the decomposition techniques so that the problem can be decomposed into several sub-problems, which can be better underline the problem structure and applied with parallel computation.

3. Finally, uncertainties caused by random variables makes the problem even more complicated by adding another dimension of variables. The problem becomes non-deterministic and the randomness of certain variables needs to be added to the decision making process.

The following provides a summary of variables for AC-OPF, AC-SCOPF, AC-OPF with uncertainties, DC-SCOPF, Robust DC-SCOPF, taking the IEEE14-bus system with two wind farms as an example.

AC OPF:

$$\mathbf{u} = [\mathbf{p_g^T}, \mathbf{q_g^T}, \mathbf{tr^T}, \varphi^{\mathbf{T}}]^{\mathbf{T}} \tag{5.1}$$
$$\mathbf{x} = [\mathbf{V}, \theta]^{\mathbf{T}} \tag{5.2}$$

AC-SCOPF

$$\mathbf{u} = [\mathbf{p_{g,k}^T}, \mathbf{q_{g,k}^T}, \mathbf{tr_k^T}, \varphi_{\mathbf{k}}^{\mathbf{T}}]^{\mathbf{T}} \tag{5.3}$$
$$\mathbf{x} = [\mathbf{V_k^T}, \theta_{\mathbf{k}}^{\mathbf{T}}]^{\mathbf{T}} \tag{5.4}$$

DC-SCOPF(Linearised SCOPF)

$$\mathbf{u} = [\mathbf{p_{g,k}}] \tag{5.5}$$
$$\mathbf{x} = [\theta_{\mathbf{k}}] \tag{5.6}$$

AC-SCOPF with Uncertainties(scenario based)

$$\mathbf{u} = [\mathbf{p_{g,k,s}^T}, \mathbf{q_{g,k,s}^T}, \mathbf{tr_{k,s}^T}, \varphi_{\mathbf{k,s}}^{\mathbf{T}}]^{\mathbf{T}} \tag{5.7}$$
$$\mathbf{x} = [\mathbf{V_{k,s}^T}, \theta_{\mathbf{k,s}}^{\mathbf{T}}, \mathbf{p_{r,s}^T}, \mathbf{p_{d,s}^T}]^{\mathbf{T}} \tag{5.8}$$

DC-Robust SCOPF

$$\mathbf{u} = [\mathbf{p_{g,k}}] \tag{5.9}$$
$$\mathbf{x} = [\theta_{\mathbf{k}}] \tag{5.10}$$

As shown in table 5.1, the number of variables increases by n_k times for security consideration and n_s for uncertainties realisation. The concerns related to the aforementioned computation difficulties are addressed one by one through Chapter 2 to Chapter 5. In particular, the robust SCOPF used in Chapter 2 has the minimum number of variables but capability

Table 5.1 Number of Variables for Several Types of Optimisation Problem Formulation

	AC OPF	AC SCOPF	DC SCOPF	AC SCOPF Uncertianties (scenario based)	DC Robust SCOPF
n_u	$2n_g + n_{tr} + n_\varphi$	$n_k(2n_g + n_{tr} + n_\varphi)$	$n_k n_g$	$n_k n_s(2n_g + n_{tr} + n_\varphi)$	$n_k n_g$
n_x	$2n_b$	$2n_k n_b$	$n_k n_b$	$n_k n_s(2n_b + n_r)$	$n_k n_b$

to consider the uncertainties that is equavalent to that of DC-SCOPF with uncertainties using a scenario based approach, which increased the number of variables by n_s times. Furthermore, the whole problem is decomposed into a master and n_k sub-problems, giving each problem a number of n_g control variables and n_b state variables. In this way, the uncertainties and securities are addressed in a computationally efficient manner.

Chapter 3 extended the model by considering the ac power flow into the SCOPF problem. Instead of formulating a whole AC-SCOPF problem, BD is employed to take advantages the problem structure, where a DC-OPF is used in the master problem for optimisation while ac power flow is used in the sub-problems for the N-1 contingency analysis for the constraints check.In this case, the problem can not only benefit from fast convergence by approximation in the OPF model, but can also check the solution solved from the approximated model with network constraints that are normally neglected by the traditional linearised OPF model.

5.2 Distributed Algorithms with Fast Convergence Rate Application in Real-Time Pricing Strategy and Convex Relaxation

Chapters 2 to 4 all examined the problems on the transmission or sub-transmission level in the scope of SCOPF considering uncertainties, which the aim of introducing an efficient way to integrate the large scaled renewable generation sources in the electricity operation, such as an hourly based OPF problem for economic dispatch. Various approaches were introduced to accommodate the uncertainties brought by both load and renewable generation sources, and a robust formulation was introduced and demonstrated in the simulation.

On the other hand, ensuring flexibility on the demand side to compensate for the uncertainties on the generation side is an alternative approach to accommodate the increasing penetration on RESs. This section introduces an optimal energy scheduling model in a real time pricing (RTP) environment [92] for DSM, and two aspects are considered:

1. The increasing penetration of distributed renewable sources in the electricity grid on the demand side has been observed in many countries. Consumers are becoming 'prosumers' [93] and the traditional 'generation follows demand' way of operation has been challenged. With the advance of smart grid application, the end users have gained more control and flexibility regarding their electricity behaviours. Therefore, a DSM model is designed to study the feasibility of 'demand follows generation' behaviour under the RTP environment.

2. A social welfare model is used to simulate the consumers' behaviours. Since some information on consumer consumption, such as upper and lower limit of consumption in a certain time frame and individual consumption preference at each time slot, is only known by the consumers, a centralised algorithm is not suitable in this case. Therefore, a distributed algorithm is applied to find the optimal solution. However, the model is not strongly convex and therefore when the distributed algorithm is applied, the gradient method suffers from a slow convergence rate. A convex relaxation and smoothing technique is introduced to improve the convergence, and the convergence analysis is provided.

5.2.1 Background

The increasing penetration of RESs has been evidently increasing the risk of reliable electricity grid operation. In recent years, the increasing pressure on the power grid has also been caused by the rising peak load demand, which is partly due to the rapid growth in the use of air conditioners and other appliances, as well as the introduction of some new types of demand to the grid, e.g. plug-in electric vehicles (EVs). Moreover, the increasing amount of renewable generations is not always capable of providing support to reduce the peak load. This problem was observed back in 2013, when California's grid operator CAISO released a report on how the growth of solar power was going to change the state's energy balance over the coming years. In this report, the famous 'duck curve', shown in figure 5.1, drew enormous attention. This graph illustrates a deep drop in the net load around noon, which is driven by a large amount of PV power injected into the grid, followed by a sharp ramp-up from the late afternoon until the early night time, when PV power fades as residents start to come home from work and to consume electricity at the same time. It should also be noted that peak demand occurs only a limited number of times per year. Thus, many new assets are in fact idle and operated at a mere fraction of their capacity. For example, in the US, 10%–20% of electricity costs are determined by peak demand summing up to only 100 hours

annually. In the Australian National Electricity Market (NEM), around 20%–30% of the $60 billion of electricity network capacity is operated for no more than 90 hours per year.

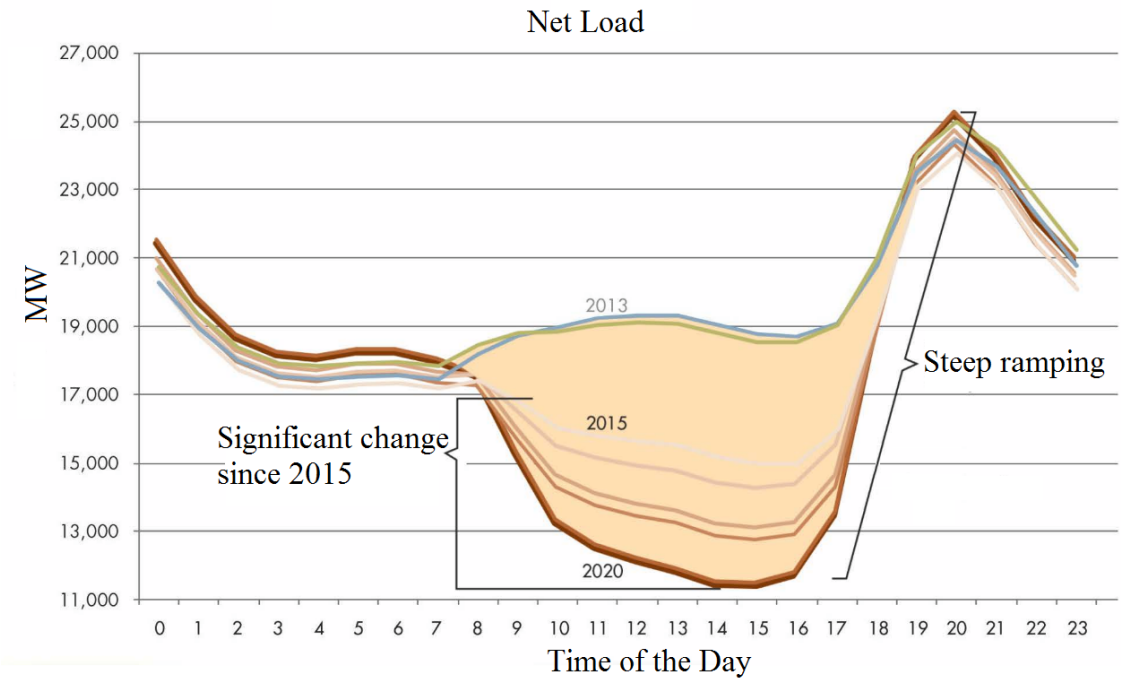

Fig. 5.1 The duck chart, showing a deep midday drop in net load and a steep ramp-up starting in the late afternoon and extending into evening peak load; the observation of oversupply risks is attributable to variable generation resources[7]

To tackle aforementioned issue, DSM has been developed and employed. DSM includes manifold programs depending on the different electricity markets and policy. Time-of-use pricing (TOU) [94] is a popular scheme. In gneral, under this scheme, electricity is priced with different rates for different time periods, normally 2 to 5 periods, such as peak, shoulder and off-peak hours. The prices are predetermined and typically adapted on a monthly or seasonal basis, so as to capture consumers' expected demand. However, the main drawback of the TOU scheme is that the prices are set well in advance, and cannot be adjusted to capture an actual situation if the demand changes widely from the expected values. It is known a large number of users tend to favour consumption when the price is cheap, consequently resulting in a new peak. This phenomenon is called the 'rebound effect'.

An alternative to TOU is the RTP. In this scheme, prices are not predetermined and are adapted to each time slot, typically an hour. The price can be increased when the demand rises, and lowered when the demand drops. In other words, if an increasing number of users begin tend to consume electricity (the rebounding effect is about to start), the price

will rise accordingly and thus mitigate the 'rebounding effect'. This scheme can reflect the current conditions and effectively capture the actual demand. Therefore, the RTP scheme can overcome the disadvantage of TOU. Mohsenian-Rad et al. [92, 95, 96] proposed innovative models for RTP. Their models have received much attention and citations in the last several years. In general, these models aim to maximise the aggregated welfare for users while minimising the cost for the energy provider through an optimal RTP strategy. Furthermore, based on Mohsenian-Rad et al' models, some extended models have been proposed for different applications. For sintance, Chai et al. extended this work to a two-level game model given for multiple utility companies [97]. The authors argue that the equilibrium points can be achieved in games formulated between users and utility companies through distributed algorithms. A load scheduling strategy is proposed in [98], where the RESs and storages are installed. The problem is again solved in a distributed fashion. Study [99] extends the work by considering load uncertainty in the optimisation constraints. Similar schemes can also be found in [100, 101].

In general, these models [92, 95–101] are concave maximisation problem and can be solved by using the IPM in a centralised fashion to obtain global optimal solutions if all parameters are known to the energy provider. However, when these models are applied in practice such as the optimal RTP problems, it is difficult to collect the parameters of all households due to privacy concerns. Moreover, when the user number is large, centralised techniques may not be feasible. Instead, a distributed sub-gradient algorithm is widely applied [92, 95–101]. This algorithm simulates the dynamic behaviours between users and the energy provider, and finally converges to an equilibrium point. Furthermore, the smart grid environment with two-way communication networks provides such a platform for the bi-directional information exchange between customers and the energy provider. In general, a one-day operation can be divided into several time slots. For example, a one-hour-based time slot is often adopted. The price for each time slot is computed in real-time and then has to be announced at the beginning of each time slot. However, there are still some problems that require further discussion. For example, it is unknow that whether the equilibrium point is unique or the same as the solution from the centralised algorithm (IPM). On the other hand, during the optimising process, although the distributed sub-gradient algorithm [102] is widely used in many RTP models to achieve an optimal solution, this algorithm in fact suffers from a slow convergence and numeric sensitivity to the step size, or even from non-convergence. More specifically, the step size parameter in the distributed algorithm has a strong impact on the convergence rate. In practice, it is difficult to adapt the step size efficiently because oscillation occurs when the step size is big, while convergence becomes too slow when the step size is small.

5.2.2 Problem Formulation

Let $\mathscr{N}$ denote the set of consumers who subscribe to an energy provider where $N \triangleq \mathscr{N}$. A whole-day cycle is divided into T time slots, where $T \triangleq \mathscr{T}$. On the customer side, the appliances are categorised into two types, deferrable and non-deferrable. For each user $i \in \mathscr{N}$, let x_i^t denote the user i_u's consumption in time slot t, where x_i^t satisfies $\underline{x_i^t} \leq x_i^t \leq \overline{x_i^t}$. $\underline{x_i^t}$ and $\overline{x_i^t}$ denote the minimum and the maximum consumption in time slot t of user i_u, respectively. The minimum consumption is the summation of all consumption from non-deferrable appliances. The maximum consumption represents the total consumption of all appliances. Denote set $I_{p,i}^t = [\underline{x_i^t}, \overline{x_i^t}]$.

User's Utility Function

Each user is assumed to behave independently to various prices and to have different preferences for energy demand. The concept of utility function $U(\mathbf{x}, \xi)$ from microeconomics is used to describe users' different responses and represents the satisfaction obtained from consuming $\mathbf{x}$ amount of energy. Herein, ξ is a parameter specifying each user's preference of each user and may vary in different time slots. In general, the following utility function is widely adopted,

$$U(x,\xi) = \begin{cases} \xi x - \alpha x^2 & if \quad 0 \leq x \leq \frac{\xi}{\alpha} \\ \frac{\xi^2}{2\alpha} & if \quad x \geq \frac{\xi}{\alpha} \end{cases} \tag{5.11}$$

Provider's Utility

The energy provider's cost function $C_t(L_t)$ describes the cost of providing L_t units of energy to its subscribers in time slot t. In general, the cost function should fulfil the properties described below. Characteristics: The cost function is strictly convex and increases with the provided capacity, for example the cost function that has been used for OPF throughout this thesis:

$$C(L) = aL^2 + bL + c \tag{5.12}$$

where $a > 0, b \geq 0 and c \geq 0$. In the time slot t, denote set $J_t = [J_t^{min}, J_t^{max}]$, where $J_t^{min} = \sum_{i=1}^{n} \underline{x_i^t}$ and $J_t^{max} = \sum_{i_u=1}^{n} \overline{x_i^t}$

Objective Function Formulation

The interactions between the energy provider and its customers can be formulated as optimisation problems in various models based on different scenarios. To identify the common features of these models, three typical models are reviewed briefly in the following. A generalised comprehensive model is then described.

For each time slot t, the objective is to maximise the sum of the utility functions of all users and minimise the cost imposed on the energy provider. Mathematically, this can be expressed as:

Objective:

$$maximise \sum_{i_u=1}^{N} U(x_i^t, \xi_i^t) - C_t(L_t)$$

Subject to:

$$\begin{aligned} &\sum_{i_u=1}^{x_i^t} = L_t \\ &x_i^t \in [\underline{x_i^t}, \overline{x_i^t}] \\ &L_t \in [J_t^{min}, J_t^{max}] \end{aligned} \tag{5.13}$$

The constraint indicates that the aggregated load of all users should be equal to the generation of the energy provider at each time slot t. As mentioned in the introduction, the parameters $\underline{x_i^t}$, $\overline{x_i^t}$ and ξ_i^t are private information for each user. It is difficult for the energy provider to solve this problem with a centralised algorithm. Alternatively, the primal problem can be transformed into its dual problem. The Lagrangian function of problem (5.13) can be written as follows:

$$\mathscr{L}(x, L_t, \lambda^t) = sum_{i \in \mathscr{N}}(U(x_i^t, \xi_i^t) - \lambda^t x_i^t) + \lambda^t L_t - C_t(L_t) \tag{5.14}$$

where λ^t is the Lagrangian multiplier, often used to indicate the electricity rate of a given time slot. Then the primal problem can be transformed into:

$$\mathscr{D}(\lambda^t) = \max \mathscr{L}(x, L_t, \lambda^t) \tag{5.15}$$

and the dual problem is:

$$\min_{\lambda^t \in \Re} \mathscr{D}(\lambda^t) \tag{5.16}$$

According to the distributed sub-gradient algorithm, at the beginning of each time slot t, the energy provider randomly generates a price λ^t and sends it to each user. All users and the provider can determine their optimal x_i^t and L_t, by solving the following sub-problems.

$$\max_{x_i^t \in I_{p,i}^t} U(x_i^t, \xi_i^t) - \lambda^t x_i^t \tag{5.17}$$

$$\max_{L_t \in J_t} \lambda^t L_t - C_t(L_t) \tag{5.18}$$

Then each user sends his or her own load information, i.e. x_i^t, back to the provider. Thus, the user's private information is not revealed. If the total load from users, i.e. $\sum_{i \in \mathscr{N}}$, is different from the generation L_t, the provider applies the following iterative rule (5.26) to update the price.

$$\lambda_{\tau+1}^t = \zeta_\tau^t - \gamma \frac{\partial \mathscr{D}(\lambda_\tau^t)}{\partial \lambda_\tau} \tag{5.19}$$

$$= \lambda_\tau^t + \gamma \Big(\sum_{i \in \mathscr{N}} (x_i^{t,*}(\lambda_\tau^t) - L_t^*(\lambda_\tau^t)) \tag{5.20}$$

where $x_i^{t,*}(\lambda_\tau^t)$ and $L_t^*(\lambda_\tau^t)$ are the optimal solutions for a given price λ_τ^t by solving (5.17) and (5.18) respectively at the τ_{th} iteration and γ is the step size. The equation (5.26) illustrates the process of computing the optimal RTP. Once the difference between $\sum_{i \in \mathscr{N}} x_i^t$ and L_t is less than a preset small quantity ε, the algorithm terminates and converges to an equilibrium point. The final announced price is the optimal one for that time slot. Parameter τ is the number of iterations, which indicates the amount of information exchange between users and the provider. The RTP scheme requires that the final price must be announced at the beginning of each time slot. Thus, a short period of computation time is important in a practical situation. Figure 5.2 below illustrates convergence performances when different step sizes γ are selected.

It is clear that when a suitable step size γ is selected, the convergence rate can be fast. For instance, at time slot t=18, the number of iterations is around 350 when the step size is selected as 0.06. However, if the step size is not chosen wisely, there could be more than 700 iterations, with a step size of 0.0001, or even non-convergence for 0.007, as shown in figure 5.2. Thus, an inappropriate step size can lead to the failure of the implementation of RTP. However, there is no effective way to determine the step size. Furthermore, a step

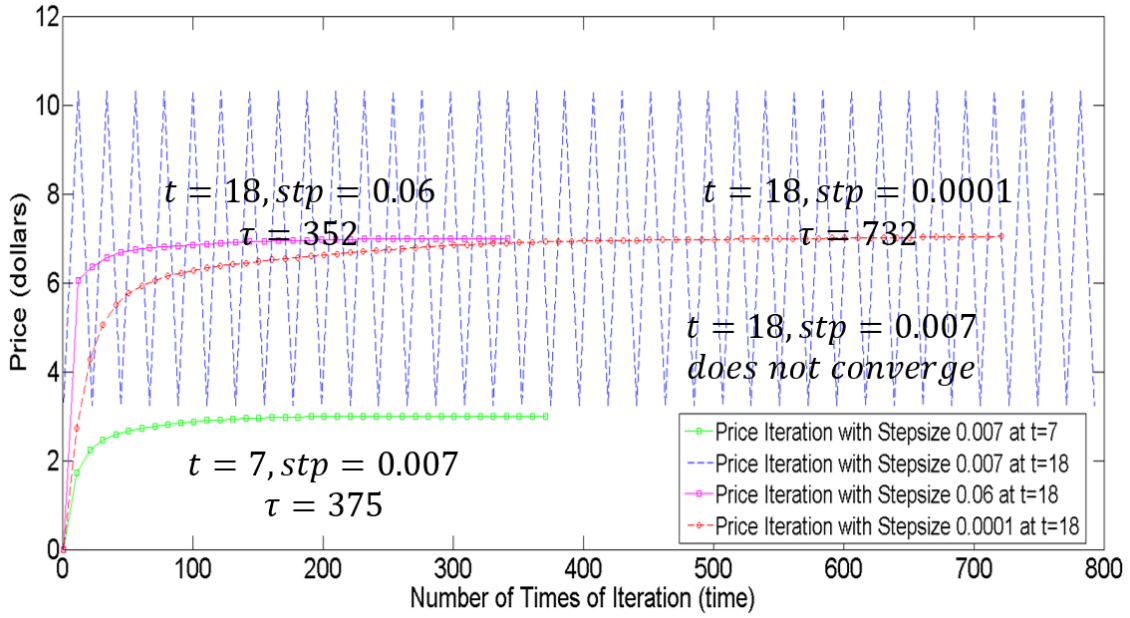

Fig. 5.2 Different computation times of sub-gradient projection method by using different time slots and step sizes

size that is suitable for one time slot may be inappropriate for another one. For example, at time slot t=7, the iteration stops after 375 times when the step size of 0.007 is selected. However, when the same step size is applied to the time slot t=18, the iteration does not converge. This result indicates that for each time slot, a new and appropriate step size γ needs to be determined. This requirement makes the distributed sub-gradient algorithm difficult in practical application. To overcome this disadvantage, an efficient and self-tuned algorithm with a fast convergence rate is imperative. Although the above algorithm has its defect, the distributed manner can allow the energy consumers and the provider to pursue their welfare optimisation individually. All in all, these kinds of innovative models have drawn dramatic attention.

Comprehensive Model for DSM in an RTP Environment Using Distributed Algorithm

In this section, a comprehensive model is introduced that can be used to express the energy scheduling RTP problems. In this model, diverse schemes can be formed according to different requirements. Moreover, a criterion is derived to guide the design of these schemes so that the optimal solution obtained from a distributed method is globally optimal. First, the

users' welfare function can be defined as,

$$W_i(x_i^t) = U(x_i^t, \xi_i^t) - \lambda^t x_i^t \tag{5.21}$$

and the energy provider's welfare function is defined as,

$$W(L_t) = \lambda^t L_t - C_t(L_t) \tag{5.22}$$

Both $W_i(x_i^t)$ and $W(L_t)$ are concave and coupled with the dynamic price signal λ^t. Normally, most energy scheduling problems can be generalised as different interactions among users and the energy provider. Thus the process of a comprehensive model can be illustrated in figure 5.3. According to the presented comprehensive model, different energy scheduling

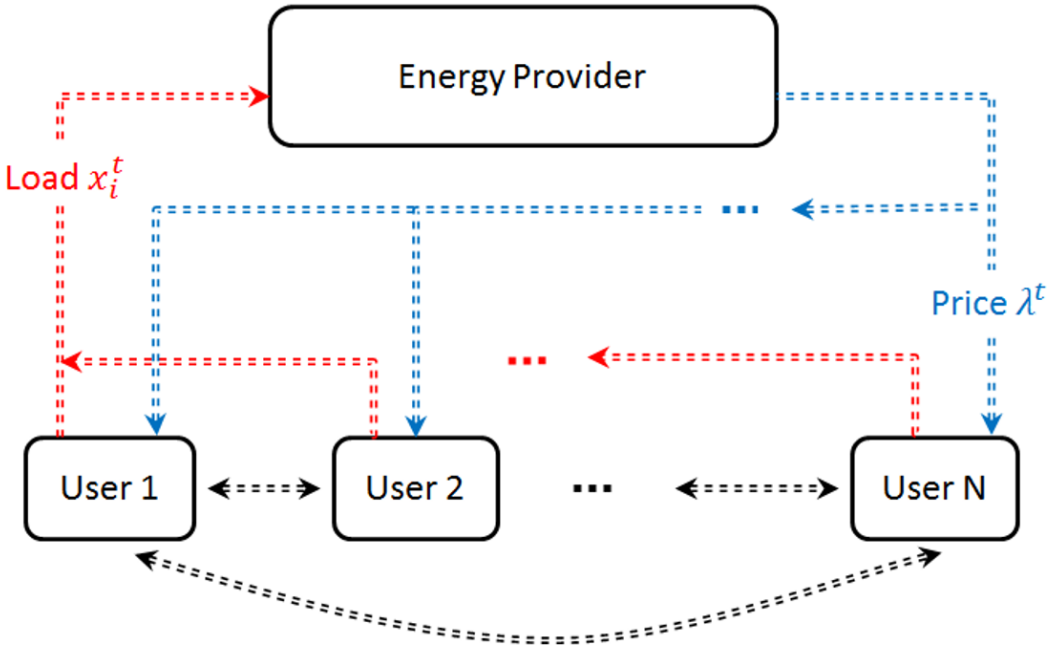

Fig. 5.3 The blue and red lines represent the information exchange, where users send their own consumptions and the energy provider announces the price signal

schemes can be generated based on different problems by using the forms of (5.21) and (5.22). For example, by simply combining (5.21) and (5.22) to achieve social welfare, model (5.13) and its equivalent (5.14) can be formed. In general, no matter how these models are designed, the following criterion is provided, which is able to guarantee that the optimisation solution achieved from a distributed method is equivalent to the optimal solution computed using a centralised method.

Model Design Criterion: The objective functions based on the welfare functions (5.21) and (5.22) for the designed model should be convex subject to coupling linear constraints. The optimal solution is existence and uniqueness. The detailed proof can be found in [103].

It is important to note that the iterative rule used in a distributed way suffers the step size and convergence issues. To address these issues, the following introduces a new distributed algorithm that can guarantee a fast convergence. This innovative algorithm can be applied to many energy scheduling RTP problems that fall within the scope of the presented comprehensive model.

5.2.3 Fast Distributed Dual Gradient Algorithm

It is observed that the main reason for the previous issue is that the dual function $\mathscr{D}(\lambda_t)$ or the payoff function is generally non-differentiable in general. In other words, the maximization problems have multiple optimal points for a given λ_t. Thus, unlike from the ordinary gradient method, the sub-gradient method is not always descent during the process. The function value may increase in some cases, resulting in a slower convergence rate. To accelerate the convergence so that the algorithm could be more efficient for the presented model, in this thesis the dual objective is smoothed twice and then becomes a strongly convex and differentiable function. In this case, an accelerated gradient algorithm can be utilised to solve the smoothed dual problem. In theory, the gradient algorithm is faster than the sub-gradient method.

Without the loss of generality, herein (5.13) is applied as a basic model composed from the presented generalised forms (5.21) and (5.22) to illustrate the effectiveness and efficiency of the presented fast distributed dual gradient algorithm(FDDGA). In General, the model (5.13) can be rewritten as:

Objective:

$$\max_{x_i^t \in I_{p,i}^t, L_t \in J_t} W(x_i^t, L_t) \triangleq \sum_{i \in \mathscr{N}} W_i(x_i^t) + W(L_t)$$

Subject to:

$$\sum_{i \in \mathscr{N}} x_i^t = L_t \tag{5.23}$$

and its dual objective function can be written in the following form:

$$\mathscr{D}(\lambda_t) = \sum_{i \in \mathscr{N}} \max_{x_i^t \in I_{p,i}^t} W_i(x_i^t) + \max_{L_t \in J_t} W(L_t) \quad \forall t \in \mathscr{T} \tag{5.24}$$

Therefore the primal problem has been transformed into solving the dual problem, i.e. $\min_{\lambda^t>0} \mathscr{D}(\lambda^t)$, to find the optimal solution λ^{t*} for each time slot $t \in \mathscr{T}$, independently. The optimal consumption x_i^{t*} and L_t^* can then be solved according to each given λ^{t*}. As was mentioned in the previous section, the problem (20) can be solved by the distributed method, and theλ^{t*} can be achieved as follows,

$$\lambda_{\tau+1}^t = \lambda_\tau^t - \gamma \frac{\partial \mathscr{D}(\lambda_\tau^t)}{\partial \lambda_\tau} \tag{5.25}$$

$$= \lambda_\tau^t + \gamma(\sum_{i\in\mathscr{N}} (x_i^{t,*}(\lambda_\tau^t) - L_t^*(\lambda_\tau^t)) \tag{5.26}$$

In the next section, the smoothing technique will be applied to improve objective functions. In this way, the convergence rate can be improved and the difficulty in step size selection can be eliminated.

Smoothing

It is important to note that the dual objective $\mathscr{D}(\lambda_t)$ is non-smooth because the maximization problem defined in (5.24) has multiple optimal solutions for a given λ^t. To guarantee the uniqueness of the optimal solution for each $\lambda^t \geq 0$, a natural method is to modify the optimisation problem $\mathscr{D}(\lambda_t)$ by smoothing approximately the objective $\mathscr{D}(\lambda_t)$. For any parameter $\mu > 0$, the dual objective $\mathscr{D}(\lambda_t)$ is smoothed as follows.

$$\mathscr{D}(\lambda_t) \triangleq \sum_{i\in\mathscr{N}} \max_{x_i^t \in I_{p,i}^t, L_t \in J_t} (W_i(x_i^t) + W(L_t) - \mu \sum_{i\in\mathscr{N}} p_i(x_i^t) - \mu p_t(L_t)) \quad \forall t \in \mathscr{T} \tag{5.27}$$

Using (5.21) and (5.22) in (5.27), we have,

$$\mathscr{D}(\lambda_t) \triangleq \sum_{i\in\mathscr{N}} \max_{x_i^t \in I_{p,i}^t} (U(x_i^t, \xi_i^t) - \lambda^t x_i^t - \mu p_i(x_i^t)) + \max_{L_t \in J_t} (\lambda^t L_t - C_t(L_t) - \mu p_t(L_t)) \tag{5.28}$$

where $p_i(\bullet)$ and $p_t(\bullet)$ are proximity functions with convex parameters $\sigma_i > 0$ and $\sigma_t > 0$ respectively, introduced by [104]. After the improvement, each feasible set $I_{p,i}^t$, $i \in \mathscr{N}$ equipped with a proximity function p_i which has a convexity parameter $\sigma_i > 0$. Moreover, it is assumed that $0 \leq d_i := \max L_t \in J_t p_i(x_i^t) < \infty$. The feasible set J_t is also equipped with a prox-function $p_t()$ which has a convexity parameter $\sigma_t > 0$. Furthermore, $0 \leq d_t := \max L_t \in J_t p_t(L_t) < \infty$. Since $p_i(x_i^t)$ is continuous on the feasible set $I_{p,i}^t$ and the objective function $\mathscr{D}(\lambda_t)$ defined in (5.27) is separable in x_i^t and L_t, denote $x_i^t(\lambda^t)$ and $L_t(\lambda^t)$ by the unique optimal solution of the maximization problem (5.28) in x_i^t and L_t, respectively. The following lemma shows useful properties of $\mathscr{D}(\lambda_t)$, whose proof can be found in [104, 105].

Lemma 1 The function $\mathscr{D}(\lambda_t)$ has the following properties:

1. $\mathscr{D}(\lambda_t)$ is convex and continuously differentiable on $\lambda^t > 0$
2. Its gradient $\triangledown \mathscr{D}_\mu(\lambda^t) = -(\sum_{i\in\mathscr{N}} x_i^t(\lambda^t) - L^t(\lambda^t))$ is Lipschitz-continuous with Lipschitz constant $L_\mu = \sum_{i\in\mathscr{N}} 1/(\mu\sigma_i) + 1/(\mu\sigma_t)$; and
3. $\mathscr{D}_\mu(\lambda_t) \leq \mathscr{D}(\lambda_t) \leq \mathscr{D}_\mu(\lambda_t) + \mu(\sum_{i\in\mathscr{N}} d_i + d_t)$, $\forall\lambda \in \Re_+^m$

Remark 1: If function $W(L_t)$ defined in (5.22) is taken, there is no need to apply the smoothing to $W(\bullet)$ in the function $\mathscr{D}(\lambda_t)$, since $C_t(L_t)$ is strongly convex.

Second smoothing is applied to $\mathscr{D}_\mu$, which allows the use of a fast gradient method with a good convergence rate for the decrease of $\left\|\triangledown \mathscr{D}_\mu(\bullet)\right\|$. Therefore, a strongly convex function $\frac{\upsilon}{2}\|\bullet\|^2$ to $\mathscr{D}_\mu$ is simply added for a scalar $\upsilon > 0$, which is a special case of prox-function. It should be noted that the second smoothing is motivated by [104]. Thus we have the following objective function is obtained:

$$\mathscr{D}_{\mu,\upsilon}(\lambda^t) := \mathscr{D}_\mu(\lambda^t) + \frac{\upsilon}{2}\left\|\lambda^t\right\|^2 \tag{5.29}$$

Similarly, the new dual objective function $\mathscr{D}_{\mu,\upsilon}(\lambda^t)$ has the following good properties [104].

Lemma 2: For the function $\mathscr{D}_{\mu,\upsilon}(\lambda^t)$,

1. $\mathscr{D}_{\mu,\upsilon}(\lambda^t)$ is υ-strongly convex and continuously differentiable on λ^t; and
2. Its gradient $\triangledown \mathscr{D}_{\mu,\upsilon}(\lambda^t) = \triangledown \mathscr{D}_\mu(\lambda^t) + \upsilon\lambda^t$ is Lipschitz continuous with Lipschitz constant $L_{\mu,\upsilon} = L_\mu + \upsilon$.

The section now focuses on solving the optimisation problem below

$$\min_{\lambda^t\in\Re} \mathscr{D}_{\mu,\upsilon}(\lambda^t) \tag{5.30}$$

FDDGA

An FDDGA to solve the problem (5.30) is presented. The algorithm can be described as follows:

FDDGA

Initialisation: Set $\lambda^{t,0} = \varkappa^{t,0} =: 0 \in \Re$; and compute $\beta = \frac{\sqrt{L_{\mu,\upsilon}}-\sqrt{\upsilon}}{\sqrt{L_{\mu,\upsilon}}+\sqrt{\upsilon}}$

iteration for $\tau \leq 0$, execute the following steps:

Step 1. Broadcast the price $\lambda^{t,\tau}, \varkappa^{t,\tau}$

- **Capacity update** for energy provider

$$L_{t,\tau} = \arg\max_{L_t \in J_t} W(L_t) = \arg\max_{L_t \in J_t} \varkappa^{t,\tau} L_t - C_t(L_t) \tag{5.31}$$

- **Load update** of each user $i \in \mathscr{N}$.

$$\begin{aligned} x_i^{t,\tau} &= \arg\max_{x_i^{t,\tau} \in I_i^t} W_i(x_i^t) - \mu p_i(x_i^t) \\ &= \arg\max_{x_i^{t,\tau} \in I_i^t} -\varkappa^t x_i^t - \mu p_i(x_i^t) \end{aligned} \tag{5.32}$$

Step 2. Collect $L_{t,\tau}$ and $x_i^{t,\tau}$, $\forall i \in \mathscr{N}$, and compute:

$$\nabla \mathscr{D}_\mu(\varkappa^{t,\tau}) = -(\sum_{i \in \mathscr{N}} x_i^t - L^t) + \upsilon \varkappa^{t,\tau} \tag{5.33}$$

Piece update with two steps:

$$\lambda^{t,\tau+1} = \varkappa^{t,\tau} - \frac{1}{L_{\mu,\upsilon}} \nabla \mathscr{D}_{\mu,\upsilon}(\varkappa^{t,\tau}) \tag{5.34}$$

$$\varkappa^{t,\tau+1} = \lambda^{t,\tau} + \beta(\lambda^{t,\tau+1} - \lambda^{t,\tau}) \tag{5.35}$$

Step 3. If the given stopping criteria is satisfied, then terminate at τ:

1. Dual variables satisfies $\left|\lambda^{t,\tau+1} - \lambda^{t,\tau}\right| \leq \varepsilon$
2. Primal objective function value satisfies:

$$\max\left\{\max_{i \in \mathscr{N}} \left|\frac{W_i(x_i^{t,\tau+1}) - W_i(x_i^{t,\tau})}{W_i(x_i^{t,\tau})}\right|, \left|\frac{W(L_{t,\tau+1}) - W(L_{t,\tau})}{W(L_{t,\tau})}\right|\right\} \leq \varepsilon; \tag{5.36}$$

3. Primal feasibility satisfies

$$\left|\sum_{i \in \mathscr{N}} x_i^{t,\tau+1} - L_{t,\tau+1}\right| \leq \varepsilon \tag{5.37}$$

Terminate

Here Theorem 1 is provided; its convergence is given in Appendix

Theorem 1:

For any given accuracy $\varepsilon > 0$, let the sequence $\{\lambda^{t,\tau}\}_{\tau \geq 0}$ and $\{x^{t,\tau}, L_{t,\tau}\}_{t,\tau}$ be generated by the FDDGA. Then a $\tau_0 = \mathscr{O}(\frac{1}{\varepsilon}\ln\frac{1}{\varepsilon}) > 0$ exists such that for any $\tau > \tau_0$, $|W(x_{t,\tau}, L_{t,\tau}) - W^*| \leq 5\varepsilon$ and $\left|\sum_{i\in\mathscr{N}} x_i^{t,\tau} - L_{t,\tau}\right| \leq \frac{\varepsilon}{\Lambda}$. That is, the iteration complexity of the FDDGA for achieving a ε-optimal solution is $\mathscr{O}(\frac{1}{\varepsilon}\ln\frac{1}{\varepsilon})$

5.2.4 Numerical Simulation

The FDDGA formulations were programmed in MATLAB. The simulations were carried out on an Intel Core I5 CPU running at 3.20 GHz with 4 GB of RAM. The numerical simulation here serves to compare the performance of the presented algorithm with the previous dual sub-gradient algorithm for to solve the problems (5.24) and other similar problems that fall into the generalised comprehensive model.

For numerical simulation, it is assumed that the standard utility function and the cost function are adopted from (5.11) and (5.12) respectively. Choose the proximity function $p_i(x_i^t) = \frac{1}{2}\|x_i^t\|^2$ with $\sigma_i = 1$ and $L_(\mu, \upsilon)$ as Lemma 2. Let $\mu = \frac{1}{3(\sum_{i\in\mathscr{N}} d_i + d_t)}$ and $\upsilon = \frac{2\varepsilon}{2\Lambda^2}$, where ε is the desired accuracy. Λ is an upper bound of the solution of the dual problem (5.24), and this simulation we uses $\Lambda = \lambda^t + \Delta_0$, where Δ_0 is a small positive real number to guarantee that Λ is always larger than λ^t. Both algorithms are terminated when all of the termination conditions are satisfied at iteration $\tau + 1$ with required accuracy $\varepsilon = 0.01$.

This section provides several results of the numerical simulations to illustrate that the performance of the convergence of the presented algorithm is superior to the widely adopted sub-gradient method [92, 95–101]. Two kinds of analysis cases are examined.

Case 1

Figures 5.4 and 5.5 display the comparison results of the FDDGA and the sub-gradient method, showing the dynamic progress of iteration for achieving optimal values in a randomly selected time slot. Two different group sizes are studied, i.e. N=10 and N=500.

As shown in figure 5.4, at the beginning of the iteration, the price signal (red line) is low. Therefore, the aggregated load (blue line) is high due to the cheap price while the optimised generation is low. Clearly, the large gap between the aggregated load and the provided energy requires further iterations. With the price signal increases, the difference between load and generation continues to decrease, until the termination criteria are met. By illustrating the

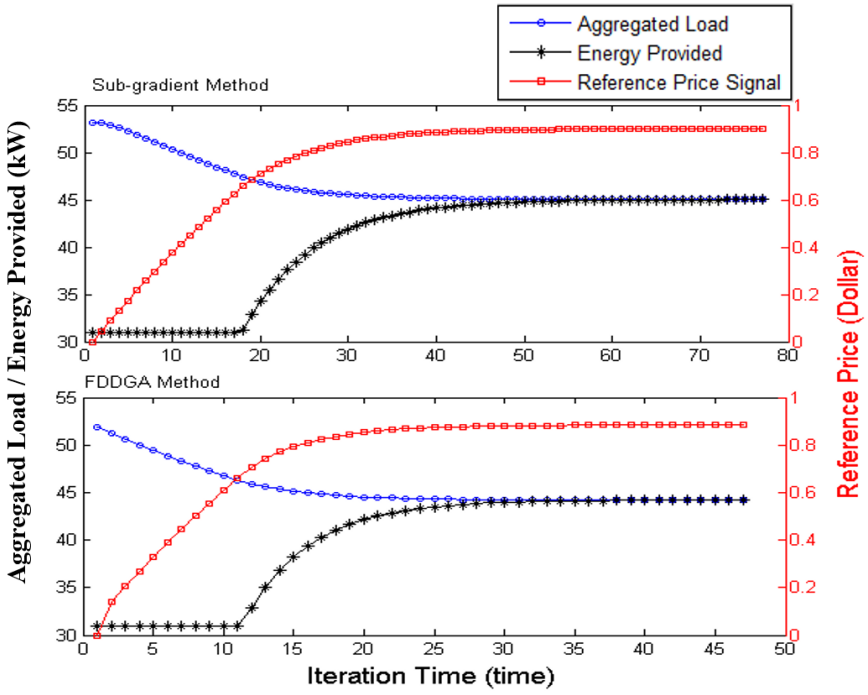

Fig. 5.4 Comparison between sub-gradient method and FDDGA when N=10

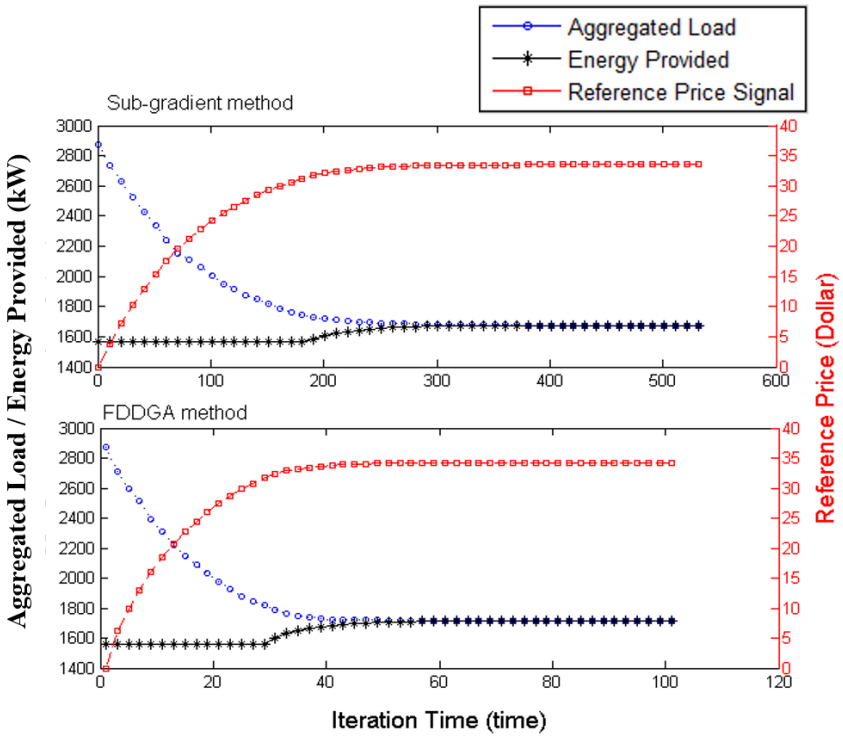

Fig. 5.5 Comparison between sub-gradient method and FDDGA when N=500

dynamic iteration process, figure 5.4 shows that the FDDGA has a faster convergence rate, though both algorithms are able to converge to the same optimal values, including aggregated load (consumption), provided energy (generation) and the pricing value (λ). As described in the previous section, the parameters(step size) in the FDDGA can be automatically computed and fixed, once the particular prox-functions and the required accuracy ε are given. Then the algorithm automatically updates its step size so as to converge rapidly to the optimal values without requiring any step size adjustments, unlike the sub-gradient method.

From the figure 5.5, it can be seen that when a larger number of users is chosen, the disadvantage of the slow convergence rate of the sub-gradient method is more severe. The iteration runs over 500 times. In contrast, with the FDDGA, the iteration stops at the 101^{th} step.

Case 2

Figure 5.6 compares the convergence performances of both algorithms via a selected time slot with regard to chosen and randomly selected step-size (e.g. t=7) and the sum of the entire study horizon (e.g. t=1, 2,...,24), further showing that the FDDGA outperforms the sub-gradient method especially well with a rise in the user number N from 10 to 1000. It can be seen that when N=1000, for time slot t=7, the iteration times for the sub-gradient method is 679 *(blue bars)* while the FDDGA only needs 110 iterations (red bars).

The convergence is also tested with randomly selected step size for the sub-gradient method, illustrated by the green bars. The step sizes are randomly generated from 0 to 0.001. As can be seen, the number of iterations dramatically increases and there is non-convergence in the case with a larger number of users.

Furthermore, when considering the sum of the total number of iteration for the entire study horizon against different user numbers, the advantage of the FDDGA is clearer. For the sub-gradient method, the number of iterations grows rapidly with the increase in users, While conversely, the FDDGA shows the capability to maintain a small number of iterations even as the number of users increases.

Table 5.2 shows the computation time for both sub-gradient method and FDDGA. Different user numbers are selected for the same time slot t=7. The computation time grows for both algorithms with the increasing user number. It is evident that the FDDGA converges faster than the sub-gradient method does. It should also be noted that with the increasing user number, the single iteration time for the FDDGA is slightly longer than for the sub-gradient method, but computation time is mainly decided by the number of iterations in this case. The selected step size for sub-gradient method is also listed for reference.

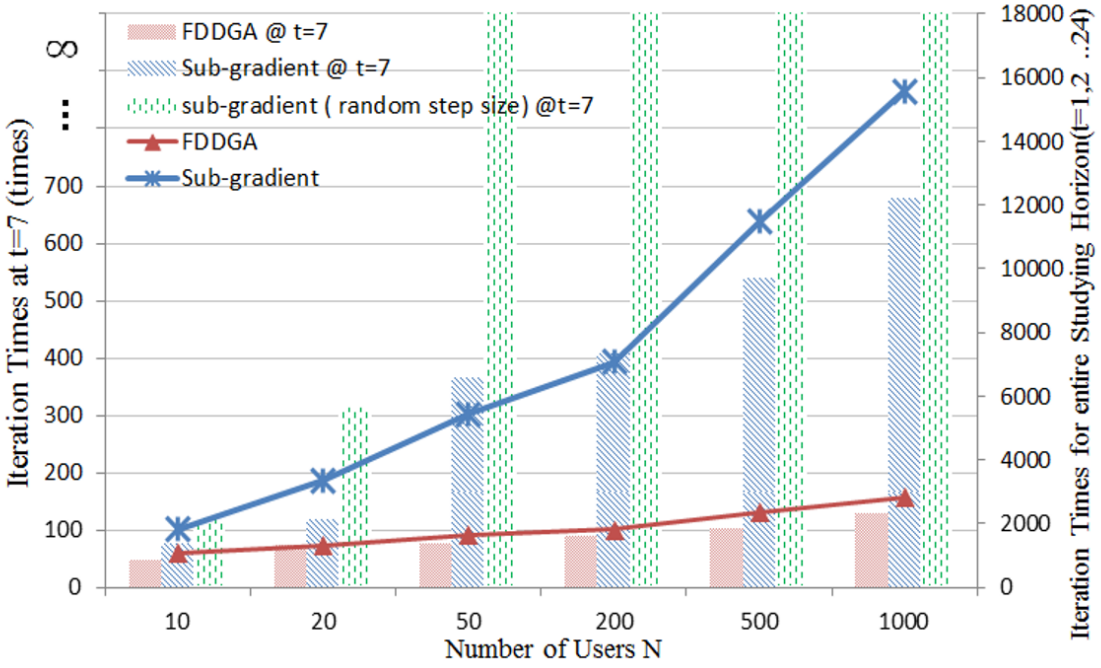

Fig. 5.6 Comparison of number of iterations between the sub-gradient method and the FDDGA with increasing user number N

Table 5.2 Computation Time for Both the Sub-gradient Method and the FDDGA. Different User Numbers at Time Slot t=7

N	FDDGA	Sub-gradient Method	
	Computation Time (Seconds)	Computation Time (Seconds)	Step Size
10	0.450	0.740	0.002
20	0.790	12.52	0.00124
50	0.851	4.052	0.00150
200	1.040	4.722	0.00089
500	1.397	6.660	0.00069
1000	1.902	9.019	0.00030

As mentioned previously, the final price should be announced at the beginning of each time slot. The FDDGA with faster convergence rate can provide more efficient ways to obtain an optimal RTP and is more suitable for practical application.

5.3 Conclusion

This chapter has examined the complexity and the scale of the problem of SCOPF when random energy generation is considered in the formulation. It discussed a few different approaches to reduce the computation burden, which were are applied throughout Chapter 2 to 4 for demonstration.

This chapter has also investigated the use of DSM to compensate for the uncertainties caused by high fraction RESs generation in the grid. In particular, a distributed algorithm is required in this case, which is further smoothed by the FDDGA algorithm to improve the convergence performance, so that the real-time computation can be ensured. The convergence analysis is provided in the appendix.

Chapter 6

Conclusion and Future Work

6.1 Conclusion

This thesis has presented several methods of power system operation and optimisation with the ultimate goal of accommodating the ever-increasing level of penetration of RESs at all different levels of electricity grids. RESs such as PV and wind introduce additional difficulties, which in turn increase the complexity of operating and planning for the grid, and pose challenges in the reliable and secure operation and optimisation for system operators. Intermittency, randomness in generation, and spattered and remote locations of RESs also require the grid expansion in both new transmission lines and larger line capacity. Traditional operation and optimisation models become inadequate both for handling the uncertainties and for finding a solution, a they are overwhelmed by the problem size and computation load. Designing an effective model to consider the randomness of uncertainties and security requirements, and proposing efficient methods to solve these problems could mitigate these issues. For example, a generalised framework of robust SCOPF is introduced in Chapter 2. Moreover, realising that a meshed MTDC grid and an ac grid could coexist in the future grid, Chapter 3 investigated a hierarchical SCOPF model for offshore wind farm optimal dispatch operation. Subsequently, Chapter 4 investigated the coordination of multiple microgrids in the post-contingency recovery, in the scenarios with large renewable generation penetration on both the transmission and MG levels. Finally, Chapter 5 examined the DSM, which is considered to be an alternative way to use the flexibility from the demand side to compensate for the uncertainties caused by the generation side.

The problems and solutions considered in this thesis have raised an additional and crucial issue regard to computation efficiency as the optimisation problem becomes computationally expensive, especially when security and reliability requirements are considered. In particular, a nonlinear formulation of an OPF problem is employed, which is non-convex and NP-

hard, and it becomes even more computationally expensive when the security constraints and uncertainties are involved. Therefore, a linearised model, also called a dc power flow model, is normally adopted as an approximation to study the OPF, neglecting some network constraints and physical losses. Another approach considered in this thesis to reduce the computation complexity is to apply decomposition techniques, on both linearised and nonlinear SCOPF, which functions well in parallel with the robust formulation developed to accommodate uncertainties brought by both load and RESs. The numerical simulations in each chapter have demonstrated encouraging outcomes with regard to the tractability of the problem. In addition, a smoothing technique has been developed to be applied to the distributed algorithm with a widely used gradient method to improve the convergence of the algorithm.

6.2 Future work

Since the penetration of RESs continues to increase in the electricity grid, some interesting research questions that could not be investigated in this thesis are discussed and formulated here as inspiration for future studies in mainly two aspects: modelling and computation.

Modelling

- **Models for OPF and SCOPF considering uncertainties should be further developed.** Control strategies of multiple MGs should be investigated. It might be valuable to study and develop a concept of operational flexibility [106] to evaluate the capability of MGs to participate in system operations and the electricity market.

- **Models of high or 100% power electronics-based grid with small or no inertia need to be studied.** An MG is a good candidate for a heavy inverter-based grid, which features high penetration of renewable sources and distributed generators, as well as low inertia. A plug-and-play feature [107] with its enabler controller design and granular integration into the grid might change the basic structure of the electricity grid operation.

- **Since there are few meshed MTDC systems in operation now, it would be of great value to further investigate detailed models.** This includes different converters, losses models, droop control strategies and different operation schemes.

Computation

- **Relaxation and approximation** could be applied to reduce the complexity of calculating the SCOPF under uncertainties, apart from linearisation.
- **Data-driven optimisation [108, 109], online algorithms [110] and machine learning [111–113]** could be more suitable techniques to deal with uncertainties brought by renewable sources with advanced development in computation and communication technologies.

Chapter 7

List of Publication

Journal paper

[1] W. Zhang, J. Li, G. Chen, Z. Y. Dong, and K. P. Wong. A comprehensive model with fast solver for optimal energy scheduling in rtp environment. *IEEE Transactions on Smart Grid*, PP(99):1–10, 2016.

[2] W. Zhang, Y. Xu, Z. Dong, and K. P. Wong. Robust security-constrained optimal power flow using multiple microgrids for corrective control under uncertainty. *IEEE Transactions on Industrial Informatics*, PP(99):1–1, 2016.

[3] W. Zhang, Y. Xu, K. Meng, and Z. Y. Dong. SCOPF using multi-microgrids for corrective control in energy internet. *Southern Power System Technology*, PP(8):67–73, 2016.

[4] K. Meng, W. Zhang, Y. Li, Z. Y. Dong, Z. Xu, K. P. Wong, and Y. Zheng. [submitted] Hierarchical scopf considering wind energy integration through multi-terminal vsc-hvdc grids. *IEEE Transactions on Power Systems*, 2016(submitted).

[5] B. Zeng, C. Li, G. Chen, and W. Zhang. Verhulst model of interval grey number based on information decomposing and model combination. *Journal of Applied Mathematics*, 2013.

Conference paper

[1] W. Zhang, Yan Xu, Zhao Yang Dong, Yijia Wang, and Rui Zhang. An efficient approach for robust scopf considering load and renewable power uncertainties. In 2016 *Power Systems Computation Conference (PSCC)*, pages 1–7, June 2016.

[2] W. Zhang, G. Chen, Z. Dong, J. Li, and Z. Wu. An efficient algorithm for optimal realtime pricing strategy in smart grid. In 2014 *IEEE PES General Meeting | Conference Exposition*, pages 1–5, July 2014.

[3] W. Zhang, X. Yan, Z. Y. Dong, K. Meng, and R. Zhang. Robust opf considering load and renewable power uncertainties in multi-terminal hvdc grids. In 2016 *IEEE PES Asia-Pacific Power and Energy Engineering Conference (APPEEC)*,pages 24–27, Oct 2016.

[4] W. Zhang, G. Chen, and Z. Y. Dong. Demand side management given distributed generation and storage: A comparison for different pricing and regulation scenarios. In *10th International Conference on Advances in Power System Control, Operation & Management*, pages 29–34, November 2015.

[5] W. Zhang, G. Chen, Y. Su, Z. Dong, and J. Li. A dynamic game behavior: Demand side management based on utility maximization with renewable energy and storage integration. In 2014 *Australasian Universities Power Engineering Conference (AUPEC)*, pages 1–5, Sept 2014.

[6] R. Zhang, Y. Xu, W. Zhang, Z. Y. Dong, and Yu Zheng. Impact of dynamic load models on transient stability-constrained optimal power flow. In 2016 *IEEE PES Asia-Pacific Power and Energy Engineering Conference (APPEEC)*, pages 18–23, Oct 2016.

[7] Z. Wang, W. Zhang, L. Zhang, G. Chen, Z. Dong, and T. Huang. Impact of different penetrations of renewable sources and demand side management on australian future grid. In 2015 *First Workshop on Smart Grid and Renewable Energy (SGRE)*, pages 1–6, March 2015.

References

[1] Thomas B Johansson. *Renewable energy: sources for fuels and electricity*. Island press, 1993.

[2] Gustav Resch, Anne Held, Thomas Faber, Christian Panzer, Felipe Toro, and Reinhard Haas. Potentials and prospects for renewable energies at global scale. *Energy Policy*, 36(11):4048–4056, 2008.

[3] Walter Musial, Sandy Butterfield, Bonnie Ram, et al. Energy from offshore wind. In *Offshore technology conference*. Offshore Technology Conference, 2006.

[4] Y. Xu, Z. Y. Dong, Z. Xu, K. Meng, and K. P. Wong. An intelligent dynamic security assessment framework for power systems with wind power. *IEEE Transactions on Industrial Informatics*, 8(4):995–1003, Nov 2012.

[5] Z. Dong, K. P. Wong, K. Meng, F. Luo, F. Yao, and J. Zhao. Wind power impact on system operations and planning. In *IEEE PES General Meeting*, pages 1–5, July 2010.

[6] Renewables 2016 Global Status Report ren21. http://www.ren21.net/wp-content/uploads/2016/06/GSR_2016_Full_Report.pdf. Accessed: 2017-01-15.

[7] Paul Denholm, Matthew O'Connell, Gregory Brinkman, and Jennie Jorgenson. Overgeneration from solar energy in california: A field guide to the duck chart. *National Renewable Energy Laboratory, Tech. Rep. NREL/TP-6A20-65023*, 2015.

[8] S. Taggart, G. James, Z. Dong, and C. Russell. The future of renewables linked by a transnational asian grid. *Proceedings of the IEEE*, 100(2):348–359, Feb 2012.

[9] Thierry Van Cutsem and Costas Vournas. *Voltage stability of electric power systems*, volume 441. Springer Science & Business Media, 1998.

[10] M. N. Kabir, Y. Mishra, G. Ledwich, Z. Y. Dong, and K. P. Wong. Coordinated control of grid-connected photovoltaic reactive power and battery energy storage systems to improve the voltage profile of a residential distribution feeder. *IEEE Transactions on Industrial Informatics*, 10(2):967–977, May 2014.

[11] Raul Banos, Francisco Manzano-Agugliaro, FG Montoya, Consolacion Gil, Alfredo Alcayde, and Julio Gómez. Optimization methods applied to renewable and sustainable energy: A review. *Renewable and Sustainable Energy Reviews*, 15(4):1753–1766, 2011.

[12] Aoife M Foley, Paul G Leahy, Antonino Marvuglia, and Eamon J McKeogh. Current methods and advances in forecasting of wind power generation. *Renewable Energy*, 37(1):1–8, 2012.

[13] J. Zhao, F. Wen, Y. Xue, Z. Y. Dong, and J. Xin. Power system stochastic economic dispatch considering uncertain outputs from plug-in electric vehicles and wind generators. *Dianli Xitong Zidonghua(Automation of Electric Power Systems)*, 34(20):22–29, 2010.

[14] R. Zhang, Y. Xu, W. Zhang, Z. Y. Dong, and Y. Zheng. Impact of dynamic load models on transient stability-constrained optimal power flow. In *2016 IEEE PES Asia-Pacific Power and Energy Engineering Conference (APPEEC)*, pages 18–23, Oct 2016.

[15] Narayana Prasad Padhy. Unit commitment-a bibliographical survey. *IEEE Transactions on power systems*, 19(2):1196–1205, 2004.

[16] Z. Y. Dong, M. Lu, Z. Lu, and K. P. Wong. A differential evolution based method for power system planning. In *2006 IEEE International Conference on Evolutionary Computation*, pages 2699–2706, 2006.

[17] K. Meng, H. Yang, Z. Y. Dong, W. Guo, F. Wen, and Z. Xu. Flexible operational planning framework considering multiple wind energy forecasting service providers. *IEEE Transactions on Sustainable Energy*, 7(2):708–717, April 2016.

[18] A Monticelli, MVF Pereira, and S Granville. Security-constrained optimal power flow with post-contingency corrective rescheduling. *IEEE Transactions on Power Systems*, 2(1):175–180, 1987.

[19] KWOK-LEUNG TSUI. An overview of taguchi method and newly developed statistical methods for robust design. *IIE Transactions*, 24(5):44–57, 1992.

[20] Antonio J Conejo, Enrique Castillo, Roberto Minguez, and Raquel Garcia-Bertrand. *Decomposition techniques in mathematical programming: engineering and science applications*. Springer Science & Business Media, 2006.

[21] W. Zhang, Y. Xu, Z. Y. Dong, Y. Wang, and R. Zhang. An efficient approach for robust scopf considering load and renewable power uncertainties. In *2016 Power Systems Computation Conference (PSCC)*, pages 1–7, June 2016.

[22] A.J. Wood and B.F. Wollenberg. *Power Generation, Operation, and Control*. A Wiley-Interscience publication. Wiley, 1996.

[23] J Carpentier. Optimal power flows. *International Journal of Electrical Power and Energy Systems*, 1(1):3 – 15, 1979.

[24] R. C. Burchett, H. H. Happ, D. R. Vierath, and K. A. Wirgau. Developments in optimal power flow. *IEEE Transactions on Power Apparatus and Systems*, PAS-101(2):406–414, Feb 1982.

[25] M. Huneault and F. D. Galiana. A survey of the optimal power flow literature. *IEEE Transactions on Power Systems*, 6(2):762–770, May 1991.

[26] P. Kundur, N.J. Balu, and M.G. Lauby. *Power System Stability and Control*. Discussion Paper Series. McGraw-Hill Education, 1994.

[27] Jamal A Baroudi, Venkata Dinavahi, and Andrew M Knight. A review of power converter topologies for wind generators. *Renewable energy*, 32(14):2369–2385, 2007.

[28] Bonmin (Basic Open-source Nonlinear Mixed INteger programming) p. belotti and p. bonami and c. d'ambrosio and etc. https://projects.coin-or.org/Bonmin. Accessed: 2017-02-08.

[29] CPLEX Optimizer ibm. http://www-01.ibm.com/software/commerce/optimization/cplex-optimizer/index.html. Accessed: 2017-02-08.

[30] Inc. Gurobi Optimization. Gurobi optimizer reference manual, 2016.

[31] A. Wächter and L. T. Biegler. On the implementation of an interior-point filter line-search algorithm for large-scale nonlinear programming. *Mathematical programming*, 106(1):25–57, 2006.

[32] R. H. Byrd, J. Nocedal, and R. A. Waltz. Knitro: An integrated package for nonlinear optimization. In *Large-scale nonlinear optimization*, pages 35–59. Springer, 2006.

[33] X.F. Wang, Y. Song, and M. Irving. *Modern Power Systems Analysis*. Power electronics and power systems. Springer US, 2010.

[34] Robert V Hogg and Allen T Craig. *Introduction to mathematical statistics.(5"" edition)*. Upper Saddle River, New Jersey: Prentice Hall, 1995.

[35] M. Shukla and G. Radman. Optimal power flow using probabilistic load model. In *Proceedings of the Thirty-Seventh Southeastern Symposium on System Theory, 2005. SSST '05.*, pages 439–442, March 2005.

[36] H. Ahmadi and H. Ghasemi. Probabilistic optimal power flow incorporating wind power using point estimate methods. In *2011 10th International Conference on Environment and Electrical Engineering*, pages 1–5, May 2011.

[37] C. Wan, Z. Xu, P. Pinson, Z. Y. Dong, and K. P. Wong. Probabilistic forecasting of wind power generation using extreme learning machine. *IEEE Transactions on Power Systems*, 29(3):1033–1044, May 2014.

[38] T. Yong and R. H. Lasseter. Stochastic optimal power flow: formulation and solution. In *2000 Power Engineering Society Summer Meeting (Cat. No.00CH37134)*, volume 1, pages 237–242 vol. 1, 2000.

[39] G. Li and X. P. Zhang. Stochastic optimal power flow approach considering correlated probabilistic load and wind farm generation. In *IET Conference on Reliability of Transmission and Distribution Networks (RTDN 2011)*, pages 1–7, Nov 2011.

[40] Y. Zhang and G. B. Giannakis. Robust optimal power flow with wind integration using conditional value-at-risk. In *2013 IEEE International Conference on Smart Grid Communications (SmartGridComm)*, pages 654–659, Oct 2013.

[41] B. Chen, J. Wang, L. Wang, Y. He, and Z. Wang. Robust optimization for transmission expansion planning: Minimax cost vs. minimax regret. *IEEE Transactions on Power Systems*, 29(6):3069–3077, Nov 2014.

[42] T. Summers, J. Warrington, M. Morari, and J. Lygeros. Stochastic optimal power flow based on convex approximations of chance constraints. In *2014 Power Systems Computation Conference*, pages 1–7, Aug 2014.

[43] H. Zhang and P. Li. Probabilistic analysis for optimal power flow under uncertainty. *IET Generation, Transmission Distribution*, 4(5):553–561, May 2010.

[44] H. Yu and W. D. Rosehart. An optimal power flow algorithm to achieve robust operation considering load and renewable generation uncertainties. *IEEE Transactions on Power Systems*, 27(4):1808–1817, Nov 2012.

[45] Dimitris Bertsimas, David B Brown, and Constantine Caramanis. Theory and applications of robust optimization. *SIAM review*, 53(3):464–501, 2011.

[46] John M Mulvey, Robert J Vanderbei, and Stavros A Zenios. Robust optimization of large-scale systems. *Operations research*, 43(2):264–281, 1995.

[47] S. Marin and A. Garces. Robust optimal power flow in distribution systems with high penetration of wind energy using a model-based evolutionary strategy. In *2014 IEEE PES Transmission Distribution Conference and Exposition - Latin America (PES T D-LA)*, pages 1–6, Sept 2014.

[48] B. Zou and Q. Xiao. Solving probabilistic optimal power flow problem using quasi monte carlo method and ninth-order polynomial normal transformation. *IEEE Transactions on Power Systems*, 29(1):300–306, Jan 2014.

[49] E. M. Constantinescu, V. M. Zavala, M. Rocklin, S. Lee, and M. Anitescu. A computational framework for uncertainty quantification and stochastic optimization in unit commitment with wind power generation. *IEEE Transactions on Power Systems*, 26(1):431–441, Feb 2011.

[50] A. Alabdulwahab, A. Abusorrah, X. Zhang, and M. Shahidehpour. Coordination of interdependent natural gas and electricity infrastructures for firming the variability of wind energy in stochastic day-ahead scheduling. *IEEE Transactions on Sustainable Energy*, 6(2):606–615, April 2015.

[51] Christopher Z Mooney. *Monte carlo simulation*, volume 116. Sage Publications, 1997.

[52] Z. Wang and F. L. Alvarado. Interval arithmetic in power flow analysis. *IEEE Transactions on Power Systems*, 7(3):1341–1349, Aug 1992.

[53] P. Zhang and W. Li. Boundary analysis of distribution reliability and economic assessment. *IEEE Transactions on Power Systems*, 25(2):714–721, May 2010.

[54] J. M. Morales, S. Pineda, A. J. Conejo, and M. Carrion. Scenario reduction for futures market trading in electricity markets. *IEEE Transactions on Power Systems*, 24(2):878–888, May 2009.

[55] Z. Wang, B. Chen, J. Wang, and M. M. Begovic. Stochastic dg placement for conservation voltage reduction based on multiple replications procedure. *IEEE Transactions on Power Delivery*, 30(3):1039–1047, June 2015.

[56] R. D. Zimmerman, C. E. Murillo-Sanchez, and R. J. Thomas. Matpower: Steady-state operations, planning, and analysis tools for power systems research and education. *IEEE Transactions on Power Systems*, 26(1):12–19, Feb 2011.

[57] T.T. Soong. *Fundamentals of Probability and Statistics for Engineers*. Wiley, 2004.

[58] W. Zhang, Y. Xu, Z. Y. Dong, K. Meng, and R. Zhang. Robust opf considering load and renewable power uncertainties in multi-terminal hvdc grids. In *2016 IEEE PES Asia-Pacific Power and Energy Engineering Conference (APPEEC)*, pages 24–27, Oct 2016.

[59] K. Meng, W. Zhang, Y. Li, Z. Y. Dong, Z. Xu, K. P. Wong, and Y. Zheng. [submitted]hierarchical scopf considering wind energy integration through multi-terminal vsc-hvdc grids. *IEEE Transactions on Power Systems*, 2016.

[60] P. Pinson, C. Chevallier, and G. N. Kariniotakis. Trading wind generation from short-term probabilistic forecasts of wind power. *IEEE Transactions on Power Systems*, 22(3):1148–1156, Aug 2007.

[61] Sandy Butterfield, Walt Musial, Jason Jonkman, Paul Sclavounos, and Libby Wayman. Engineering challenges for floating offshore wind turbines. In *Copenhagen Offshore Wind Conference, Copenhagen, Denmark*, pages 377–382. Citeseer, 2005.

[62] Iñigo Martinez de Alegría, Jon Andreu, José Luis Martín, Pedro Ibanez, José Luis Villate, and Haritza Camblong. Connection requirements for wind farms: A survey on technical requierements and regulation. *Renewable and Sustainable Energy Reviews*, 11(8):1858–1872, 2007.

[63] J. Beerten, O. Gomis-Bellmunt, X. Guillaud, J. Rimez, A. van der Meer, and D. Van Hertem. Modeling and control of hvdc grids: A key challenge for the future power system. In *2014 Power Systems Computation Conference*, pages 1–21, Aug 2014.

[64] Anna J Wieczorek, Simona O Negro, Robert Harmsen, Gaston J Heimeriks, Lin Luo, and Marko P Hekkert. A review of the european offshore wind innovation system. *Renewable and Sustainable Energy Reviews*, 26:294–306, 2013.

[65] P. Bresesti, W. L. Kling, R. L. Hendriks, and R. Vailati. Hvdc connection of offshore wind farms to the transmission system. *IEEE Transactions on Energy Conversion*, 22(1):37–43, March 2007.

[66] RJ Barthelmie and SC Pryor. Potential contribution of wind energy to climate change mitigation. *Nature Climate Change*, 4(8):684–688, 2014.

[67] Gene Russo. Renewable energy: Wind power tests the waters. *Nature*, 513(7519):478–480, 2014.

[68] Colin Macilwain. Supergrid. *Nature*, 468(7324):624–625, 2010.

[69] M Milligan, E Ela, J Hein, T Schneider, G Brinkman, and P Denholm. Renewable electricity futures study bulk electric power systems: Operations and transmission planning. *National Renewable Energy Laboratory (NREL), USA, Tech. Rep*, 2012.

[70] E. Iggland, R. Wiget, S. Chatzivasileiadis, and G. Anderson. Multi-area dc-opf for hvac and hvdc grids. *IEEE Transactions on Power Systems*, 30(5):2450–2459, Sept 2015.

[71] S. H. Low. Convex relaxation of optimal power flow x2014;part i: Formulations and equivalence. *IEEE Transactions on Control of Network Systems*, 1(1):15–27, March 2014.

[72] S. H. Low. Convex relaxation of optimal power flow x2014;part ii: Exactness. *IEEE Transactions on Control of Network Systems*, 1(2):177–189, June 2014.

[73] W. Zhang, Y. Xu, Z. Y. Dong, and K. P. Wong. Robust security-constrained optimal power flow using multiple microgrids for corrective control under uncertainty. *IEEE Transactions on Industrial Informatics*, PP(99):1–1, 2016.

[74] W. Zhang, Y. Xu, K. Meng, and Z. Y. Dong. Scopf using multi-microgrids for corrective control in energy internet. *Southern Power System Technology*, 8:67–73, 2016.

[75] F. Capitanescu and L. Wehenkel. A new iterative approach to the corrective security-constrained optimal power flow problem. *IEEE Transactions on Power Systems*, 23(4):1533–1541, Nov 2008.

[76] Y. Xu, Z. Y. Dong, R. Zhang, K. P. Wong, and M. Lai. Solving preventive-corrective scopf by a hybrid computational strategy. *IEEE Transactions on Power Systems*, 29(3):1345–1355, May 2014.

[77] S. Dong Y. Wen, C. Guo. Coordinated control of distributed and bulk energy storage for alleviation of post-contingency overloads. *Energies*, 7(3):1599–1620, 2014.

[78] S. K., K. Ng, , and J. Zhong. Security-constrained dispatch with controllable loads for integrating stochastic wind energy. In *2012 3rd IEEE PES Innovative Smart Grid Technologies Europe (ISGT Europe)*, pages 1–8, Oct 2012.

[79] Florin Capitanescu. Enhanced risk-based {SCOPF} formulation balancing operation cost and expected voluntary load shedding. *Electric Power Systems Research*, 128:151 – 155, 2015.

[80] J. Cao, W. Du, and H. F. Wang. An improved corrective security constrained opf for meshed ac/dc grids with multi-terminal vsc-hvdc. *IEEE Transactions on Power Systems*, 31(1):485–495, Jan 2016.

[81] V. Saplamidis, R. Wiget, and G. Andersson. Security constrained optimal power flow for mixed ac and multi-terminal hvdc grids. In *2015 IEEE Eindhoven PowerTech*, pages 1–6, June 2015.

[82] A. Berizzi, M. Delfanti, P. Marannino, M. S. Pasquadibisceglie, and A. Silvestri. Enhanced security-constrained opf with facts devices. *IEEE Transactions on Power Systems*, 20(3):1597–1605, Aug 2005.

[83] Alexis Kwasinski. *A microgrid architecture with multiple-input dc/dc converters: applications, reliability, system operation, and control*. ProQuest, 2007.

[84] Stephen Sewalk, Norm G Miller, Sunny Liston, and David Wenzhong Gao. Commercial buildings: Energy efficiency and reliability with electric, smart, and microgrids.

[85] N. H. Tran, C. T. Do, S. Ren, Z. Han, and C. S. Hong. Incentive mechanisms for economic and emergency demand responses of colocation datacenters. *IEEE Journal on Selected Areas in Communications*, 33(12):2892–2905, Dec 2015.

[86] P. Basak, A. K. Saha, S. Chowdhury, and S. P. Chowdhury. Microgrid: Control techniques and modeling. In *2009 44th International Universities Power Engineering Conference (UPEC)*, pages 1–5, Sept 2009.

[87] W. Zhang, J. Li, G. Chen, Z. Y. Dong, and K. P. Wong. A comprehensive model with fast solver for optimal energy scheduling in rtp environment. *IEEE Transactions on Smart Grid*, PP(99):1–10, 2016.

[88] J. A. Momoh, R. Adapa, and M. E. El-Hawary. A review of selected optimal power flow literature to 1993. i. nonlinear and quadratic programming approaches. *IEEE Transactions on Power Systems*, 14(1):96–104, Feb 1999.

[89] J. A. Momoh, M. E. El-Hawary, and R. Adapa. A review of selected optimal power flow literature to 1993. ii. newton, linear programming and interior point methods. *IEEE Transactions on Power Systems*, 14(1):105–111, Feb 1999.

[90] H. W. Dommel and W. F. Tinney. Optimal power flow solutions. *IEEE Transactions on Power Apparatus and Systems*, PAS-87(10):1866–1876, Oct 1968.

[91] Florin Capitanescu, JL Martinez Ramos, Patrick Panciatici, Daniel Kirschen, A Marano Marcolini, Ludovic Platbrood, and Louis Wehenkel. State-of-the-art, challenges, and future trends in security constrained optimal power flow. *Electric Power Systems Research*, 81(8):1731–1741, 2011.

[92] P. Samadi, A. H. Mohsenian-Rad, R. Schober, V. W. S. Wong, and J. Jatskevich. Optimal real-time pricing algorithm based on utility maximization for smart grid. In *2010 First IEEE International Conference on Smart Grid Communications*, pages 415–420, Oct 2010.

[93] I. Lampropoulos, G. M. A. Vanalme, and W. L. Kling. A methodology for modeling the behavior of electricity prosumers within the smart grid. In *2010 IEEE PES Innovative Smart Grid Technologies Conference Europe (ISGT Europe)*, pages 1–8, Oct 2010.

[94] M. Parvania, M. Fotuhi-Firuzabad, and M. Shahidehpour. Optimal demand response aggregation in wholesale electricity markets. *IEEE Transactions on Smart Grid*, 4(4):1957–1965, Dec 2013.

[95] P. Samadi, H. Mohsenian-Rad, R. Schober, and V. W. S. Wong. Advanced demand side management for the future smart grid using mechanism design. *IEEE Transactions on Smart Grid*, 3(3):1170–1180, Sept 2012.

[96] A. H. Mohsenian-Rad, V. W. S. Wong, J. Jatskevich, R. Schober, and A. Leon-Garcia. Autonomous demand-side management based on game-theoretic energy consumption scheduling for the future smart grid. *IEEE Transactions on Smart Grid*, 1(3):320–331, Dec 2010.

[97] B. Chai, J. Chen, Z. Yang, and Y. Zhang. Demand response management with multiple utility companies: A two-level game approach. *IEEE Transactions on Smart Grid*, 5(2):722–731, March 2014.

[98] Y. Zhang, N. Gatsis, and G. B. Giannakis. Robust energy management for microgrids with high-penetration renewables. *IEEE Transactions on Sustainable Energy*, 4(4):944–953, Oct 2013.

[99] P. Tarasak. Optimal real-time pricing under load uncertainty based on utility maximization for smart grid. In *2011 IEEE International Conference on Smart Grid Communications (SmartGridComm)*, pages 321–326, Oct 2011.

[100] S. Weckx, J. Driesen, and R. D'hulst. Optimal real-time pricing for unbalanced distribution grids with network constraints. In *2013 IEEE Power Energy Society General Meeting*, pages 1–5, July 2013.

[101] M. Fathi and M. Gholami. Localized demand-side management in electric power systems. In *Iranian Conference on Smart Grids*, pages 1–4, May 2012.

[102] Stephen Boyd, Lin Xiao, and Almir Mutapcic. Subgradient methods. *lecture notes of EE392o, Stanford University, Autumn Quarter*, 2004, 2003.

[103] Antimo Barbato and Antonio Capone. Optimization models and methods for demand-side management of residential users: A survey. *Energies*, 7(9):5787–5824, 2014.

[104] Yu Nesterov. Smooth minimization of non-smooth functions. *Mathematical programming*, 103(1):127–152, 2005.

[105] Olivier Devolder, François Glineur, and Yurii Nesterov. Double smoothing technique for large-scale linearly constrained convex optimization. *SIAM Journal on Optimization*, 22(2):702–727, 2012.

[106] Andreas Ulbig and Göran Andersson. On operational flexibility in power systems. In *Power and Energy Society General Meeting, 2012 IEEE*, pages 1–8. IEEE, 2012.

[107] Souvik Dasgupta, Shankar Narayan Mohan, Sanjib Kumar Sahoo, and Sanjib Kumar Panda. A plug and play operational approach for implementation of an autonomous-micro-grid system. *IEEE Transactions on Industrial Informatics*, 8(3):615–629, 2012.

[108] Jung P Shim, Merrill Warkentin, James F Courtney, Daniel J Power, Ramesh Sharda, and Christer Carlsson. Past, present, and future of decision support technology. *Decision support systems*, 33(2):111–126, 2002.

[109] Erick Delage and Yinyu Ye. Distributionally robust optimization under moment uncertainty with application to data-driven problems. *Operations research*, 58(3):595–612, 2010.

[110] Shai Shalev-Shwartz et al. Online learning and online convex optimization. *Foundations and Trends® in Machine Learning*, 4(2):107–194, 2012.

[111] X. Chen, Z. Y. Dong, K. Meng, Y. Xu, K. P. Wong, and H. W. Ngan. Electricity price forecasting with extreme learning machine and bootstrapping. *IEEE Transactions on Power Systems*, 27(4):2055–2062, Nov 2012.

[112] Christophe Andrieu, Nando De Freitas, Arnaud Doucet, and Michael I Jordan. An introduction to mcmc for machine learning. *Machine learning*, 50(1-2):5–43, 2003.

[113] Rui Zhang, Zhao Yang Dong, Yan Xu, Ke Meng, and Kit Po Wong. Short-term load forecasting of australian national electricity market by an ensemble model of extreme learning machine. *IET Generation, Transmission & Distribution*, 7(4):391–397, 2013.

Appendix A

Convergence analysis of the FDDGA used in Chapter 5

Convergence analysis

In this section, the convergence analysis of the FDDGA introduced in Chapter 5 is provided. Firstly, denote $\widetilde{\lambda}^{t*}$ as the unique optimal solution of the proposed twice smoothed dual problem (5.30) and λ^{t*} as an optimal solution of the dual problem (5.24). Then it gives:

$$\left\|\lambda^{t*}\right\| \leq \Lambda \tag{A.1}$$

where Λ is an estimated upper bound for λ^{t*}.

The goal is to compute an approximate optimal solution for primal problem (5.23), defined as follows:

Definition 1.

For any given target accuracy $\varepsilon > 0$, if there exists non-negative constants c_1, c_2 such that:

$$\left|W(\hat{x}^t, \hat{L}_t) - W^*\right| \leq c_1\varepsilon \; and \; \left|\sum_{i\in\mathcal{N}} \hat{x}_i^t - \hat{L}_t\right| \leq c_1\varepsilon \tag{A.2}$$

then $(\hat{x}^t, \hat{L}_t) \in \Re^{N+1}$ is an ε-optimal feasible solution of primal problem (5.23).

Proposition 1. Let $\{\lambda^{t,\tau}\}_{\tau\geq 0}$ be the sequence of iterates generated by (5.31)-(5.35). Then for all $\tau \geq 0$, it holds,

$$\mathscr{D}(\lambda^{t,\tau}) - \mathscr{D}(\lambda^{t*}) \leq (2+\sqrt{2})(\mathscr{D}(0) - \mathscr{D}(\lambda^*) + \mu(\sum_{i\in\mathscr{N}} d_i + d_t))e^{-\frac{\tau}{2}\sqrt{\frac{\upsilon}{L_{\mu,\upsilon}}}} + \mu(\sum_{i\in\mathscr{N}} d_i + d_t)) + \frac{\upsilon}{2}\Lambda^2 \tag{A.3}$$

Proof of proposition 1 is given in **Appendix II**.

The further analysis on the accuracy of FDDGA for achieving the optimal objective value of $\mathscr{D}(\bullet)$ is given in **Theorem 2**.

Theorem 2. For any given accuracy $\varepsilon > 0$, let $\{\lambda^{t,\tau}\}_{\tau\geq 0}$ be the sequences of dual iterates generated by (5.34) and (5.35). Then, there exists a $\tau_1 = \mathscr{O}(\frac{1}{\varepsilon}\ln\frac{1}{\varepsilon}) > 0$ such that $\tau > \tau_1$, it holds that $\mathscr{D}(\lambda^{t,\tau}) - \mathscr{D}(\lambda^{t*}) \leq \varepsilon$. Here the proof of theorem 2 is provided. To achieve $\mathscr{D}(\lambda^{t,\tau}) - \mathscr{D}(\lambda^{t*}) \leq \varepsilon$, all the three terms of Proposition 1 are forced to be less than or equal to $\varepsilon/3$. Therefore, the corresponding smoothing parameters of the given accuracy $\varepsilon \geq 0$ are:

$$\mu = \frac{1}{3\sum_{i\in\mathscr{N}} d_i + d_t)} \; and \; \upsilon = \frac{2\varepsilon}{3\Lambda^2} \tag{A.4}$$

which yields,

$$\mathscr{D}(\lambda^{t,\tau}) - \mathscr{D}(\lambda^{t*}) \leq (2+\sqrt{2})(\mathscr{D}(0) - \mathscr{D}(\lambda^* + \frac{\varepsilon}{3})e^{-\frac{\tau}{2}\sqrt{\frac{\upsilon}{L_{\mu,\upsilon}}}} + \frac{2\varepsilon}{3} \tag{A.5}$$

One can see that ε-accuracy is achieved as soon as the first term on the right-hand side of the above inequality gets less than $\varepsilon/3$ depending on the number of iterations. Thus this leads to the followings.

$$\tau \geq 2\sqrt{\frac{L_{\mu,\upsilon}}{\upsilon}}\ln\frac{3(2+\sqrt{2})(\mathscr{D}(0) - \mathscr{D}(\lambda^* + \frac{\varepsilon}{3})}{\varepsilon} = \tau_1(\varepsilon) \tag{A.6}$$

Investigating the square root term of $\tau_1(\varepsilon)$ in (A.6), and it gets back Lemma 2 and (A.5). Therefore at most $\tau_1 = \mathscr{O}(\frac{1}{\varepsilon}\ln\frac{1}{\varepsilon})$ iterations such that $\mathscr{D}(\lambda^{t,\tau}) - \mathscr{D}(\lambda^{t*}) \leq \varepsilon$ can be achieved.

In order to reconstruct a nearly optimal and feasible primal solution efficiently, an upper bound on the norm of $\nabla\mathscr{D}(\lambda^{t,\tau})$ needs to be given.

Theorem 3 For any given accuracy $\varepsilon \geq 0$, let $\{\lambda^{t,\tau}\}_{\tau\geq 0}$ be the sequences of dual iterates generated by (5.34), (5.35). Then, there exists a $\tau_2 = \mathscr{O}(\frac{1}{\varepsilon}\ln\frac{1}{\varepsilon}) > 0$ such that $l \geq l_2$. It holds,

$$\left\|\nabla\mathscr{D}(\lambda^{t,\tau})\right\| \leq \frac{\varepsilon}{\Lambda} \tag{A.7}$$

The proof of Theorem 3 is also given in the Appendix II.

Appendix B

Proof of Theorem 1, Proposition 1 and Theorem 3

This section describe the proofs for theorem 1, proposition 1 and theorem 3 presented in Chapter 5

Proof of Theorem 1

According to (5.28), (5.31) and (5.32), it gives,

$$\begin{aligned}\mathscr{D}_{\mu}(\lambda^{t,\tau}) = \sum_{i\in\mathscr{N}} U(x_i^{t,\tau},\xi) - \lambda^{t,\tau}x_i^{t,\tau} - \mu p_i(x_i^{t,\tau}) \\ + \lambda^{t,\tau}L_{t,\tau} - C(L_{t,\tau}) - \mu p_t(L_{t,\tau})\end{aligned} \tag{B.1}$$

Noting that $W^* = \mathscr{D}^*$ and $\triangledown\mathscr{D}_{\mu}(\lambda^{t,\tau}) = -[\sum_{i\in\mathscr{N}} x_i^{t,\tau} - L_{t,\tau}]$, so,

$$\begin{aligned}W(x_i^{t,\tau},L_{t,\tau}) - W^* = \lambda^{t,\tau}\triangledown\mathscr{D}_{\mu}(\lambda^{t,\tau}) + \sum_{i\in\mathscr{N}} \mu p_i(x_i^{t,\tau}) \\ + \mu p_t(L_{t,\tau}) - \mathscr{D}_{\mu}(\lambda^{t,\tau}) + \mathscr{D}(\lambda^{t*})\end{aligned} \tag{B.2}$$

Then, $|\mathscr{D}(\lambda^{t,\tau}) - \mathscr{D}(\lambda^{t*}) \leq \varepsilon|$. Therefore,

$$\left|W(x_i^{t,\tau},L_{t,\tau}) - W^*\right| \leq \|\lambda_{t,\tau}\| \left\|\triangledown\mathscr{D}_{\mu}(\lambda^{t,\tau})\right\| + 2\varepsilon \tag{B.3}$$

It holds,

$$\|\lambda_{t,\tau}\| \leq \Lambda\sqrt{\frac{3}{\varepsilon}(\mathscr{D}_\mu 0 - \mathscr{D}_\mu(\widetilde{\lambda}^{t*}))} \tag{B.4}$$

Due to the choice of l_0 and the above estimates, the following could be obtained,

$$\left|W(x_i^{t,\tau}, L_{t,\tau}) - W^*\right| \leq (3-2\sqrt{2})\varepsilon + (2+\sqrt{2})\varepsilon \leq 5\varepsilon \tag{B.5}$$

Finally, it follows from (A.2) , Lemma1 and Theorem 3 that,

$$\left|\sum_{i\in\mathscr{N}} x_i^{t,\tau} - L_{t,\tau}\right| = \left\|\triangledown\mathscr{D}_\mu(\lambda^{t,\tau})\right\| \leq \frac{\varepsilon}{\Lambda} \tag{B.6}$$

The proof of Theorem 1 is complete.

Proof of proposition 1

From (5.29), it gives $\mathscr{D}_\mu(0) \leq \mathscr{D}(0)$ and $\mathscr{D}(\lambda^*) - \mu(\sum_{i\in\mathscr{N}} d_i + d_t) \leq \mathscr{D}_\mu(\hat{\lambda}^{t*})$, thus,

$$\mathscr{D}_\mu(0) - \mathscr{D}_\mu(\widetilde{\lambda}^{t*}) \leq \mathscr{D}(0) - \mathscr{D}(\lambda^{t*}) + \mu(\sum_{i\in\mathscr{N}} d_i + d_t) \tag{B.7}$$

Since $\mathscr{D}_\mu(\widetilde{\lambda}^{t*}) + \frac{\upsilon}{2}\left\|\widetilde{\lambda}^{t*}\right\|^2 \leq \mathscr{D}_\mu(\lambda^{t*}) + \frac{\upsilon}{2}\|\lambda^{t*}\|^2$, and and follows from the above inequality, (A.1) and due to $\mathscr{D}_{\mu,\upsilon}(\lambda^{t,\tau}) = \mathscr{D}_\mu(\lambda^{t,\tau}) + \frac{\upsilon}{2}\|\lambda^{t*}\|^2$, it leads to:

$$\mathscr{D}_\mu(\lambda^{t,\tau}) - \mathscr{D}_\mu(\widetilde{\lambda}^{t*}) \leq (\mathscr{D}_\mu(0) - \mathscr{D}_\mu(\widetilde{\lambda}^{t*}))e^{-\tau\sqrt{\frac{\upsilon}{L_{\mu,\upsilon}}}} + \frac{\upsilon}{2}(\left\|\widetilde{\lambda}^{t*}\right\|^2 - \left\|\lambda^{t,\tau}\right\|^2) \tag{B.8}$$

Now it is estimated $\left\|\widetilde{\lambda}^{t*}\right\|^2 - \|\lambda^{t,\tau}\|^2$ as follow,

$$\begin{aligned}\left\|\widetilde{\lambda}^{t*}\right\|^2 - \left\|\lambda^{t,\tau}\right\|^2 &\leq \left\|\lambda^{t*} - \lambda t, \tau\right\|(\left\|\lambda^{t*} - \lambda t, \tau\right\| + 2\left\|\widetilde{\lambda}^{t*}\right\|) \\ &\leq \frac{2+2\sqrt{2}}{\upsilon}(\mathscr{D}_\mu(0) - \mathscr{D}_\mu(\widetilde{\lambda}^{t*}))e^{-\tau\sqrt{\frac{\upsilon}{L_{\mu,\upsilon}}}}\end{aligned} \tag{B.9}$$

Hence, combing with (B.7), (B.8) and (B.9) the desired result is achieved and this completes the proof.

Proof of Theorem 3

From lemma 2, the following could be obtained,

$$\left\|\nabla \mathscr{D}_{\mu}(\lambda^{t,\tau})\right\| \leq \left\|\nabla \mathscr{D}_{\mu,\upsilon}(\lambda^{t,\tau})\right\| + \upsilon \left\|\lambda^{t,\tau}\right\| \tag{B.10}$$

Moreover, noting that,

$$\begin{aligned}\mathscr{D}(\lambda^{t*}) + \frac{\upsilon}{2}\left\|\lambda^{t*}\right\|^2 &\geq \mathscr{D}_{\mu}(\lambda^{t*}) + \frac{\upsilon}{2}\left\|\lambda^{t*}\right\|^2 \\ &\geq \mathscr{D}(\lambda^{t*}) - \mu(\sum_{i\in\mathscr{N}} d_i + d_t) + \frac{\upsilon}{2}\left\|\lambda^{t*}\right\|^2\end{aligned} \tag{B.11}$$

Combing with the previous estimates, it gives rise to,

$$\left\|\nabla \mathscr{D}_{\mu}(\lambda^{t,\tau})\right\| \leq (\sqrt{L_{\mu,\upsilon}} + \sqrt{\upsilon})\sqrt{2(\mathscr{D}(0) - \mathscr{D}(\lambda^{t*}) + \frac{\varepsilon}{3})}e^{-\tau\sqrt{\frac{\upsilon}{L_{\mu,\upsilon}}}} + \frac{2\sqrt{2}\varepsilon}{3\Lambda} \tag{B.12}$$

For $\varepsilon > 0$ fixed, the first term of the above inequality decreases by the iteration counter τ. In order to ensure $\left\|\nabla \mathscr{D}_{\mu}(\lambda^{t,\tau})\right\| \leq \frac{\varepsilon}{\Lambda}$, the following is needed,

$$\tau \geq 2\sqrt{\frac{L_{\mu,\upsilon}}{\varepsilon}} \ln \frac{3\Lambda(\sqrt{L_{\mu,\upsilon}} + \sqrt{\upsilon})\sqrt{2(\mathscr{D}(0) - \mathscr{D}(\lambda^{t*}) + \frac{\varepsilon}{3})}}{(3-2\sqrt{2})\varepsilon} = \tau_2(\varepsilon) \tag{B.13}$$

Note that $\tau_2 = \mathscr{O}(\frac{1}{\varepsilon}\ln\frac{1}{\varepsilon})$ and the proof is completed.